Article

Neuron

Polarity Acquisition in Cortical Neurons Is Driven by Synergistic Action of Sox9-Regulated Wwp1 and Wwp2 E3 Ubiquitin Ligases and Intronic miR-140

Graphical Abstract

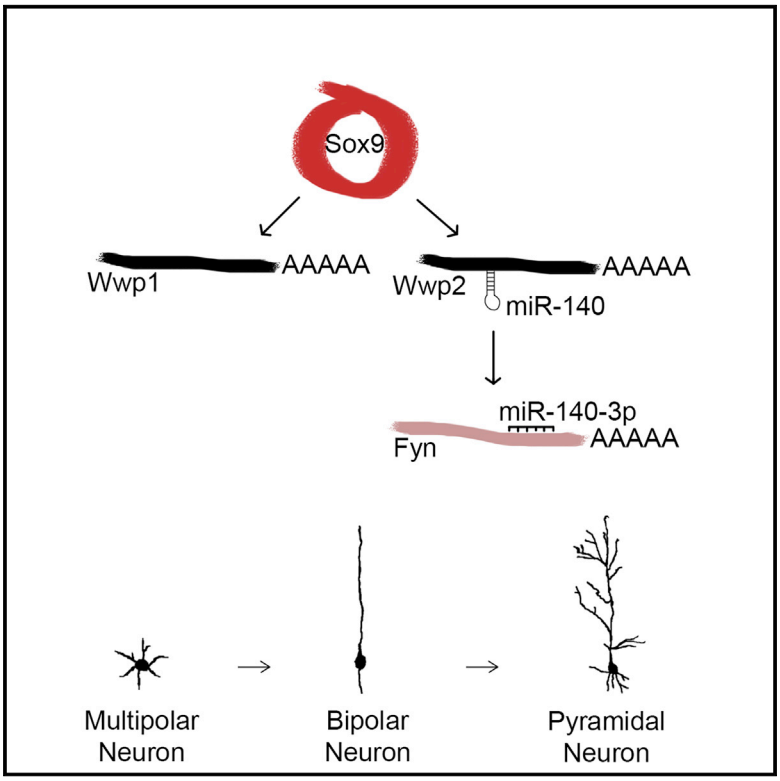

Highlights

- The ubiquitin ligases Wwp1 and Wwp2 are essential for neuronal polarity acquisition
- Wwp2 and *Wwp2*-intron-encoded *miR-140* synergistically regulate neuronal development
- miR-140 represses Fyn expression during neuronal development
- Sox9 drives expression of *Wwp1*, *Wwp2,* and *miR-140* in neurons

Authors

Mateusz C. Ambrozkiewicz, Manuela Schwark, Mika Kishimoto-Suga, ..., Mikio Hoshino, Victor Tarabykin, Hiroshi Kawabe

Correspondence

mateusz-cyryl.ambrozkiewicz@charite.de (M.C.A.), kawabe@em.mpg.de (H.K.)

In Brief

Ambrozkiewicz et al. describe a synergistic signaling pathway that involves Sox9-driven expression of the E3 ubiquitin ligases Wwp1 and Wwp2 and of *Wwp2*-intron-encoded miR-140, and miR-140-dependent control of Fyn expression to regulate axon-dendrite polarity in developing neurons.

Ambrozkiewicz et al., 2018, Neuron *100*, 1097–1115
December 5, 2018
https://doi.org/10.1016/j.neuron.2018.10.008

CellPress

Neuron
Article

Polarity Acquisition in Cortical Neurons Is Driven by Synergistic Action of Sox9-Regulated Wwp1 and Wwp2 E3 Ubiquitin Ligases and Intronic miR-140

Mateusz C. Ambrozkiewicz,[1,2,3,*] Manuela Schwark,[1] Mika Kishimoto-Suga,[1,13] Ekaterina Borisova,[3,4,13] Kei Hori,[5] Andrea Salazar-Lázaro,[3] Alexandra Rusanova,[3,4] Bekir Altas,[1,2] Lars Piepkorn,[6] Paraskevi Bessa,[3] Theres Schaub,[3] Xin Zhang,[7] Tamara Rabe,[8] Silvia Ripamonti,[1] Marta Rosário,[3] Haruhiko Akiyama,[9] Olaf Jahn,[6] Tatsuya Kobayashi,[10] Mikio Hoshino,[5] Victor Tarabykin,[3,4,14] and Hiroshi Kawabe[1,11,12,14,15,*]

[1]Department of Molecular Neurobiology, Max Planck Institute of Experimental Medicine, Hermann-Rein-Strasse 3, 37075 Göttingen, Germany
[2]International Max Planck Research School for Neurosciences, Georg-August-Universität Göttingen, Griesebachstrasse 5, 37077 Göttingen, Germany
[3]Institute of Cell Biology and Neurobiology, Charité-Universitätsmedizin Berlin, corporate member of Freie Universität Berlin, Humboldt-Universität zu Berlin, and Berlin Institute of Health, Charitéplatz 1, 10117 Berlin, Germany
[4]Institute of Neuroscience, Lobachevsky University of Nizhny Novgorod, pr. Gagarina 24, 603950 Nizhny Novgorod, Russian Federation
[5]Department of Biochemistry and Cellular Biology, National Institute of Neuroscience, NCNP, 4-1-1 Ogawahigashi, Kodaira, Tokyo 187-8502, Japan
[6]Proteomics Group, Max Planck Institute of Experimental Medicine, Hermann-Rein-Strasse 3, 37075 Göttingen, Germany
[7]Molecular Oncology, Medical University of Göttingen, Justus-von-Liebig-Weg 11, 37077 Göttingen, Germany
[8]Max Planck Institute for Biophysical Chemistry, Am Fassberg 11, 37077 Göttingen, Germany
[9]Department of Orthopaedic Surgery, Gifu University, 1-1 Yanagito, Gifu 501-1193, Japan
[10]Massachusetts General Hospital and Harvard Medical School, Boston, MA 02114, USA
[11]Division of Pathogenetic Signaling, Department of Biochemistry and Molecular Biology, Kobe University Graduate School of Medicine, 1-5-6 Minatojima-minamimachi, Chuo-ku, Kobe 650-0047, Japan
[12]Department of Gerontology, Laboratory of Molecular Life Science, Institute of Biomedical Research and Innovation, Foundation for Biomedical Research and Innovation at Kobe, 2-2 Minatojima-Minamimachi Chuo-ku, Kobe 650-0047, Japan
[13]These authors contributed equally
[14]Senior author
[15]Lead Contact
*Correspondence: mateusz-cyryl.ambrozkiewicz@charite.de (M.C.A.), kawabe@em.mpg.de (H.K.)
https://doi.org/10.1016/j.neuron.2018.10.008

SUMMARY

The establishment of axon-dendrite polarity is fundamental for radial migration of neurons during cortex development of mammals. We demonstrate that the E3 ubiquitin ligases WW-Containing Proteins 1 and 2 (Wwp1 and Wwp2) are indispensable for proper polarization of developing neurons. We show that knockout of *Wwp1* and *Wwp2* results in defects in axon-dendrite polarity in pyramidal neurons, and their aberrant laminar cortical distribution. Knockout of *miR-140*, encoded in *Wwp2* intron, engenders phenotypic changes analogous to those upon *Wwp1* and *Wwp2* deletion. Intriguingly, transcription of the *Wwp1* and *Wwp2/miR-140* loci in neurons is induced by the transcription factor Sox9. Finally, we provide evidence that *miR-140* supervises the establishment of axon-dendrite polarity through repression of Fyn kinase mRNA. Our data delineate a novel regulatory pathway that involves Sox9–[Wwp1/Wwp2/miR-140]-Fyn required for axon specification, acquisition of pyramidal morphology, and proper laminar distribution of cortical neurons.

INTRODUCTION

The assembly of the mammalian cerebral cortex follows a tightly controlled inside-first-and-outside-last pattern of development, which ultimately establishes the cellular and synaptic substrate for all cortical functions. During cortical development, sequential cohorts of newly born neurons migrate from the ventricular zone (VZ) and intermediate zone (IZ), in the cortical plate (CP), and distribute horizontally upon reaching the marginal zone (MZ). The excitatory neurons of the mammalian neocortex originate from a cluster of progenitors located in the VZ and subventricular zone (SVZ) (Noctor et al., 2001). Differentiating neurons undergo robust changes of their shape. Shortly after birth, multipolar (MP) neurons at the border between the SVZ and IZ alter their appearance to acquire a characteristic bipolar (BP) morphology. Disruptions to corresponding morphoregulatory processes may engender defects in neuronal migration that contribute to the etiology of severe neurodevelopmental disorders, and likely also to autism spectrum disorders (Hori et al., 2014).

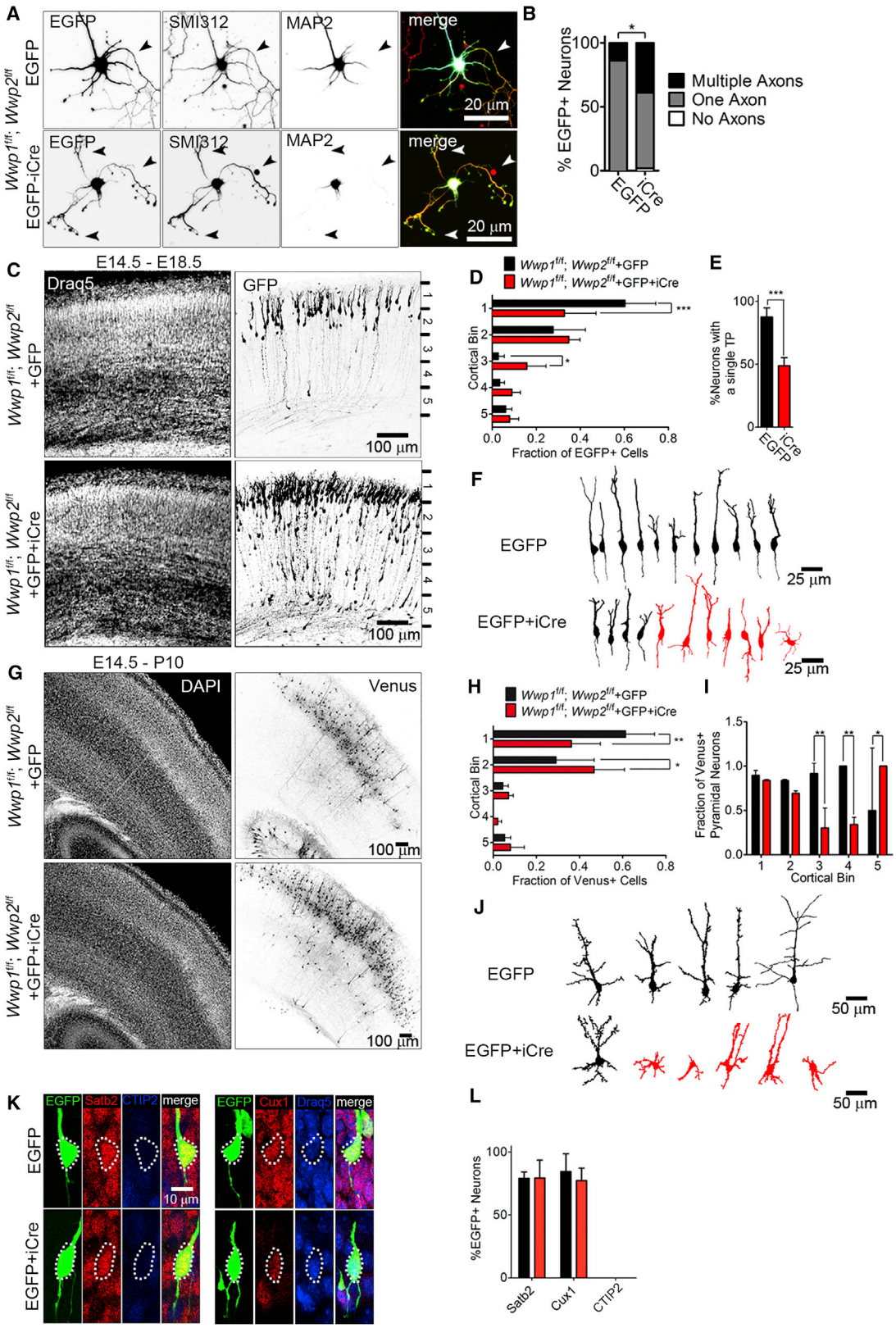

(legend on next page)

The acquisition of BP shape in migrating neurons is coupled to the emergence of neuronal polarity. The single leading process (LP) of a migrating nerve cell orients perpendicularly toward the pia, whereas the single trailing process (TP), emerging from the somatic antipode, lags behind the radially translocating neuron. Notably, pyramidal neurons derive axon-dendrite polarity from specification of the LP and the TP during migration (Barnes and Polleux, 2009). The neurite that extends in the radial direction becomes the LP, and the TP extends from the opposite pole of the nerve cell. Later in development, the LP establishes the fate of an apical dendritic shaft, and the TP extends into the axon (Hatanaka et al., 2012).

One salient feature of the mammalian cortex is its six-layered structure. Excitatory neurons of a given cortical layer display similar transcriptional signatures and connectivity. Neurons of layer II/III contribute to the establishment of cortico-cortical projections, whereas neurons in deeper layers send their axons sub-cerebrally (Rakic, 2009). Signaling pathways that control axon-dendrite polarity acquisition, radial migration, and positioning of neurons among the cortical layers contribute to the establishment of neuronal circuits.

Posttranscriptional and posttranslational regulation of gene expression plays a pivotal role in neuronal development. Recent discoveries have highlighted ubiquitination as a critical regulatory principle in fundamental biological processes that control brain development. Members of the family of Neural Precursor Cell Expressed Developmentally Down-Regulated 4 (Nedd4) E3 ligases, which are of the Homologous to E6AP Carboxyl Terminus (HECT) type, are essential regulators of nerve cell development (Ambrozkiewicz and Kawabe, 2015; Kawabe and Brose, 2011; Kawabe et al., 2010).

microRNAs (miRNAs, miRs) regulate gene expression by binding, in most cases, 3′ UTRs of mRNA transcripts. There is ample evidence for a key role of miRNAs in neuronal development (De Pietri Tonelli et al., 2008). Of note, approximately half of all identified human miRNAs are encoded in introns of protein-coding genes. This type of genomic structure enables the promoter-mediated co-regulation of the intronic miRNA and the host gene. Indeed, bioinformatic predictions indicate that intronic miRNAs and the protein products of their host gene loci often co-regulate the same cellular processes (Lutter et al., 2010). However, corresponding experimental validations and functional analyses of such putative synergistic interactions between miRNA and host gene products are largely lacking.

In the present study, we investigate the role of a subfamily of Nedd4-type E3 ligases, WW Domain Containing E3 Ubiquitin Protein Ligases 1 and 2 (Wwp1 and Wwp2; Wwp1/2), and their functional interplay with *miR-140*, encoded in a *Wwp2* intron. We demonstrate synergistic roles of *Wwp1/2* and *miR-140* in the acquisition of axon-dendrite polarity and the laminar distribution of developing pyramidal neurons. Moreover, miR-140-mediated silencing of Fyn kinase is required for the proper acquisition of a BP morphology by developing neurons. Finally, the expression of *Wwp1/2* and the intronic *miR-140* is under the control of the transcription factor Sex Determining Region Y-Box 9 (Sox9) in developing neurons, and Sox9 is essential for the proper laminar distribution and polarity formation of cortical nerve cells. We propose that Sox9 supervises two collateral signaling pathways that are mediated by *Wwp1/2* and *miR-140*, respectively, regulating proper polarity formation in developing cortical neurons.

RESULTS

Wwp1 and Wwp2 Are Essential for the Establishment of Polarized Morphology and Proper Laminar Distribution of Developing Neurons

Wwp1 and Wwp2 share a high degree of homology (Figure S1A, related to Figure 1). To circumvent the problem of redundancy in the functional analyses of Wwp1/2, we generated a $Wwp1^{f/f}$; $Wwp2^{f/f}$ ($Wwp1/2^{f/f}$) mouse line (Figures S1A–S1G) and established small hairpin RNA (shRNA)-mediated knockdown (KD) systems for Wwp1 and Wwp2 (Figure S1H). In the $Wwp1/2^{f/f}$ mice, Cre-mediated eliminations of 6^{th} exons in *Wwp1* and *Wwp2* result in an in-frame premature stop codons. To establish glia/neuron-specific *Wwp1/2* double-knockout (dKO) mouse lines, we crossed $Wwp1/2^{f/f}$ mice with an $Emx1^{Cre/+}$ driver (hereafter named *Wwp1/2* cdKO). Western blotting with antibodies against Wwp1 and Wwp2 showed a strong reduction of Wwp1 and Wwp2 levels in *Wwp1/2* cdKO mouse brains (Figure S1G), with the remaining expression of Wwp1 and Wwp2 likely reflecting protein expression in other cells of non-*Emx1* lineage.

The function of wwp-1, the *C. elegans* ortholog of Wwp1 and Wwp2, has been linked to the regulation of presynapse development (Sieburth et al., 2005). *wwp-1* has a functional correlation to *sad-1*—an ortholog of the mammalian SAD-A and SAD-B kinases, required for proper axon-dendrite polarity acquisition in mice (Barnes et al., 2007; Kishi et al., 2005).

Figure 1. Double Knockout of *Wwp1* and *Wwp2* Induces Multiple Axons and Disrupts Laminar Distribution of Developing Neurons

(A) Control primary hippocampal neurons expressing EGFP and *Wwp1/2* double-knockout neurons (*Wwp1/2* double knockout [dKO]) expressing GFP and Cre recombinase were fixed at DIV7 and immunostained as indicated. Arrowheads indicate axons.

(B) Quantification of the number of axons projected from a single neuron (see Table S1A for details).

(C and G) Representative images of immunostaining signals in E18.5 (C) and P10 (G) cortices of $Wwp1/2^{f/f}$ mice after IUE as indicated.

(D and H) Quantification of laminar distribution of control and Wwp1/2 double KO neurons *in vivo* at E18.5 (D) and P10 (H) (Tables S1B and S1D).

(E) Quantification of percentage of neurons with a single trailing process (TP) at E18.5, unpaired t test (Table S1C).

(F and J) Tracings of representative control and *Wwp1/2* double KO neurons in bin 3 and 4 of E18.5 (F) and P10 (J) brains.

(I) Average fraction of control and *Wwp1/2* double KO neurons of pyramidal morphology (Table S1E).

(K) Representative images of Draq5 and immunostaining signals in E18.5 cortices electroporated as described in (C). Dotted line encloses cell soma.

(L) Quantification of the fraction of $Wwp1/2^{f/f}$ $EGFP^{+}$ neurons expressing indicated vectors, positive for Satb2, Cux1, or CTIP2, unpaired t test (Table S1F).

Results on graphs are represented as averages ±SD. For statistical analyses, (B) chi-square test; (D), (H), and (I) two-way ANOVA with Bonferroni post hoc test; ***$p < 0.001$; ** $0.001 < p < 0.01$; * $0.01 < p < 0.05$. See also Figures S1–S4 and S8.

For this reason, we decided to study the cell-autonomous effects of loss of *Wwp1* and *Wwp2* (*Wwp1/2*) on axon formation. We prepared primary hippocampal neurons from *Wwp1/2*$^{f/f}$ mice and transfected them with a plasmid encoding EGFP alone, or with a plasmid encoding EGFP and Cre recombinase at first day *in vitro* (DIV) (Figure 1A). We found that at DIV6–7 the loss of *Wwp1/2* causes a marked increase in the number of axons per neuron (Figure 1B; Table S1A, exact values, sample numbers, and statistics, related to the whole manuscript).

Polarization in primary neurons *in vitro* recapitulates major aspects of polarity acquisition in developing nerve cells *in vivo* (Barnes and Polleux, 2009). Hence, multiple axons in Cre-expressing *Wwp1/2*$^{f/f}$ primary hippocampal neurons may reflect deficiency in the MP-to-BP transition, antecedent to aberrances in the radial migration and laminar distribution. We then deleted *Wwp1/2* by transfecting cortical progenitors of *Wwp1/2*$^{f/f}$ mice at E14.5 with a Cre/EGFP co-expression vector using *in utero* electroporation (IUE) and analyzed targeted brains at E18.5. *Wwp1/2*$^{f/f}$ neurons expressing EGFP and Cre (*Wwp1/2* double KO) exhibited a slight but significant accumulation in lower regions of the CP (Figures 1C and 1D; Table S1B). At this stage of development, migrating control neurons acquire characteristic morphology with a single LP and a single TP. Notably, *Wwp1/2* double KO induced a drastic loss of polarity, leading to specification of multiple TPs in single cortical neurons, or to misorientation of apical dendrites sometimes directing toward the ventricle (Figures 1E and 1F; Table S1C).

Aberrant laminar distribution of cortical neurons was still prominent upon *Wwp1/2* double KO postnatally at P10, when polarity of pyramidal neurons is established *in vivo* (Figures 1G and 1H; Table S1D). *Wwp1/2* double KO neurons arrested in deeper layers of the cortex exhibited loss of pyramidal morphology, with increased fractions of MP neurons, projecting multiple apical dendrites or extended the apical dendrite away from the pia (Figures 1I and 1J; Table S1E). Relatively normal pyramidal morphology of neurons in the upper layers is likely due to the compensatory effect from the extracellular signals in layer II/III or an alternative pathway at work in the neuronal polarity and migration of layer II/III cells. Altered position of neurons in the cortex upon *Wwp1/2* double KO was not caused by the neuronal fate switch, as they were labeled for marker proteins expressed in upper-layer neurons: Cut-Like 1 (Cux1) (Nieto et al., 2004), and Special AT-Rich Sequence-Binding Protein 2 (Satb2) (Britanova et al., 2008), but not with the deeper layer neuron marker Chicken Ovalbumin Upstream Promoter Transcription Factor-Interacting Protein 2 (CTIP2) (Figures 1K and 1L; Table S1F).

As negative controls, we expressed EGFP and Cre recombinase in neuronal progenitors of wild-type embryos (Figures S1I and S1J; Table S1G), and EGFP alone in *Wwp1/2*$^{f/f}$ progenitors at E14.5 (Figures 1C and 1G). Neurons in both negative controls were found to distribute within upper layers, as expected from their birthdate at E14.5, independently of mouse gender (Figure S1K).

Single knockout of *Wwp2* gene (Figure S1L and S1M; Table S1H) and single KDs of Wwp1 or Wwp2 using shRNAs (Figures S1N and S1O; Table S1I) resulted in altered distribution of cortical neurons without causing neuronal fate switch (Figures S1P and S1Q; Table S1J). However, none of these modifications engendered induction of MP morphology with multiple TPs (Figures S1R and S1S; Table S1K). This indicates functionally redundant roles for Wwp1 and Wwp2 in inhibiting the acquisition of MP neuronal morphology. For this reason, we analyze *Wwp1/2* double KO or Wwp1/2 double-KD (dKD) in the following studies.

Similar to *Wwp1/2* double KO, Wwp1/2 dKD resulted in induction of multiple axons in primary hippocampal neurons *in vitro* (Figures S2A and S2B, related to Figure 1; Table S1L), altered laminar distribution of neurons (Figures S2C–S2F; Tables S1M and S1N), and a loss of polarized morphology in neurons retained in deeper layers *in vivo* (Figures S2G–S2J; Tables S1O and S1P).

In summary, our data show that elimination of *Wwp1/2* from developing neurons induces formation of multiple axons and persistent defects in laminar distribution and polarity formation *in vivo*.

Wwp1 and Wwp2 Are Essential Regulators of Axon Formation in Cortical Neurons

Primary neurons undergo transitions through several morphological stages, from MP (DIV2), a polarized cell with a single axon (DIV4), into a cell with defined axon-dendrite polarity (DIV6) (Barnes and Polleux, 2009). Such a sequence of neurite growth is associated with specific alterations in neuron-intrinsic cellular organelle polarity. In particular, the deposition of the Golgi apparatus at the base of a neurite was shown to promote its asymmetrical outgrowth in young MP neurons (Horton et al., 2005). In a nascent neuron, localization of the Golgi apparatus is associated with the site of the axon emergence (de Anda et al., 2005).

To verify whether Wwp1/2 are necessary for polarization of newborn cortical neurons, as well as hippocampal neurons (Figures 1A and S2A), we restricted our analysis to VZ E14.5 progenitors, which give rise to layer II/III neurons, shown affected in our experiments *in vivo* (Figures 1C–1L). We used *ex utero* electroporation (EUE) to transfect E14.5 ventricular progenitor cells in *Wwp1/2*$^{f/f}$ mice with a plasmid encoding for EGFP, or for EGFP and Cre.

At DIV2 (Figure S3A, related to Figure 1), we detected no differences in the length of the longest neurite (Figure S3B; Table S1Q; Figure S3A, black arrowheads), nor in the number of primary neurites (Figure S3C; Table S1R) between control and *Wwp1/2* dKO neurons. However, the Golgi apparatus failed to align with the base of the longest neurite in *Wwp1/2* double KO, as measured by the acute Golgi-Longest Process angle θ (Horton et al., 2005) (Figure S3D; Table S1S). We observed multiple Golgi stacks deposited in the somata of *Wwp1/2* double KO neurons in contrast to a single Golgi apparatus in the control EGFP-expressing cells that was deposited in line with the longest neurite (Figure S3A, red arrowheads; Figure S3E; Table S1T).

At DIV4, the majority of control neurons specified a single axon, positive for axonal marker antigen SMI-312 and negative for dendritic Microtubule-Associated Protein 2 (MAP2), while the fraction of *Wwp1/2* double KO neurons projected multiple axons from the soma (Figures S3F and S3G; Table S1U). Axons projected from *Wwp1/2* double KO neurons were shorter than ones from control neurons (Figure S3H; Table S1V) with increased density of primary branches (Figure S3I; Table S1W),

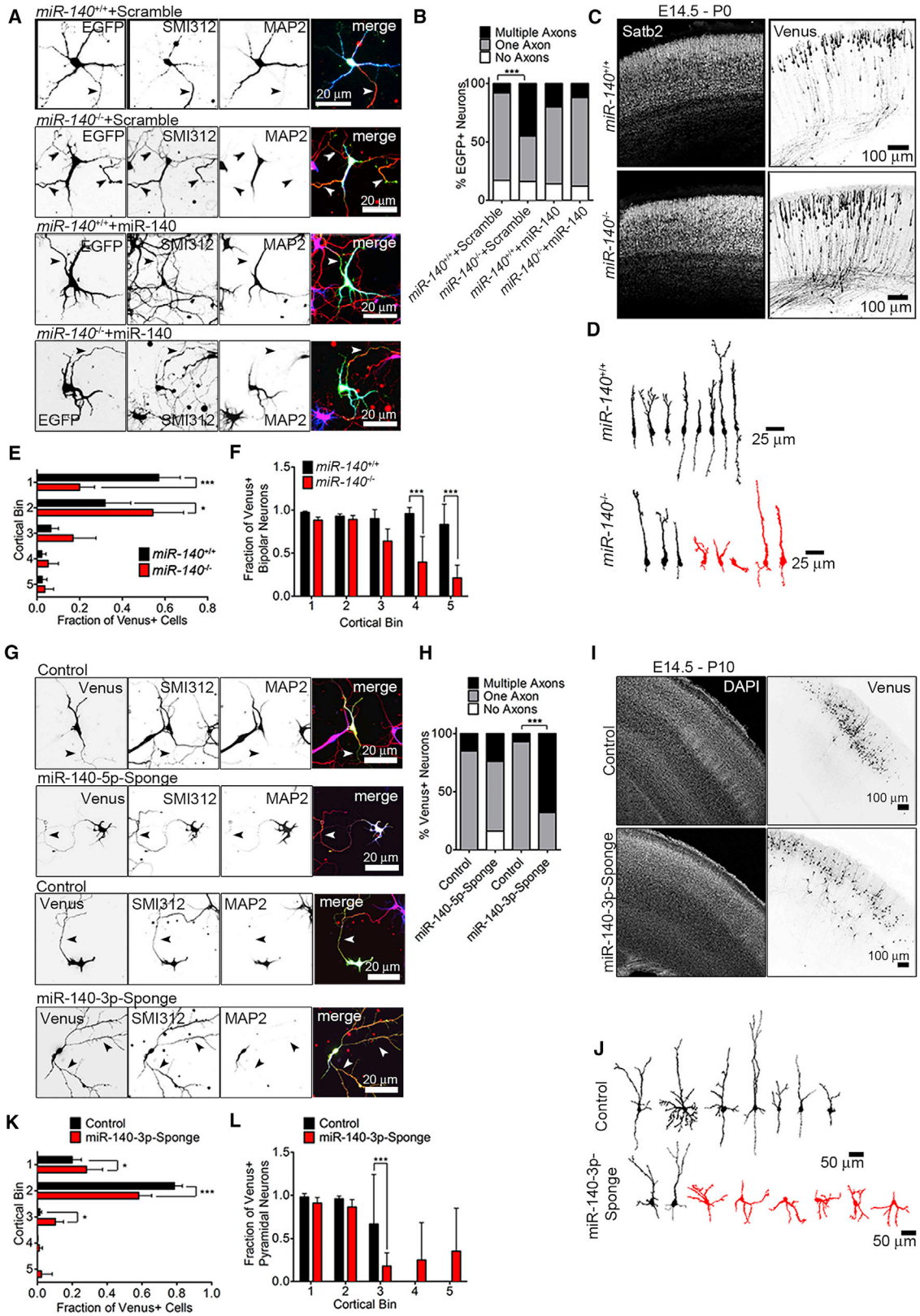

(legend on next page)

whereas complexity of dendrites was unchanged (Figures S3J–S3L; Table S1X).

At DIV6, we consistently observed an increase in the fraction of *Wwp1/2* double KO neurons with multiple axons, verified by lack of MAP2 and positive labeling for axon-enriched markers SMI312 (Figures S3M and S3N; Table S1Y), or Tau-1 (Figures S3O and S3P; Table S1Z). *Wwp1/2* double KO neurons showed shorter and more branched axons than control neurons as observed at DIV4 (Figures S3Q, S3S, and S3V; Tables S1A′ and S1C′). The aggregate length of all axons projected from a single *Wwp1/2* double KO neuron was no different from the total length of axons from control neurons (Figure S3R; Table S1B′), while the complexity of dendrites was significantly reduced at DIV6 (Figures S3T–S3V; Table S1D′).

To test whether abnormal morphological features can be induced by knocking out *Wwp1/2* after the completion of initial axon specification, cortical *Wwp1/2*$^{f/f}$ neurons were transfected with EGFP- or EGFP/Cre-expression vector at DIV4 and fixed at DIV6 (Figure S4, related to Figure 1). With this transfection protocol, *Wwp1/2* double KO cortical neurons showed phenotypes resembling neurons EUE-transfected at E14.5 (Figure S4; Tables S1E′–S1I′).

Taken together, *Wwp1/2* are essential for establishment and maintenance of axon specification and thereby polarized morphology in cortical neurons.

Loss of Intronic *miR-140* Resembles the Double KO of *Wwp1* and Host *Wwp2* in Developing Nerve Cells

Wwp2 harbors a locus for *microRNA-140*, *miR-140*. Concomitant expression of *Wwp2* and intron-encoded *miR-140* has been reported in non-neuronal tissue, where they regulate their targets post-transcriptionally and post-translationally (Yang et al., 2011). A strong *in situ* hybridization signal for *Wwp2/miR-140* mRNA was apparent in the VZ, the ganglionic eminence, and the CP in the brain at E16 (Figure S5A, related to Figure 2). We also detected the hybridization signal throughout the entire adult brain (Figure S5A). We performed quantitative real-time PCR to profile the expression of the 5p and 3p strands of the effector miR-140 (miR-140-5p and miR-140-3p, respectively) in the developing mouse cortex (Figures S5B and S5C; Tables S1J′ and S1K′). miR-140-3p showed early embryonic induction and stable levels postnatally, whereas miR-140-5p did not show such a dynamic expression pattern. In primary hippocampal neurons, brain-enriched miR-134 (Schratt et al., 2006) and miR-140-3p localize to somata, shown by *in situ* hybridization (Figure S5D).

In order to test whether *miR-140* regulates axon acquisition, we analyzed the number of axons in primary hippocampal cell cultures prepared from *miR-140*$^{-/-}$ mice (Nakamura et al., 2011a) (Figures 2A and 2B). A population of primary hippocampal neurons deficient for *miR-140* displayed multiple axons, and transfection of *miR-140*$^{-/-}$ neurons with a plasmid encoding miR-140 reversed the aberrant axon number phenotype (Figures 2A and 2B; Table S1L′). This indicates a cell-autonomous and indispensable role for miR-140 in axon acquisition.

As shown by IUE at E14.5, *miR-140*$^{-/-}$ neurons displayed an altered laminar distribution and projected multiple LPs or failed to specify a prominent neurite (Figures 2C–2F; Tables S1M′ and S1N′). Only a small fraction of *miR-140*$^{-/-}$ neurons in the deeper layers were BP in contrast to *miR-140*$^{+/+}$ neurons (Figure 2F; Table S1N′).

Consistently to aberrant distribution of *miR-140*$^{-/-}$ cortical neurons after IUE at E14.5 (Figure 2C), Cux1-positive neurons in *miR-140*$^{-/-}$ showed global altered laminar positioning in the cortex, whereas distribution of deep-layer neurons and neuronal progenitors was unaffected (Figures S5E–S5I; Tables S1O′–S1R′).

At E14.5, when Cux1-positive neurons are born at the VZ (Nieto et al., 2004), we detected no differences in apoptotic marker cleaved caspase-3 staining pattern between *miR-140*$^{+/+}$ and *miR-140*$^{-/-}$ mouse cortices, indicating no changes in ongoing apoptosis in this mutant (Figure S5J).

These data show that, during neuronal polarization *in vitro* and *in vivo*, miR-140 exerts effects on Cux1-positive upper-layer neurons similar to those of its host gene *Wwp2* and the homologous *Wwp1*.

miR-140-3p Controls Neuronal Polarization and Proper Cortical Distribution

To determine which miR-140 strand acts to regulate axon acquisition in developing neurons, we downregulated each miR-140

Figure 2. The Loss of Intronic *miR-140* and the Acute Knockdown of miR-140-3p Resembles the Loss of Its Host *Wwp2* and Homologous *Wwp1*

(A) Images of representative *miR-140*$^{+/+}$ or *miR-140*$^{-/-}$ primary hippocampal neurons transfected as indicated. Arrowheads point to axons.
(B) Quantification of number of axons specified by individual neurons (Table S1L′).
(C) Representative images of immunofluorescence in P0 cortices of *miR-140*$^{+/+}$ or *miR-140*$^{-/-}$ mice after IUE.
(D) Representative morphologies of neurons in bin 3 and 4 in *miR-140*$^{+/+}$ and *miR-140*$^{-/-}$ brains at P0.
(E) Distribution of *miR-140*$^{+/+}$ and *miR-140*$^{-/-}$ neurons in the cortex (Table S1M′).
(F) Classification of morphologies of *miR-140*$^{+/+}$ and *miR-140*$^{-/-}$ neurons (Table S1N′).
(G) Neurons expressing control or miR-140-5p-Sponge, and with control Sponge or miR-140-3p-Sponge with myr-Venus as a reporter. Arrowheads point to axons.
(H) Quantification of the number of axons projected by single neurons (Table S1S′).
(I) Representative images of DAPI staining and Venus fluorescence in P10 cortices of wild-type mice. Neuronal progenitors were electroporated *in utero* at E14.5 with plasmids encoding indicated sponges.
(J) Representative morphologies of control and miR-140-3p-Sponge-expressing neurons in bin 3 in P10 brains.
(K) Distribution of neurons expressing control or miR-140-3p-Sponge *in vivo* (Table S1T′).
(L) Classification of polarities in control and miR-140-3p-Sponge-expressing neurons. Results are represented as averages ±SD (Table S1U′).
Results on graphs are represented as averages ±SD. For statistical analyses, (B) and (H), chi-square test; (E), (F), (K), and (L), two-way ANOVA with Bonferroni post hoc test. ***$p < 0.001$; * $0.01 < p < 0.05$. See also Figures S5, S6, and S8.

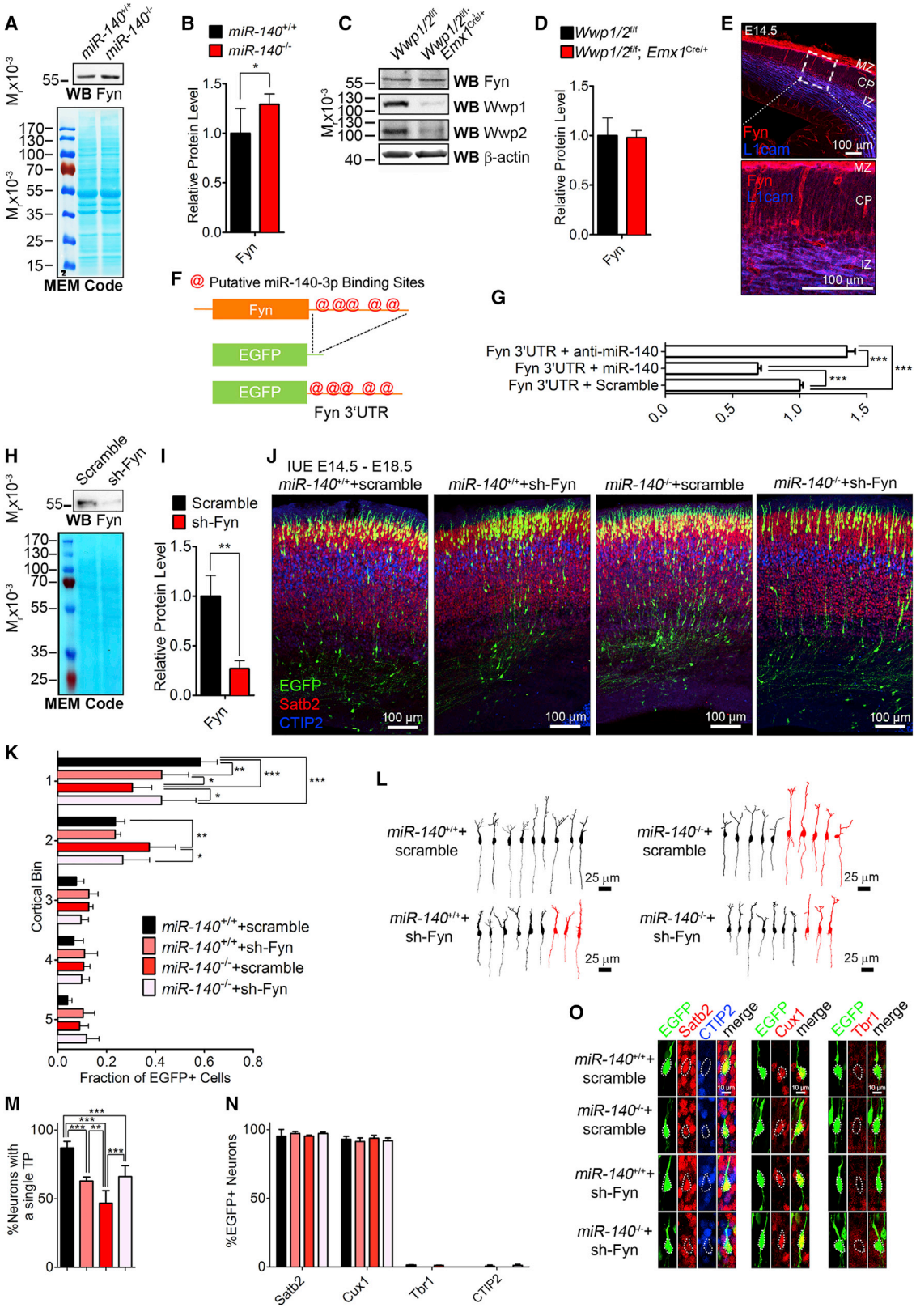

(legend on next page)

strand selectively in primary hippocampal neurons using miR-Sponge technology (Figure 2G). Sponges are molecular tools that sequester and thereby downregulate endogenous miRNAs by binding the target strand of a miRNA to their tandemly repeated complemental miRNA-binding sequences cloned downstream of a sponge reporter, such as EGFP or Venus (Ebert et al., 2007). Expression of miR-140-5p-Sponge in primary neurons did not induce multiple axons, while expression of miR-140-3p-Sponge led to an increase in the number of neurons projecting multiple axons (Figures 2G and 2H; Table S1S′).

At P10, neurons expressing miR-140-3p-Sponge after IUE at E14.5 were retained in the deeper layers of the CP, displaying an abnormal non-pyramidal morphology (Figures 2I–2L; Tables S1T′ and S1U′) in a similar way to *Wwp1/2* double KO and Wwp1/2 dKD neurons. Additionally, some miR-140-3p-Sponge-expressing neurons accumulated above the respective control Sponge-expressing ones, distributed in layers II/III (Figure 2I and Bin1 and −2 in Figure 2K).

Taken together, these data show that miR-140-3p acts as an effector miR-140 strand in cortical nerve cells, regulating axon-dendrite polarity, pyramidal morphology, and laminar distribution in the cortex.

miR-140 Regulates Axon Formation in Cortical Neurons in a Similar Fashion to Wwp1/2

Next, we performed morphological analyses of primary cortical neurons prepared after EUE of *miR-140*$^{+/+}$ and *miR-140*$^{-/-}$ brains at E14.5, analogous to the analyses of *Wwp1/2* double KO neurons (Figure S3). At DIV2, *miR-140*$^{-/-}$ neurons showed increased length of the longest neurite (Figures S6A and S6B, related to Figure 2; Table S1V′) and increased number of primary neurites (Figures S6A and S6C; Table S1W′), which were not pronounced in *Wwp1/2* double KO neurons (also see Figures S3B and S3C). Except for these two phenotypes, *miR-140*$^{-/-}$ primary cortical neurons showed phenotypes resembling those of *Wwp1/2* double KO neurons, i.e., altered morphology of Golgi apparatus at DIV2 (Figures S6D and S6E; Tables S1X′ and S1Y′), number, length, and primary branches of axons (Figures S6F–S6I; Tables S1Z′–S1B″) without affecting dendrite branching (Figures S6J–S6L; Table S1C″) at DIV4. At DIV6, *miR-140*$^{-/-}$ primary cortical neurons showed altered development of axons stained with SMI312 or Tau-1 (Figures S6M–S6S; Tables S1D″–S1H″) and of dendrites (Figures S6T–S6V; Table S1I″), again resembling *Wwp1/2* double KO neurons.

Altogether, miR-140 serves to inhibit axon formation in developing cortical neurons, in a similar fashion to its host *Wwp2* and the homologous *Wwp1*.

miR-140 Suppresses Expression of Fyn to Orchestrate Polarity Acquisition and Proper Cortical Distribution of Developing Neurons

In most cases, KO of a given miRNA gene results in an upregulation of protein expression from its target mRNAs. In order to identify downstream molecular components of miR-140-mediated regulation of neuronal development, we applied a quantitative proteomics approach and compared synaptosomal fractions from *miR-140*$^{+/+}$ and *miR-140*$^{-/-}$ cortices (Figures S7A and S7B, related to Figure 3). Prefractionation increases the depth of analysis and the likelihood of quantifying neuronal protein candidates of low abundance. Putative miR-140 targets were chosen based on the fold increase in *miR-140*$^{-/-}$ synaptosomes and q-statistics (Figure S7C, related Table S2; label-free quantification of proteins in P2C fractions from *miR-140*$^{+/+}$ and $^{-/-}$ cortices). To exclude indirect effects of miR-140 depletion, mRNAs with putative miR-140-3p binding sites in their 3′ UTRs predicted by the probability of interaction by target accessibility (PITA) algorithm were selected (Kertesz et al., 2007) (Figure S7C, filled red dots). We found five potential

Figure 3. miR-140 Induces Translational Repression of Fyn mRNA to Control Morphology and Laminar Positioning of Cortical Neurons

(A–D) Quantitative western blotting of Fyn levels in P0 cortices of *miR-140*$^{+/+}$ and *miR-140*$^{-/-}$ (A and B) and *Wwp1/2*$^{f/f}$ and *Wwp1/2*$^{f/f}$; *Emx1*$^{Cre/+}$ (C and D) mice. (A and C) Representative western blotting image with cortical lysates from control and mutant mice (MEM Code staining, which detects proteins on nitrocellulose membranes).

(B) Average relative Fyn levels in *miR-140*$^{+/+}$ and *miR-140*$^{-/-}$ cortices (Table S1J″).

(D) Average relative Fyn levels in *Wwp1/2*$^{f/f}$ and *Wwp1/2*$^{f/f}$; *Emx1*$^{Cre/+}$ cortices (Table S1K″).

(E) Immunohistochemistry using indicated antibodies: marginal zone (MZ), cortical plate (CP), intermediate zone (IZ).

(F) Scheme of a vector encoding EGFP fused to Fyn 3′ UTR with putative miR-140-3p-binding sites (@).

(G) Quantification of EGFP fluorescence intensities from HEK293T cells expressing EGFP-Fyn 3′ UTR fusion construct together with anti-miR-140 antagomiR (Fyn 3′ UTR + anti-miR-140), synthetic miR-140 (Fyn 3′ UTR + miR-140), or scramble miR (Fyn 3′ UTR + Scramble) (Table S1L″).

(H and I) Quantitative western blotting of Fyn levels in N2A cells transfected with Fyn overexpression construct together with either scramble shRNA or sh-Fyn.

(H) Representative western blotting image.

(I) Average relative Fyn levels in cells transfected with indicated vectors (Table S1M″).

(J) Representative images of immunostaining in E18.5 *miR-140*$^{+/+}$ or *miR-140*$^{-/-}$ cortices electroporated *in utero* at E14.5 to express either EGFP and scramble shRNA, or EGFP and sh-Fyn.

(K) Quantification of laminar distribution of cortical neurons in *miR-140*$^{+/+}$ or *miR-140*$^{-/-}$ mouse brains after IUE with indicated vectors (Table S1N″).

(L) Representative EGFP-fluorescence-based tracings of *miR-140*$^{+/+}$ or *miR-140*$^{-/-}$ neurons transfected with indicated vectors. Neurons with aberrant morphology (i.e., multiple trailing processes) are colored red.

(M) Quantification of the number of neurons with a single trailing process (TP) (Table S1O″). Legend for the graph is in (K).

(N) Quantification of the fraction of EGFP-positive *miR-140*$^{+/+}$ or *miR-140*$^{-/-}$ neurons expressing indicated fate markers after IUE with vectors indicated on (K) (Table S1P″).

(O) Representative images of immunostaining against EGFP, Satb2, CTIP2, Cux1, and Tbr1 after IUE with indicated vectors. Cell soma is marked with a dotted line.

Results on other graphs are represented as averages ±SD. For statistical analyses, (B), (D), (I), unpaired t test; (M), (N), (G), one-way ANOVA with Bonferroni post hoc test; (K), two-way ANOVA with Bonferroni post hoc test. ***$p < 0.001$; ** $0.001 < p < 0.01$; * $0.01 < p < 0.05$. See also Figures S7 and S8.

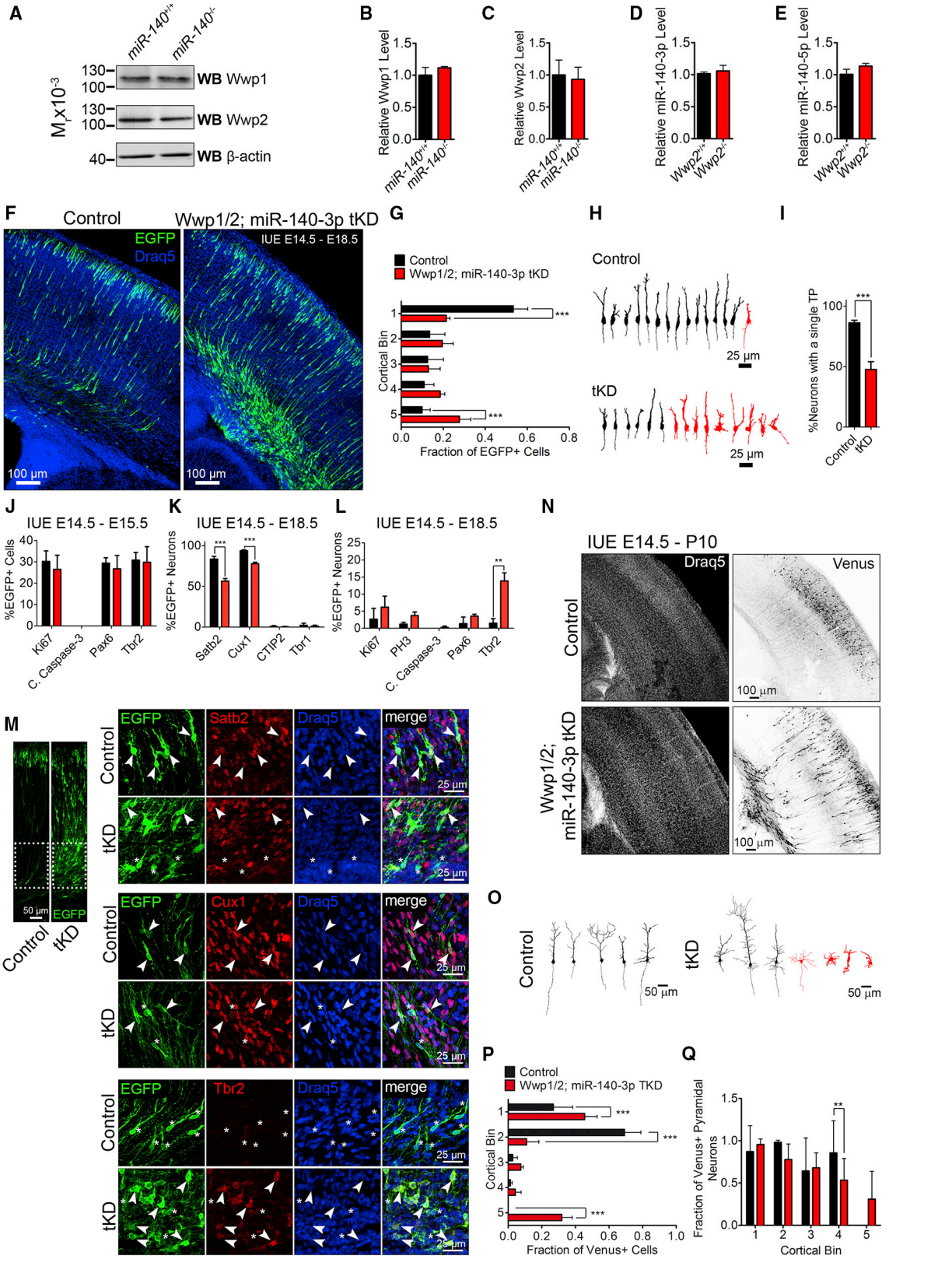

(legend on next page)

binding sites of miR-140-3p in the 3′ UTR of the Src family tyrosine kinase, Fyn, which plays a major role in neuronal morphogenesis and regulation of lamination (Sasaki et al., 2002; Simó and Cooper, 2013).

In quantitative western blotting experiments, the loss of miR-140 was associated with an upregulation of Fyn expression, while Fyn levels were unaltered in *Wwp1/2* cdKO (Figures 3A–3D; Tables S1J″ and S1K″). These results implicate miR-140 in the specific regulation of Fyn in a Wwp1/2-independent manner.

Analysis of Fyn expression in the developing neocortex from E14.5 embryo revealed prominent labeling in the IZ, where developing neurons undergo MP-to-BP transition and initiate migration to their future destination (Figure 3E). Such a pattern of expression and a recent study demonstrating that Fyn mediates MP-to-BP transitions and neurite morphogenesis (Huang et al., 2017) suggest that upregulation of Fyn may indeed be responsible for perturbations observed in *miR-140*$^{-/-}$ cortex.

We then tested whether miR-140 binds the 3′ UTR of Fyn mRNA and might thereby induce its direct repression. For this purpose, the 3′ UTR of Fyn was cloned downstream of the EGFP-coding sequence and co-expressed in HEK293T cells together with miR-140 (Rybak et al., 2008) (Figure 3F). Co-transfection of HEK293T cells with the EGFP-Fyn 3′ UTR fusion reporter construct together with miR-140 decreased EGFP signal while co-transfection with the reporter construct and a miR-140 antagonist yielded an increase in fluorescence intensity (Figure 3G; Table S1L″). Collectively, miR-140 is able to mediate inhibition of Fyn mRNA.

To test whether reducing Fyn levels in *miR-140*$^{-/-}$ cortex restores proper laminar distribution and polarized morphology of developing cortical neurons, we generated an shRNA for Fyn KD (Figures 3H and 3I; Table S1M″) to perform rescue experiments by Fyn KD in *miR-140*$^{-/-}$ cortices using IUE (Figure 3J). Strikingly, Fyn KD in cortical neurons partially restored their laminar distribution and the fraction of neurons with a single TP in *miR-140*$^{-/-}$ (Figures 3K–3M; Tables S1N″, S1O″ and S3, details on mice for IUE; Table S4. Genotyping summary of mouse lines related to STAR Methods) without altering the neuronal fate (Figures 3N and 3O; Table S1P″).

As observed upon *miR-140* KO, Fyn overexpression altered the laminar distribution of cortical neurons at P0 (Figures S7D and S7E; Table S1R″). The majority of Fyn overexpressing neurons that settled in deeper cortical layers expressed Cux1 (Figure S7F; Table S1S″) and displayed non-BP morphology as compared to control P0 cells (Figures S7G and S7H; Table S1T″). At P10, the laminar distribution pattern of neurons overexpressing Fyn resembled the ones expressing miR-140-3p-Sponge, with slight accumulation of neurons in Bin 1 (Figures S7I and S7J; Table S1U″), indicative of overmigration together with arrest of cells in deeper cortical layers. In these cells, we observed loss of pyramidal morphology, as compared to control neurons (Figures S7K and S7L; Table S1V″).

Altogether, these data show that miR-140 translationally inhibits Fyn expression to control laminar distribution and polarized morphology in cortical neurons.

Lack of Reciprocal Regulation between Wwp1, Wwp2, and miR-140

Western blotting with *miR-140*$^{+/+}$ and *miR-140*$^{-/-}$ cortical lysates using antibodies specific for Wwp1/2 ligases (Figures 4A, S1G, and S1H for specificity of antibodies) revealed no changes of Wwp1/2 levels in *miR-140* KO cortices (Figures 4A–4C; Tables S1W″ and S1X″). Similarly, no alterations in *miR-140* levels were detected in *Wwp2*$^{-/-}$ cortices (Figures 4D and 4E; Tables S1Y″ and S1Z″). These data indicate that *miR-140* and *Wwp1/2* do not regulate each other and that Cre-mediated excision of floxed Wwp2 exon does not affect the expression of *miR-140*.

Intact Fyn expression upon *Wwp1/2* cdKO (Figures 3C and 3D) led us to hypothesize that miR-140 and Wwp1/2 employ divergent cascades to regulate neuronal development. Supporting this hypothesis, Fyn KD in *Wwp1/2* double KO neurons failed to revert aberrant laminar distribution of cortical neurons (Figures S8A and S8B, related to Figures 1, 2, 3, and 4; Table S1A‴). Interestingly, miR-140 overexpression in *Wwp1/2* double KO neurons restored their proper laminar distribution (Figures S8A and S8C; Table S1B‴). Notably, neither reducing Fyn levels, nor overexpressing miR-140 in *Wwp1/2* double KO neurons was sufficient to reinstate BP morphology of cortical neurons (Figures S8D–S8F; Tables S1C‴ and S1D‴). Observed

Figure 4. Lack of Epistatic Regulation between Wwp1, Wwp2, and miR-140

(A) Representative images of western blotting using lysates of *miR-140*$^{+/+}$ and *miR-140*$^{-/-}$ cortices.

(B and C) Average relative levels of Wwp1 (B) and Wwp2 (C) in *miR-140*$^{+/+}$ and *miR-140*$^{-/-}$ cortices (Tables S1W″ and S1X″).

(D and E) Quantitative real-time PCR for of miR-140-3p (D) and −5p (E) in P0 cortices of *Wwp2*$^{+/+}$ and *Wwp2*$^{-/-}$ mice (Tables S1Y″ and S1Z″).

(F) Representative images of anti-EGFP immunostaining signals and Draq5 fluorescence after IUE with indicated vectors.

(G) Quantification of laminar distribution of control and tKD neurons across the CP (Table S1G″).

(H) Representative EGFP-fluorescence-based tracings of neurons expressing indicated vectors. Neurons with multiple TPs are colored red.

(I) Quantification of the number of neurons with a single TP (Table S1H″).

(J–L) Quantification of percentage of of EGFP^{+} control and tKD neurons positive for apoptotic and mitotic markers (J and L) or layer identity markers (K) (Tables S1I″–S1K″).

(M) Representative images of immunostaining in E18.5 CP after IUE with indicated vectors. The area marked with a dotted line is magnified on the right. Arrowheads point to EGFP^{+} cells positive for indicated marker. Stars mark EGFP^{+} neurons negative for indicated marker protein.

(N) Representative images of Draq5 fluorescence and anti-GFP immunolabeling of Venus in P10 control and tKD neurons.

(O) Representative morphologies of control and tKD neurons in bins 3–4 of P10 brains. Neurons with non-pyramidal morphology are colored red.

(P) Distribution of control and tKD neurons *in vivo* (Table S1L″).

(Q) Quantification of morphologies of control and tKD neurons (Table S1M″).

Results on other graphs are represented as averages ±SD. For statistical analyses, (B–E), (I–L), unpaired t test; for (G), (P), and (Q), two-way ANOVA with Bonferroni post hoc test. ***$p < 0.001$; ** $0.001 < p < 0.01$. See also Figures S8 and S9.

alterations in laminar distribution of neurons were not caused by changes of neuronal fate switch (Figures S8G–S8I; Tables S1E‴ and S1F‴).

Lack of mutual regulation between miR-140 and Wwp1/2 implies that simultaneous loss of the trio engenders aberrances more severe than the ones observed for loss of each, independently. To test this, we performed a triple KD (tKD) in neuronal progenitors at E14.5 with shRNAs for Wwp1/2 and miR-140-3p-Sponge. As a control, we transfected the progenitors with non-silencing shRNA and control Sponge. Remarkably, tKD led to a failure in translocation initiation of neurons to upper cortical layers and their retention at the SVZ/VZ (Figures 4F and 4G; Table S1G‴), a phenotype more severe than that observed for Wwp1/2 dKD (Figure S2C). tKD neurons exhibited marked loss of BP morphology and displayed multiple TPs (Figures 4H and 4I; Table S1H‴). One day after IUE, no changes were detected between control and tKD neurons regarding expression of markers for proliferation (Ki67 antigen), apoptosis (cleaved caspase-3), and fate (Paired box protein-6 [Pax6] expressed in radial glia [Götz et al., 1998] and T-Box Brain Protein 2 [Tbr2] expressed in intermediate progenitors [Bulfone et al., 1999] [Figure 4J; Table S1I‴]). At E18.5, we noted a marked decrease in the fraction of tKD neurons positive for upper-layer neuron markers and a concomitant increase in the proportion of tKD neurons positive for Tbr2, without changes in their expression of Ki67, or Phospho-Ser10-Histone H3 (PH3) (Figures 4K–4M; Tables S1J‴ and S1K‴). Persistence of Tbr2 expression and unchanged immunoreactivity of mitotic markers indicates the inability of tKD cells to transition into postmitotic neurons and reflects delay/aberrances in neuronal differentiation, thereby preventing tKD cells from entering into the CP.

Such a pronounced retention and the perturbed polarity persisted until P10 (Figures 4N and 4O). Additionally, tKD neurons that entered the CP over-migrated toward the pia (Figures 4N and 4P; Table S1L‴). A large fraction of tKD neurons exhibited non-pyramidal morphology (Figures 4O and 4Q; Table S1M‴).

To characterize the mode of migration of tKD neurons, we traced the dynamics of their translocation online. Live imaging of tKD neurons unveiled MP cells arrested at the bottom of the CP while control neurons exhibited characteristic saltatory translocations toward the pia and BP morphology during migration (Figures S9A–S9C, related to Figure 4). The displacement of tracked tKD neurons were shorter in length as compared to control neurons (Figure S9D; Table S1N‴), without noted changes for total distance traveled (Figure S9E; Table S1O‴), or the speed of their movement (Figure S9F; Table S1P‴). This indicates loss of directionality in the movement of tKD neurons, likely reflecting their inability to initiate radial translocation.

Postnatally, arrested tKD neurons exhibited a persistent loss of Cux1 staining, however, were positive for Neuronal Nuclear Antigen, NeuN, indicative of their postmitotic neuronal fate (Figures S9G–S9I; Table S1Q‴).

Altogether, synthetic phenotypes and more severe aberrances observed for tKD neurons support the notion that miR-140 and Wwp1/2 regulate divergent, Fyn-dependent and Fyn-independent molecular cascades in developing nerve cells.

Sox9 Induces Expression of *Wwp1*, *Wwp2*, and *miR-140* in Developing Neurons

Both *Wwp2* and *miR-140* are major targets of Sox9 transcription factor in chondrocytes (Yang et al., 2011). We then tested whether Sox9 is expressed in neurons. Sox9 labeling was pronounced in control neurons and significantly reduced in $Sox9^{f/f}$ cells expressing Cre (Figure 5A-5B; Table S1R‴). Sox9 was prominent in all postmitotic cortical neurons, expressing nuclear NeuN and all analyzed markers (Figures S10A–S10D, related to Figure 5; Tables S1S‴ and S1T‴). Moreover, apart from prominent labeling of Sox9 mRNA and protein in the VZ/SVZ, we detected weak but significant Sox9 expression throughout the CP (Figures S10E and S10F). Sox9 immunolabeling also detected non-neuronal cells, infiltrating the CP (Figures S10B and S10E).

Next, we performed expression profiling of Sox9, Wwp1, and Wwp2 during cortex development. Sox9 protein levels correlated with the amount of Wwp2 showing developmental downregulation, while Wwp1 levels were developmentally upregulated (Figure 5C). To test whether Sox9 serves as a transcriptional regulator of *Wwp1* and *Wwp2/miR-140* in neurons, we infected primary cortical neurons with lentiviruses encoding either scramble shRNA (control) or sh-Sox9 (Sox9 KD). Sox9 KD samples revealed marked losses of Wwp1/2, miR-140-5p, and -3p (Figure 5D to 5G; Tables S1U‴–S1W‴).

The reduction of Wwp2 and miR-140 levels upon Sox9 KD in neurons, which we observed, seems to be due to perturbed transcriptional effects (Figures 5E and 5F, related Table S5. The parameters of RT-PCR), as reported in cartilage cells previously (Nakamura et al., 2011b; Yang et al., 2011). A previous study reported a strong Sox9 binding peak at the promoter region of *Wwp1* in mouse chondrocytes (Ohba et al., 2015). To assess the interaction between Sox9 and Wwp1, we performed luciferase assays using sequences upstream of the transcriptional start site of *Wwp1* and *Wwp2/miR-140* (the latter included previously published Sox9 binding sites and was used as a positive control). Sox9 induced transcription of both the *Wwp1* and the *Wwp2/miR-140* luciferase reporter construct (Figure 5H; Table S1X‴). Taken together, our data show that Sox9 acts as a strong transcriptional regulator of *Wwp1* and *Wwp2/miR-140*, promoting their expression in neurons.

Sox9 Regulates Axon Acquisition, Establishment of Pyramidal Morphology, and Proper Positioning of Developing Neurons

Similarly to inactivation of Wwp1/2 or miR-140, Sox9 KD led to the emergence of multiple axons in primary neurons (Figures 6A and 6B; Table S1Y‴), and to the appearance of cortical neurons delayed at the bottom of the CP (Figures 6C and 6D; Table S1Z‴) with a loss of pyramidal morphology in neurons *in vivo* (Figures 6E and 6F; Table S1A‴). Genetical depletion of *Sox9* by transfecting $Sox9^{f/f}$ neuronal progenitors with a Cre expression plasmid by IUE resulted in similar morphological changes (Figures 6G–6J; Tables S1B‴ and S1C‴) without affecting neuronal cell fate (Figure 6K; Table S1D‴). These data demonstrate that Sox9 has a pivotal role in regulating neuronal polarity and the migration of layer II/III neurons, similar to the activities of Wwp1 and Wwp2/miR-140.

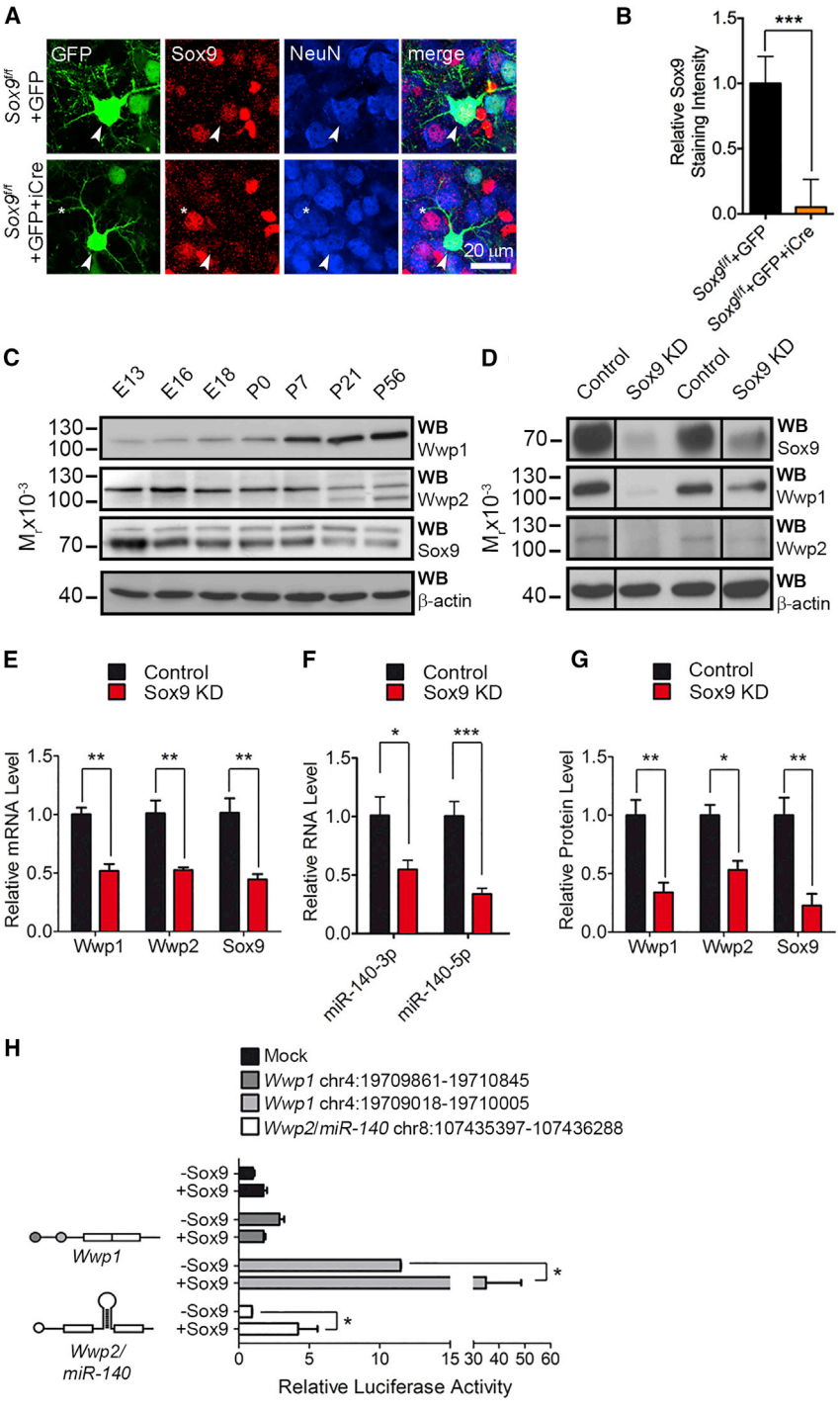

Figure 5. Sox9 Induces Expression of Wwp1, Wwp2, and miR-140 in Developing Neurons

(A) Expression of Sox9 in postmitotic neurons. Cortical neurons of *Sox9*$^{f/f}$ mice express GFP, or GFP and Cre. Brains at P10 were immunostained against Sox9 and NeuN. Arrowheads indicate GFP-expressing cells. Asterisk indicates untransfected Sox9-positive neuron.

(B) Quantification of Sox9 immunostaining intensity in *Sox9*$^{f/f}$ neurons expressing GFP, or GFP and Cre (Table S1R″′).

(C) Western blotting for Wwp1, Wwp2, Sox9, and β-actin using mouse cortical lysates prepared at indicated ages.

(D) Western blotting using antibodies for Sox9, Wwp1, Wwp2, and β-actin using lysates of cultured neurons expressing non-silencing shRNA (Control) or sh-Sox9 (Sox9 knockdown [KD]). The first and the fourth lanes were run in the same gel but were noncontiguous.

(E and F) Quantitative real-time PCR for Wwp1, Wwp2, and Sox9 mRNA (E) or miR-140-3p and miR-140-5p (F) in control and Sox9 KD neurons (Tables S1U″′ and S1V″′).

(G) Average relative Wwp1, Wwp2, and Sox9 protein levels in control and Sox9 KD neurons (Table S1W″′).

(H) Luciferase activity assay for *Wwp1* and *Wwp2/miR-140* promoter activities in HEK293T cells co-expressing mock DNA or Sox9 (Table S1X″′).

Bars on (B) and (E)–(H) represent average ±SD. For statistical analyses, unpaired t test. ***$p < 0.001$; ** $0.001 < p < 0.01$; * $0.01 < p < 0.05$. See also Figure S10.

Sox9, Wwp1/2, and miR-140 Establish a Signaling Cascade to Regulate Polarized Neuronal Morphology and Laminar Position of Cortical Neurons

Next, we investigated whether the effects of Sox9 KD could be rescued by overexpressing the Wwp1/2/miR-140 trio *in vivo* (Figure 7A). At E18.5, Sox9 KD neurons displayed aberrant laminar distribution (Figure 7B; Table S1E″″) with decreased proportion of polarized cells (Figures 7C and 7D; Table S1F″″). Notably, restoration of Wwp1/2 and miR-140 expression in Sox9 KD neurons partially reinstated laminar distribution and polarization (Figures 7B–7E), independently of cell fate (Figures 7F–7H; Tables S1G″″ and S1H″″), supporting the model wherein Wwp1/2 and miR-140 regulate neuronal positioning and polarization downstream of Sox9.

We then investigated the possible causes of observed positioning defects upon altering levels of the counterparts of Sox9-Wwp1/2-miR-140-Fyn cascade. To quantify CP entry of neurons upon Wwp1/2 dKD, miR-140-3p Sponge expression, tKD, Sox9 KD, or Fyn OE (Figure 8A), we quantified proportion of EGFP-expressing cells in VZ/SVZ, IZ, and CP (Figure 8B) (Namba et al., 2014). Notably, all listed modifications resulted in a reduced fraction of neurons in the CP (Figure 8C; Table S1I″″), implicating that disturbance of any part of the cascade leads to retention of neurons in the VZ/SVZ/IZ. Interestingly, axon intensity ratio was reduced for every modification tested without changes in cell proliferation or apoptosis (Figures 8D and 8E; Tables S1J″″ and S1K″″; see also Tables S6, antibodies used in this study,

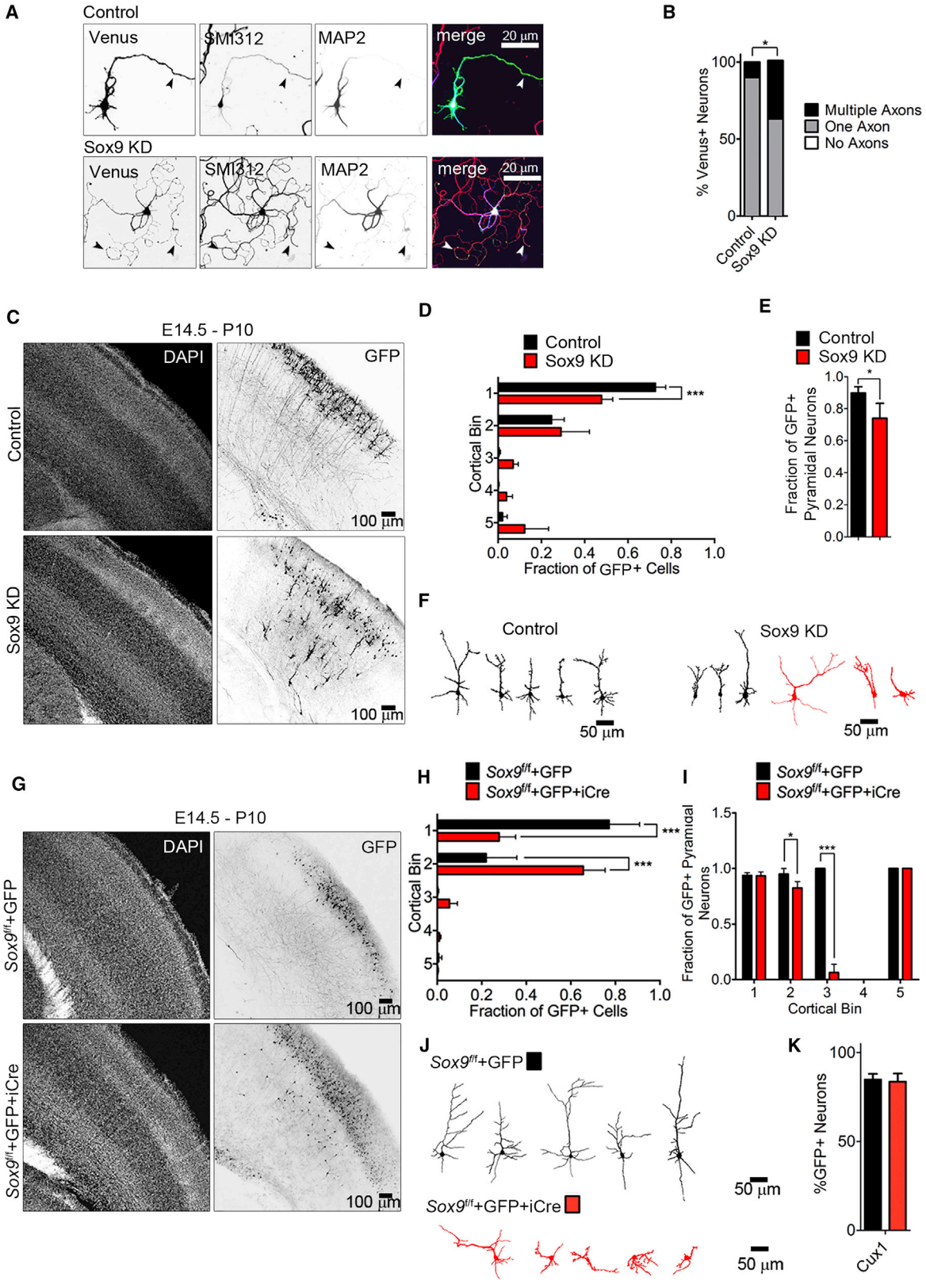

(legend on next page)

and S7, oligonucleotides used in this study, related to STAR Methods and Key Resources Table).

To further explain the decreased axonal projection in our experiment, we investigated the polarity establishment sequence in *in vitro* cortical neurons after EUE to modify components of Sox9-Wwp1/2-miR-140-Fyn cascade.

At DIV2, although we found almost no change in the length of the longest neurite or the number of primary neurites after listed modifications (Figures S11A–S11C, related to Figures 6, 7, and 8; Tables S1L′′′′ and S1M′′′′), we detected multiple depositions of *cis*-Golgi network in somata (Figures S11A, red arrowheads, S11D, and S11E; Tables S1N′′′′ and S1O′′′′). Neurons with altered levels of Sox9 cascade components showed significantly shorter and less complex axons than control (Figures S11F–S11H; Tables S1P′′′′ and S1Q′′′′) without drastically affecting the initial dendrite formation or branching (Figures S11I–S11K; Tables S1R′′′′–S1T′′′′) at DIV4, and multiple axons in a large proportion of cortical neurons at DIV6 (Figures S12A–S12D, related to Figures 7 and 8; Tables S1U′′′′ and S1V′′′′).

In accord with our experiments *in vivo* (Figure 3), KD of Fyn in miR-140-3p-Sponge-expressing neurons reestablished the properly polarized neurons with a single axon (7 in Figures S12A–S12D). Similarly, restoration of Wwp1/2 and miR-140 expression in Sox9 KD neurons rescued the neuronal polarity defect (8 in Figures S12A–S12D). Neurons with modified expression levels of Sox9 cascade elements projected shorter axons (Figure S12E; Table S1W′′′′) than controls; however, the total length of all axons projected from a single neuron remained unaltered (Figure S12F; Table S1X′′′′). These axons displayed increased primary branching density (Figure S12G; Table S1Y′′′′). Notably, normalizing Fyn levels in neurons expressing miR-140-3p Sponge restored normal length of single axons (3 versus 7, Figure S12E), and, similarly, reexpressing Wwp1/2 and miR-140 in Sox9 KD neurons reinstated axon length and branching (5 versus 8, Figures S12E and S12G). We detected significantly decreased dendritic tree complexity upon Wwp1/2 dKD, miR-140-3p Sponge expression, and Sox9 KD. Overexpressing Wwp1/2 and miR-140 in Sox9 KD neurons or Fyn KD in miR-140-3p-Sponge-expressing neurons failed to restore the phenotypes in dendrite complexity (Figures S12H–S12K; Table S1Z′′′′), indicating that other targets of Sox9 and of miR-140 play an important role in dendrite development. These data suggest that Sox9-Wwp1/2-miR-140-Fyn cascade is a specific regulator of axon development (Figure 8F).

DISCUSSION

Sox9, Wwp1/2, and miR-140 Regulate Axon-Dendrite Polarity in Neurons

In this report, we describe a regulatory cascade that supervises neuronal polarization. Precise positioning of Golgi apparatus at the emergence of the longest neurite correlates for the development of the neurite to an axon (de Anda et al., 2005). *Wwp1/2* double KO, *miR-140* KO, Fyn OE or Sox9 KD neurons failed to localize Golgi at the base of the longest process (Figures S3D, S6D, and S11D), exhibiting multiple Golgi stacks deposited in the soma and along the differentiating neurites (Figures S3E, S6E, and S11E). Altered Golgi apparatus orientation in a developing neuron is associated with its disrupted polarization (Wiegreffe et al., 2015), indicating the possible cell biological basis of phenotypes observed in our mutants. Further, the multiple-axon phenotype observed in our mutants *in vitro* (Figures 1, 2, and 6) might be associated with an aberrant apico-basal polarity acquisition in neuronal progenitors, or with an aberrant MP-BP transition. Supportive of the latter is the finding that modifying the expression levels of the counterparts of Sox9 cascade increased the proportion of neurons residing in VZ/SVZ/IZ, where most of the cells undergo polarization prior to initiation of migration. Indeed, live imaging in Figure S9 indicates that tKD neurons lack the ability to initiate radial translocation.

We report that loss of *Wwp1/2* and/or *miR-140*, Fyn OE, or Sox9 KD in cortical neurons results in induction of multiple axons (Figures 1, 2, 6, S3, S6, and S12). In our assay, multiple axons were distinguished as neurites with a distinct emergence from the soma. Similarly, observed multiple TPs might reflect origins of multiple axons in the developing cortex (Figures 1F, 2D, 3L, 4H, and 7C). Moreover, axons of *Wwp1/2* double KO and/or *miR-140* KO, Fyn OE, or Sox9 KD were shorter than those of control neurons (Figures S3, S6, and S12); yet the aggregate length of all axons projected from a single cell remained unchanged. Multiple shorter axons projected from these neurons are likely to be the reason of observed reduced axon intensity ratio (Figure 8D). Altogether, when the expression of the components of Sox9 cascade is modified, the intrinsic cellular capacity to

Figure 6. Depletion of *Sox9* Engenders Disruption in Axon Acquisition, Establishment of Proper Morphology, and Laminar Distribution in Developing Neurons

(A) Representative images of primary hippocampal neurons expressing myr-Venus with non-silencing shRNA (Control) or sh-Sox9 (Sox9 KD), immunostained with indicated markers. Arrowheads point to axons.

(B) Quantification of the number of axons projected by a single neuron by chi-square test (Table S1Y′′).

(C) Representative images of DAPI staining and anti-GFP immunolabeling in P10 cortices after IUE.

(D) Distribution of control and Sox9 KD neurons in the cortex *in vivo* (Table S1Z′′).

(E) Quantification of pyramidal morphology in control and Sox9 KD cortical neurons (Table S1A′′′′).

(F) Representative morphologies of control and Sox9 KD neurons in P10 cortices.

(G) Representative images of DAPI staining and anti-GFP immunolabeling in P10 $Sox9^{f/f}$ cortices expressing GFP (control) or GFP and Cre (*Sox9* KO).

(H) Quantification of neuronal distribution of control and *Sox9* KO in the cortex *in vivo* (Table S1B′′′′).

(I) Average relative fraction of neurons of pyramidal morphology in control and *Sox9* KO neurons (Table S1C′′′′).

(J) Representative morphologies of control and *Sox9* KO neurons in bin 3 of P10 brains.

(K) Average percentage of $EGFP^{+}$ $Sox9^{f/f}$ neurons expressing indicated vectors and positive for Cux1 (Table S1D′′′′).

Bars on (D), (E), (H), (I), and (K) represent average ±SD. For statistical analyses, (B), Fisher's exact test; (E) and (K), unpaired t test; (D), (H), and (I), two-way ANOVA with Bonferroni post hoc test. ***$p < 0.001$; * $0.01 < p < 0.05$. See also Figure S11.

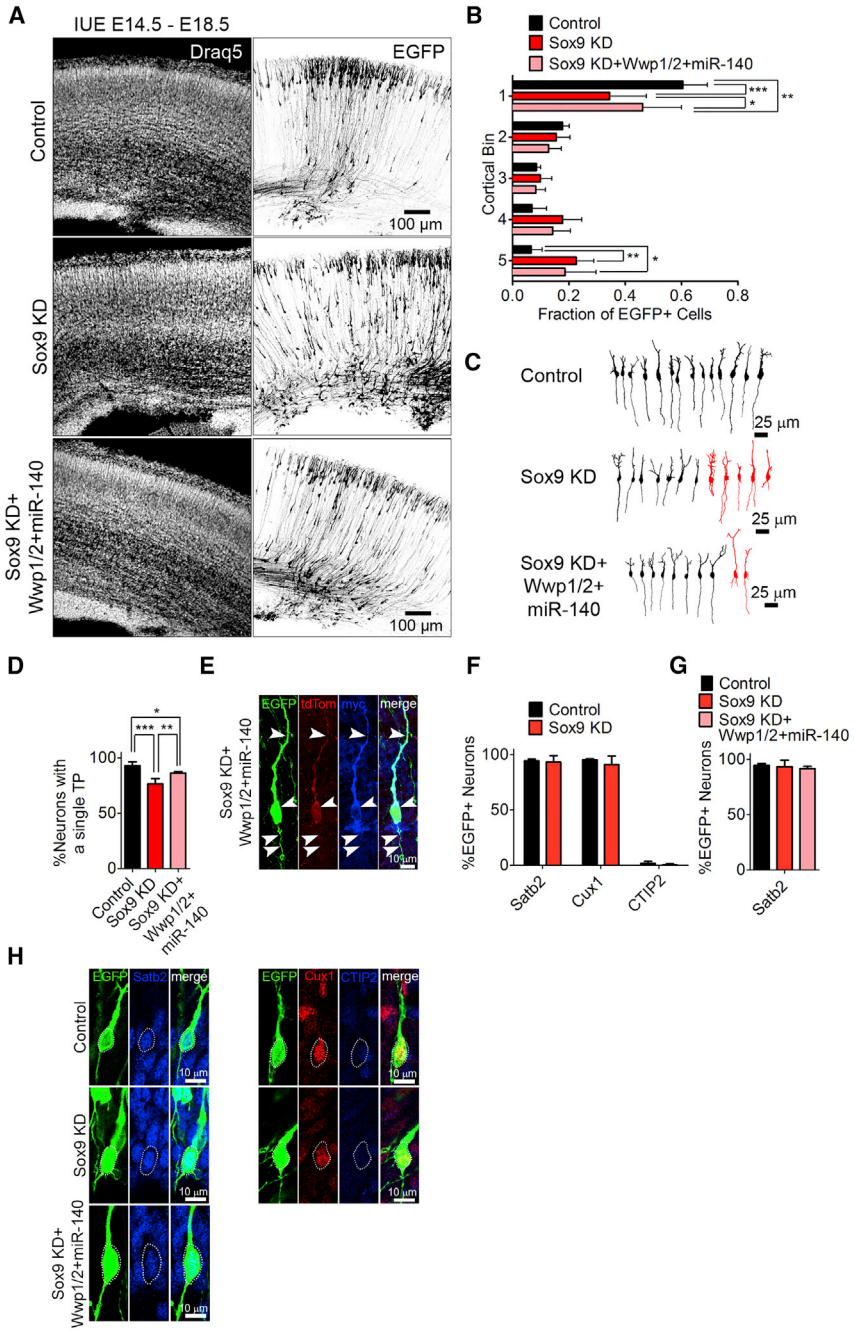

Figure 7. Overexpression of Wwp1/2 and miR-140 in Sox9 Knockdown Developing Cortical Neurons Partially Restores Their Polarized Morphology and Laminar Distribution

(A) Representative images of EGFP immunostaining signals and Draq5 labeling in E18.5 cortices expressing EGFP, scramble shRNA, and mock DNA (Control); EGFP, sh-Sox9, and mock DNA (Sox9 KD); or EGFP, sh-Sox9, myc-Wwp1, myc-Wwp2, and simultaneous miR-140/tdTomato overexpression constructs at E14.5.

(B) Quantification of laminar distribution of cortical neurons in mouse brains after IUE with indicated vectors (Table S1E‴).

(C) Representative EGFP-fluorescence-based tracings of neurons expressing indicated vectors. Neurons with aberrant morphology (i.e., multiple TPs) are colored red.

(D) Quantification of the number of neurons with a single and multiple TP (Table S1F‴).

(E) Representative images of immunostaining against EGFP, tdTomato, and myc after IUE with indicated vectors. Arrowheads point to a dendrite and an axon.

(F and G) Quantification of the fraction of EGFP-positive neurons expressing indicated fate markers, Satb2, Cux1, and CTIP2 (F), or Satb2 (G) after IUE with indicated vectors (Tables S1G‴ and S1H‴).

(H) Representative images of immunostaining against EGFP, Satb2, Cux1, and CTIP2 after IUE with indicated vectors. Cell soma is marked with a dotted line.

Bars represent average ±SD. For statistical analyses, (B), two-way ANOVA with Bonferroni post hoc test; (F), unpaired t test; (D) and (G), one-way ANOVA with Bonferroni post hoc test. ***$p < 0.001$; ** $0.001 < p < 0.01$. See also Figures S11 and S12.

grow an axon remains unaffected, rather that it leads to induction of multiple shorter axons.

In the primary culture system, counterparts of Sox9 cascade play crucial roles in dendritogenesis (Figures S3T– S3V, S4G and S4H, S6T–S6V, and S12H–S12K). However, this role of Sox9 cascade is likely to be dispensable for the formation of BP morphology of neurons. In our earlier study where axon/dendrite branching was selectively perturbed in mutant mouse lines, polarity and pyramidal shape was unaffected (Hsia et al., 2014).

We observed that Sox9 is strongly expressed in the VZ and weakly in postmitotic cortical neurons, compared to the abundant immunoreactivity of non-neuronal cells. Sox9 KD in neuronal cultures caused a marked reduction in the levels of Wwp1, Wwp2, and miR-140 (Figure 5), indicating—along with the data of corresponding luciferase reporter assays (Figure 5H)—that Sox9 plays a critical role in the induction of the *Wwp1* and *Wwp2/miR-140* loci in neurons. Given that the expression of Sox9 and Wwp2 is developmentally downregulated, while Wwp1 levels are developmentally upregulated, it appears that Sox9 operates as a main regulator of *Wwp2* expression in neurons, whereas the regulation of *Wwp1* expression depends partially, but significantly, on Sox9. Strong expression of Sox9 in VZ/SVZ implies that *Wwp1/2/miR-140* transcription might be activated in ventricular cells, and sustained in newly born neurons that express Sox9 modestly in the CP. In neurons, Sox9 KD leads to significant reduction, but not entire eliminations of Wwp1/2/miR-140 levels (Figures 5D–5G),

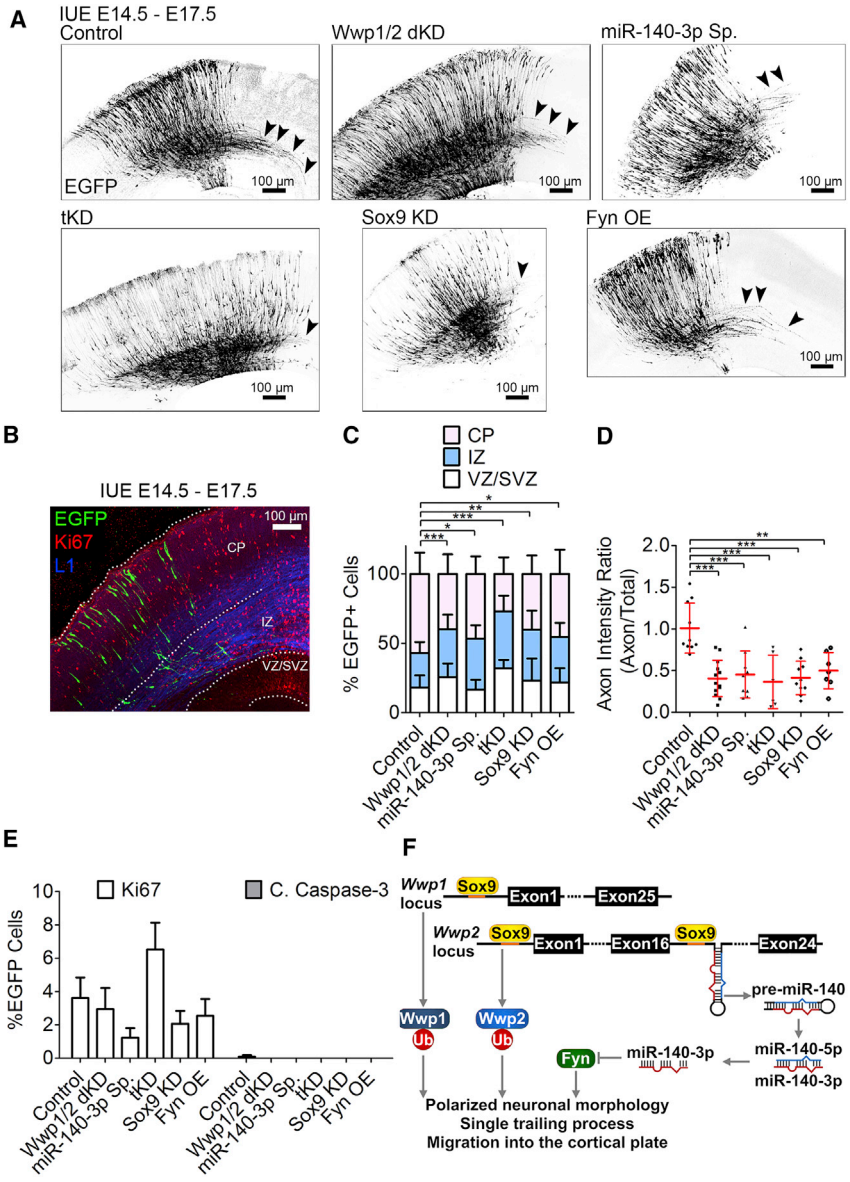

Figure 8. Sox9, Wwp1, Wwp2, and miR-140 Regulate Cortical Plate Entry by Developing Neurons

(A) Representative images of immunostaining signals in E17.5 CP after IUE with vectors to achieve indicated effects. Arrowheads point to axons extending toward the midline.

(B) EGFP, Ki67, and L1 immunostaining signals. Depicted are 3 zones in the developing cortex, VZ/SVZ, IZ, and CP.

(C) Quantification of the cortical entry (Table S1I‴).

(D) Quantification of axon intensity ratio (Table S1J‴).

(E) Quantification of the proliferation and apoptosis in cells expressing indicated vectors (Table S1K‴).

(F) Sox9 induces Wwp1/2 and miR-140 to regulate establishment of BP neuronal morphology. Intronic *miR-140* inhibits Fyn mRNA.

Scatter dot plot on (D) with the red line as mean, error bars represent ±SD. Bars on (C) and (E) represent average ±SD. For statistical analyses, (C) two-way ANOVA with Bonferroni post hoc test; (D) and (E), D'Agostino and Pearson omnibus normality test and one-way ANOVA with Bonferroni post hoc test. ***$p < 0.001$; ** $0.001 < p < 0.01$; * $0.01 < p < 0.05$. See also Figures S11 and S12.

whereas acute downregulation of Wwp1/2 using shRNA almost completely eliminates the protein expression (Figure S1H). Similar but not identical phenotypes of tKD and Sox9 KD may reflect an effect of a targeted depletion of Wwp1/2miR-140-3p trio, whereas Sox9 KD eliminates one of the many inductory factors for the trio expression.

miR-140 Controls Fyn Expression to Regulate Neuronal Morphology

A single miRNA molecule holds a potent regulatory capacity. It is tempting to hypothesize that eliminating a single miRNA gene leads to discreet additive disinhibitions of its multiple target mRNAs, which result in added net effect on a certain cellular process. Here, we report that *miR-140* KO in neurons engenders upregulation of Fyn. Reducing Fyn level in *miR-140* KO partially reinstated polarized morphology and laminar distribution of neurons (Figure 3). At P10, the effects of Fyn OE resembled miR-140-3p-Sponge overexpression, with MP neurons delayed in deeper cortical layers and very similar fraction of cells accumulating above layer II/III (Figures 2I, 2K, S7I, and S7J). These data indicate that Fyn serves as a miR-140 target critical for regulating neuronal morphology and laminar distribution. Moreover, no rescue of cortical aberrances in *Wwp1/2* double KO with Fyn KD but restoration of *Wwp1/2* double KO phenotype by miR-140 OE indicates the presence of other, Fyn-unrelated miR-140 targets that regulate pathways specific for radial migration, but not for polarity establishment (Figure S8).

Overshooting migration observed for Wwp1/2/miR-140-3p tKD and miR-140-3p-Sponge expression may reflect a change in the sensitivity to reelin-mediated go or stop signals in the CP, mediated among others by expression level and Fyn-dependent phosphorylation of Dab1. miR-140-mediated downregulation of Fyn might be a key regulator of this pathway (Feng et al., 2007; Nishimura et al., 2010; Simó and Cooper, 2013).

Synergistic Activities of Host Wwp2 and Intronic miR-140 in Neurons

The coordinated expression of host genes and their intragenic miRNAs is a known phenomenon, and functional reciprocity between the host gene and the intragenic miRNAs have been predicted (Lutter et al., 2010). The evolutionary emergence of miRNA loci residing within protein coding genes allows for the use of preexisting gene regulatory machineries and, in parallel,

for the exposure of miRNAs to the same cellular context and molecular networks in which the host gene and its protein product operate (França et al., 2016). A genomic organization, like that between *Wwp2* and *miR-140*, indicates critical functions of the linked genes in the control of similar fundamental cellular pathways, such as axon-dendrite polarity establishment. Nested transcriptional units, such as host *Wwp2* and intronic *miR-140*, add an additional layer of regulation to the processes that control principal aspects of neuronal development. While the functional relevance of this type of genomic organization is generally rather poorly understood, our study provides experimental evidence for synergistic activities of host *Wwp2* and *miR-140* in neurodevelopment, which were previously only assumed and/or modeled.

According to our data, Sox9 induces expression of intragenic *miR-140* and host *Wwp2*, both of which act in synergy, but employ divergent, Fyn-dependent and Fyn-independent molecular pathways (Figure 8F). The emergence of unique phenotypes observed in tKD, but not in Wwp1/2 dKD only or expression of miR-140-3p-Sponge only, further supports the hypothesis that intragenic miRNAs and their host genes are evolutionarily favored to regulate principal cellular processes, such as neuronal polarity formation and neuronal migration.

STAR★METHODS

Detailed methods are provided in the online version of this paper and include the following:

- KEY RESOURCES TABLE
- CONTACT FOR REAGENTS AND RESOURCE SHARING
- EXPERIMENTAL MODEL AND SUBJECT DETAILS
  - Animals
  - Sex and age/developmental stage of animals for *in vivo* experiments
  - Cell lines and primary cultures
- METHOD DETAILS
  - Generation of Wwp1/2$^{f/f}$ mouse line
  - Mutant mouse genotyping
  - Expression vectors
  - Cloning strategies for constructs generated in this study
  - Isolation of RNA
  - First-Strand cDNA synthesis
  - Real Time PCR (RT-PCR) for mRNA detection and quantification
  - Detection of miRNA by quantitative real-time PCR
  - Isolation of the genomic DNA from Embryonic Stem Cells (ES Cells)
  - Southern blotting of Wwp1 and Wwp2 mutants
  - Probe synthesis for *in situ* hybridization
  - *In situ* hybridization (DIG-labeled probes)
  - LNA-based *in situ* detection of miRNA
  - Biochemical experiments
  - Cell culture
  - Murine primary hippocampal neurons
  - Immunocytochemistry
  - Histology
  - *In utero* electroporation (IUE)
  - Image acquisition, analysis and statistics
- QUANTIFICATION AND STATISTICAL ANALYSIS
  - Quantitative western blotting
  - Label-free protein quantification
  - Axon counting assays *in vitro*
  - Quantification of distribution of cortical neurons and polarity classification
  - Statistical analyses

SUPPLEMENTAL INFORMATION

Supplemental Information includes 12 figures and seven tables and can be found with this article online at https://doi.org/10.1016/j.neuron.2018.10.008.

ACKNOWLEDGMENTS

This work was supported by the German Research Foundation (SPP1365/KA3423/1-1 and KA3423/3-1, H.K.; DFG TA 303/6-1, V.T.) and the Russian Scientific Foundation (15-14-10021, V.T., for the IUE experiments in *miR-140*$^{-/-}$ line), JSPS KAKENHI Grant Number 15K21769 (H.K.), The Mother and Child Health Foundation (H.K.), and the Fritz Thyssen Foundation (H.K.). We would like to acknowledge Nils Brose for his help with project administration and insightful remarks regarding the conceptualization. We thank Fritz Benseler, Klaus-Peter Hellman, Bernd Hesse-Niessen, Ivonne Thanhäuser, Dayana Warnecke, Christiane Harenberg, Maik Schlieper, Dörte Hesse, Rike Dannenberg, and Denis Lajkó and animal facilities of Max Planck Institute of Experimental Medicine and of Charité University Hospital. We acknowledge Fred Rehfeld, Andreas Schedl, Prim Singh, Bob Weinberg, Didier Trono, Richard Huganir, David Baltimore, Anna-Katerina Hadjantonakis, and Kevin R. Jones for providing materials; Judith Stegmüller, Anne Schaefer, Ahmed Mansouri, and Matthias Dobbelstein for their feedback. We thank Stephen Horan for help with editing of the manuscript.

AUTHOR CONTRIBUTIONS

Conceptualization, Data Curation, Formal Analysis, Methodology, Writing – Original Draft and Editing, M.C.A.; Data Curation, Methodology, and/or Formal Analysis, M.K.-S., A.S.-L., M.S., E.B., A.R., K.H., B.A., O.J., L.P., P.B., T.S., M.R., X.Z., T.R., S.R., and M.H.; Resources, H.A. and T.K.; Project Administration and Conceptualization, V.T.; Conceptualization, Formal Analysis, Methodology, Project Administration, Writing –Original Draft, Editing, and Review, H.K.

DECLARATION OF INTERESTS

The authors declare no competing interests.

Received: October 12, 2017
Revised: July 31, 2018
Accepted: October 4, 2018
Published: November 1, 2018

REFERENCES

Akiyama, H., Chaboissier, M.C., Martin, J.F., Schedl, A., and de Crombrugghe, B. (2002). The transcription factor Sox9 has essential roles in successive steps of the chondrocyte differentiation pathway and is required for expression of Sox5 and Sox6. Genes Dev. *16*, 2813–2828.

Ambrozkiewicz, M.C., and Kawabe, H. (2015). HECT-type E3 ubiquitin ligases in nerve cell development and synapse physiology. FEBS Lett. *589*, 1635–1643.

Barnes, A.P., and Polleux, F. (2009). Establishment of axon-dendrite polarity in developing neurons. Annu. Rev. Neurosci. *32*, 347–381.

Barnes, A.P., Lilley, B.N., Pan, Y.A., Plummer, L.J., Powell, A.W., Raines, A.N., Sanes, J.R., and Polleux, F. (2007). LKB1 and SAD kinases define a pathway required for the polarization of cortical neurons. Cell *129*, 549–563.

Britanova, O., de Juan Romero, C., Cheung, A., Kwan, K.Y., Schwark, M., Gyorgy, A., Vogel, T., Akopov, S., Mitkovski, M., Agoston, D., et al. (2008). Satb2 is a postmitotic determinant for upper-layer neuron specification in the neocortex. Neuron *57*, 378–392.

Bulfone, A., Martinez, S., Marigo, V., Campanella, M., Basile, A., Quaderi, N., Gattuso, C., Rubenstein, J.L., and Ballabio, A. (1999). Expression pattern of the Tbr2 (Eomesodermin) gene during mouse and chick brain development. Mech. Dev. *84*, 133–138.

de Anda, F.C., Pollarolo, G., Da Silva, J.S., Camoletto, P.G., Feiguin, F., and Dotti, C.G. (2005). Centrosome localization determines neuronal polarity. Nature *436*, 704–708.

De Pietri Tonelli, D., Pulvers, J.N., Haffner, C., Murchison, E.P., Hannon, G.J., and Huttner, W.B. (2008). miRNAs are essential for survival and differentiation of newborn neurons but not for expansion of neural progenitors during early neurogenesis in the mouse embryonic neocortex. Development *135*, 3911–3921.

Ebert, M.S., Neilson, J.R., and Sharp, P.A. (2007). MicroRNA sponges: Competitive inhibitors of small RNAs in mammalian cells. Nat. Methods *4*, 721–726.

Feng, L., Allen, N.S., Simo, S., and Cooper, J.A. (2007). Cullin 5 regulates Dab1 protein levels and neuron positioning during cortical development. Genes Dev. *21*, 2717–2730.

França, G.S., Vibranovski, M.D., and Galante, P.A. (2016). Host gene constraints and genomic context impact the expression and evolution of human microRNAs. Nat. Commun. *7*, 11438.

Gorski, J.A., Talley, T., Qiu, M., Puelles, L., Rubenstein, J.L., and Jones, K.R. (2002). Cortical excitatory neurons and glia, but not GABAergic neurons, are produced in the Emx1-expressing lineage. J. Neurosci. *22*, 6309–6314.

Götz, M., Stoykova, A., and Gruss, P. (1998). Pax6 controls radial glia differentiation in the cerebral cortex. Neuron *21*, 1031–1044.

Guo, W., Keckesova, Z., Donaher, J.L., Shibue, T., Tischler, V., Reinhardt, F., Itzkovitz, S., Noske, A., Zürrer-Härdi, U., Bell, G., et al. (2012). Slug and Sox9 cooperatively determine the mammary stem cell state. Cell *148*, 1015–1028.

Hatanaka, Y., Yamauchi, K., and Murakami, F. (2012). Formation of axon-dendrite polarity in situ: Initiation of axons from polarized and non-polarized cells. Dev. Growth Differ. *54*, 398–407.

Hori, K., Nagai, T., Shan, W., Sakamoto, A., Taya, S., Hashimoto, R., Hayashi, T., Abe, M., Yamazaki, M., Nakao, K., et al. (2014). Cytoskeletal regulation by AUTS2 in neuronal migration and neuritogenesis. Cell Rep. *9*, 2166–2179.

Horton, A.C., Rácz, B., Monson, E.E., Lin, A.L., Weinberg, R.J., and Ehlers, M.D. (2005). Polarized secretory trafficking directs cargo for asymmetric dendrite growth and morphogenesis. Neuron *48*, 757–771.

Hsia, H.E., Kumar, R., Luca, R., Takeda, M., Courchet, J., Nakashima, J., Wu, S., Goebbels, S., An, W., Eickholt, B.J., et al. (2014). Ubiquitin E3 ligase Nedd4-1 acts as a downstream target of PI3K/PTEN-mTORC1 signaling to promote neurite growth. Proc. Natl. Acad. Sci. USA *111*, 13205–13210.

Huang, Y., Li, G., An, L., Fan, Y., Cheng, X., Li, X., Yin, Y., Cong, R., Chen, S., and Zhao, S. (2017). Fyn regulates multipolar-bipolar transition and neurite morphogenesis of migrating neurons in the developing neocortex. Neuroscience *352*, 39–51.

Jiang, M., and Chen, G. (2006). High Ca2+-phosphate transfection efficiency in low-density neuronal cultures. Nat. Protoc. *1*, 695–700.

Kammers, K., Cole, R.N., Tiengwe, C., and Ruczinski, I. (2015). detecting significant changes in protein abundance. EuPA Open Proteom. *7*, 11–19.

Kawabe, H., and Brose, N. (2011). The role of ubiquitylation in nerve cell development. Nat. Rev. Neurosci. *12*, 251–268.

Kawabe, H., Neeb, A., Dimova, K., Young, S.M., Jr., Takeda, M., Katsurabayashi, S., Mitkovski, M., Malakhova, O.A., Zhang, D.E., Umikawa, M., et al. (2010). Regulation of Rap2A by the ubiquitin ligase Nedd4-1 controls neurite development. Neuron *65*, 358–372.

Kertesz, M., Iovino, N., Unnerstall, U., Gaul, U., and Segal, E. (2007). The role of site accessibility in microRNA target recognition. Nat. Genet. *39*, 1278–1284.

Kishi, M., Pan, Y.A., Crump, J.G., and Sanes, J.R. (2005). Mammalian SAD kinases are required for neuronal polarization. Science *307*, 929–932.

Lakso, M., Pichel, J.G., Gorman, J.R., Sauer, B., Okamoto, Y., Lee, E., Alt, F.W., and Westphal, H. (1996). Efficient in vivo manipulation of mouse genomic sequences at the zygote stage. Proc. Natl. Acad. Sci. USA *93*, 5860–5865.

Liu, P., Jenkins, N.A., and Copeland, N.G. (2003). A highly efficient recombineering-based method for generating conditional knockout mutations. Genome Res. *13*, 476–484.

Lois, C., Hong, E.J., Pease, S., Brown, E.J., and Baltimore, D. (2002). Germline transmission and tissue-specific expression of transgenes delivered by lentiviral vectors. Science *295*, 868–872.

Lutter, D., Marr, C., Krumsiek, J., Lang, E.W., and Theis, F.J. (2010). Intronic microRNAs support their host genes by mediating synergistic and antagonistic regulatory effects. BMC Genomics *11*, 224.

Mertin, S., McDowall, S.G., and Harley, V.R. (1999). The DNA-binding specificity of SOX9 and other SOX proteins. Nucleic Acids Res. *27*, 1359–1364.

Nakamura, Y., Inloes, J.B., Katagiri, T., and Kobayashi, T. (2011a). Chondrocyte-specific microRNA-140 regulates endochondral bone development and targets Dnpep to modulate bone morphogenetic protein signaling. Mol. Cell. Biol. *31*, 3019–3028.

Nakamura, Y., Yamamoto, K., He, X., Otsuki, B., Kim, Y., Murao, H., Soeda, T., Tsumaki, N., Deng, J.M., Zhang, Z., et al. (2011b). Wwp2 is essential for palatogenesis mediated by the interaction between Sox9 and mediator subunit 25. Nat. Commun. *2*, 251.

Namba, T., Kibe, Y., Funahashi, Y., Nakamuta, S., Takano, T., Ueno, T., Shimada, A., Kozawa, S., Okamoto, M., Shimoda, Y., et al. (2014). Pioneering axons regulate neuronal polarization in the developing cerebral cortex. Neuron *81*, 814–829.

Nieto, M., Monuki, E.S., Tang, H., Imitola, J., Haubst, N., Khoury, S.J., Cunningham, J., Gotz, M., and Walsh, C.A. (2004). Expression of Cux-1 and Cux-2 in the subventricular zone and upper layers II-IV of the cerebral cortex. J. Comp. Neurol. *479*, 168–180.

Nishimura, Y.V., Sekine, K., Chihama, K., Nakajima, K., Hoshino, M., Nabeshima, Y., and Kawauchi, T. (2010). Dissecting the factors involved in the locomotion mode of neuronal migration in the developing cerebral cortex. J. Biol. Chem. *285*, 5878–5887.

Noctor, S.C., Flint, A.C., Weissman, T.A., Dammerman, R.S., and Kriegstein, A.R. (2001). Neurons derived from radial glial cells establish radial units in neocortex. Nature *409*, 714–720.

Ohba, S., He, X., Hojo, H., and McMahon, A.P. (2015). Distinct transcriptional programs underlie Sox9 regulation of the mammalian chondrocyte. Cell Rep. *12*, 229–243.

Polleux, F., and Ghosh, A. (2002). The slice overlay assay: A versatile tool to study the influence of extracellular signals on neuronal development. Sci. STKE *2002*, pl9.

Rakic, P. (2009). Evolution of the neocortex: A perspective from developmental biology. Nat. Rev. Neurosci. *10*, 724–735.

Ripamonti, S., Ambrozkiewicz, M.C., Guzzi, F., Gravati, M., Biella, G., Bormuth, I., Hammer, M., Tuffy, L.P., Sigler, A., Kawabe, H., et al. (2017). Transient oxytocin signaling primes the development and function of excitatory hippocampal neurons. eLife *6*, e22466.

Ritchie, M.E., Phipson, B., Wu, D., Hu, Y., Law, C.W., Shi, W., and Smyth, G.K. (2015). limma powers differential expression analyses for RNA-sequencing and microarray studies. Nucleic Acids Res. *43*, e47.

Rybak, A., Fuchs, H., Smirnova, L., Brandt, C., Pohl, E.E., Nitsch, R., and Wulczyn, F.G. (2008). A feedback loop comprising lin-28 and let-7 controls pre-let-7 maturation during neural stem-cell commitment. Nat. Cell Biol. *10*, 987–993.

Sasaki, Y., Cheng, C., Uchida, Y., Nakajima, O., Ohshima, T., Yagi, T., Taniguchi, M., Nakayama, T., Kishida, R., Kudo, Y., et al. (2002). Fyn and

Cdk5 mediate semaphorin-3A signaling, which is involved in regulation of dendrite orientation in cerebral cortex. Neuron *35*, 907–920.

Schneider, C.A., Rasband, W.S., and Eliceiri, K.W. (2012). NIH Image to ImageJ: 25 years of image analysis. Nat. Methods *9*, 671–675.

Schratt, G.M., Tuebing, F., Nigh, E.A., Kane, C.G., Sabatini, M.E., Kiebler, M., and Greenberg, M.E. (2006). A brain-specific microRNA regulates dendritic spine development. Nature *439*, 283–289.

Sieburth, D., Ch'ng, Q., Dybbs, M., Tavazoie, M., Kennedy, S., Wang, D., Dupuy, D., Rual, J.F., Hill, D.E., Vidal, M., et al. (2005). Systematic analysis of genes required for synapse structure and function. Nature *436*, 510–517.

Silva, J.C., Gorenstein, M.V., Li, G.Z., Vissers, J.P., and Geromanos, S.J. (2006). Absolute quantification of proteins by LCMSE: A virtue of parallel MS acquisition. Mol. Cell. Proteomics *5*, 144–156.

Simó, S., and Cooper, J.A. (2013). Rbx2 regulates neuronal migration through different cullin 5-RING ligase adaptors. Dev. Cell *27*, 399–411.

Storey, J.D., and Tibshirani, R. (2003). Statistical significance for genomewide studies. Proc. Natl. Acad. Sci. USA *100*, 9440–9445.

Thomas, K.R., and Capecchi, M.R. (1987). Site-directed mutagenesis by gene targeting in mouse embryo-derived stem cells. Cell *51*, 503–512.

Wiegreffe, C., Simon, R., Peschkes, K., Kling, C., Strehle, M., Cheng, J., Srivatsa, S., Liu, P., Jenkins, N.A., Copeland, N.G., et al. (2015). Bcl11a (Ctip1) Controls Migration of Cortical Projection Neurons through Regulation of Sema3c. Neuron *87*, 311–325.

Yang, J., Qin, S., Yi, C., Ma, G., Zhu, H., Zhou, W., Xiong, Y., Zhu, X., Wang, Y., He, L., and Guo, X. (2011). MiR-140 is co-expressed with Wwp2-C transcript and activated by Sox9 to target Sp1 in maintaining the chondrocyte proliferation. FEBS Lett. *585*, 2992–2997.

STAR★METHODS

KEY RESOURCES TABLE

REAGENT or RESOURCE	SOURCE	IDENTIFIER
Antibodies		
Mouse anti-SMI312	Millipore	RRID:AB_509993
Mouse anti-SMI312	Covance	SMI-312R; RRID:AB_2314906
Mouse anti-Tau-1	Millipore	Clone PC16C; MAB3420; RRID:AB_94855
Chicken anti-MAP2	Novus	RRID:AB_350528
Rabbit anti-GFP	MBL	#598; RRID:AB_591818
Goat anti-GFP	Rockland	600-101-215M; RRID:AB_2612804
Chicken anti-GFP	Abcam	ab13970; RRID:AB_300798
Goat anti-tdTomato	Sicgen	AB8181-200; RRID:AB_2722750
Mouse anti-GM130	BD	610823; RRID:AB_398142
Rat anti-Ki67	Gift from Prim Singh	N/A
Anti-PH3	Abcam	ab5176; RRID:AB_304763
Rabbit anti-Pax6	Millipore	AB2237; RRID:AB_1587367
Rabbit anti-Tbr1	Abcam	ab31940; RRID:AB_2200219
Rabbit anti-Tbr2 / Eomes	Abcam	ab23345; RRID:AB_778267
Rabbit anti-Cleaved Caspase-3	Cell Signaling	#9662; RRID:AB_331439
Rabbit anti-Satb2	Generated in-house	N/A
Mouse anti-myc	Cell Signaling	9B11; RRID:AB_331783
Rabbit anti-Wwp1	This paper, SySy	0221
Rabbit anti-Wwp2	This paper, SySy	7425A
Mouse anti-actin	Sigma-Aldrich	AC40; RRID:AB_262137
Rabbit anti-Cux1 (CDP)	SCBT	M-222; RRID:AB_2261231
Mouse anti-PSD-95	NeuroMab	RRID:AB_2307331
Rabbit anti-RabGDI	SySy	130011
Mouse anti-Fyn	SCBT	15; RRID:AB_627642
Rabbit anti-Sox9	Millipore	5535; RRID:AB_2239761
Rat anti-CTIP2	Abcam	25B6; RRID:AB_2064130
Rabbit anti-Cre	SySy	257003; RRID:AB_2619968
Anti-NeuN	Chemicon	RRID:AB_2298772
Rat anti-L1cam	Millipore	RRID:AB_2133200
Goat anti-Brn-2	SCBT	RRID:AB_2167385
Goat anti-mouse IgG HRP	BioRad	#1721011; RRID:AB_11125936
Goat anti-rabbit IgG HRP	BioRad	#1706515; RRID:AB_11125142
Goat anti-mouse IgG IR-Dye-680RD	Li-COR	925-68070; RRID:AB_2651128
Goat anti-mouse IgG IR-Dye-800CW	Li-COR	925-32210; RRID:AB_2687825
Goat anti-rabbit IgG IR-Dye-680RD	Li-COR	925-68071; RRID:AB_2721181
Goat anti-rabbit IgG IR-Dye-800CW	Li-COR	925-32212; RRID:AB_2716622
Goat anti-chicken IgY AlexaFluor-633	Thermo Fisher Scientific	A-21103; RRID:AB_2535756
Goat anti-mouse IgG AlexaFluor-488	Thermo Fisher Scientific	A-11001; RRID:AB_2534069
Goat anti-mouse IgG AlexaFluor-555	Thermo Fisher Scientific	A-21422; RRID:AB_2535844
Goat anti-mouse IgG AlexaFluor-633	Thermo Fisher Scientific	A-21052; RRID:AB_2535719
Goat anti-rabbit IgG AlexaFluor-488	Thermo Fisher Scientific	A-11008; RRID:AB_143165
Goat anti-rabbit IgG AlexaFluor-555	Thermo Fisher Scientific	A-21428; RRID:AB_2535849
Goat anti-rabbit IgG AlexaFluor-633	Thermo Fisher Scientific	A-21070; RRID:AB_2535731
Goat anti-rat IgG AlexaFluor-555	Thermo Fisher Scientific	A-21434; RRID:AB_2535855

(*Continued on next page*)

Continued

REAGENT or RESOURCE	SOURCE	IDENTIFIER
Donkey anti-goat AlexaFluor-488	Jackson Immunoresearch	705-546-147; RRID:AB_2340430
Donkey anti-chicken AlexaFluor-488	Jackson Immunoresearch	703-545-155; RRID:AB_2340375
Donkey anti-goat AlexaFluor-Cy3	Jackson Immunoresearch	705-165-147; RRID:AB_2307351
Donkey anti-rabbit AlexaFluor-488	Jackson Immunoresearch	711-545-152; RRID:AB_2313584
Donkey anti-rabbit AlexaFluor-Cy3	Jackson Immunoresearch	711-167-003; RRID:AB_2340606
Donkey anti-rabbit AlexaFluor-Cy3	Jackson Immunoresearch	711-165-152; RRID:AB_2307443
Donkey anti-rat AlexaFluor-Cy3	Jackson Immunoresearch	712-165-153; RRID:AB_2340667
Donkey anti-rat AlexaFluor-Cy5	Jackson Immunoresearch	712-175-153; RRID:AB_2340672
Donkey anti-mouse AlexaFluor-Cy3	Jackson Immunoresearch	715-165-150; RRID:AB_2340813
Donkey anti-mouse AlexaFluor-594	Invitrogen	A-21207
Donkey anti-mouse AlexaFluor-Cy5	Jackson Immunoresearch	715-175-151; RRID:AB_2340820
Draq5	Biostatus Limited	RRID:AB_2314341
Bacterial and Virus Strains		
Escherichia coli XL-1 Blue competent cells	Stratagene	N/A
Escherichia coli Electro10-Blue competent cells	Stratagene	N/A
Escherichia coli JM109 competent cells	Promega	L2005
Escherichia coli TOP10 competent cells	Invitrogen	C404052
Control lentivirus; pLKO.1-Venus-Scramble	This paper	N/A
Sox9 KD lentivirus; pLKO.1-sh-mSox9	This paper	N/A
Critical Commercial Assays		
Secrete-Pair Dual Luminescence Assay Kit	GeneCopoeia	LF032
Pierce Reversible Protein Stain Kit for Nitrocellulose Membranes	ThermoFisher	24580
Experimental Models: Cell Lines		
HEK293FT	GIBCO	R700–07; RRID: CVCL_6911
HEK293T	Leibniz Institute DSMZ-German Collection of Microorganisms and Cell Cultures	ACC 635; RRID: CVCL_0063
N2A	Thermo Fisher	RRID: CVCL_0470
Primary murine hippocampal and cortical neurons	This paper	N/A
Experimental Models: Organisms/Strains		
Wwp1$^{f/f}$ mouse line	This paper	N/A
Wwp2$^{f/f}$ mouse line	This paper	N/A
Wwp1/2$^{f/f}$ mouse line	This paper	N/A
Emx1$^{Cre/+}$ mouse line	(Gorski et al., 2002)	B6.129S2-Emx1$^{tm1(cre)Krj}$/J
E2A$^{Cre/+}$ mouse line	(Lakso et al., 1996)	B6.FVB-Tg(EIIa-cre)^{C5379Lmgd}/J
Flip recombinase expressing mouse line	Jackson Laboratory	B6;SJL-Tg(ACTFLPe)^{9205Dym}/J
C57BL6/N wild type mouse strain	Charles Rivers	N/A
FVBN wild type mouse strain	Charles Rivers	RRID:CVCL_F046
NMRI wild type mouse strain	Charles Rivers and Janvier Labs	RRID:IMSR_TAC:nmri
miR-140$^{-/-}$ mouse line	(Nakamura et al., 2011a)	N/A
Sox9$^{f/f}$ mouse line	(Akiyama et al., 2002)	N/A
Oligonucleotides		
Information regarding the oligonucleotides used in this study can be found in the Table S7.		
Recombinant DNA		
P0 mouse cortex cDNA library	This paper	N/A
pMD2.G	Unpublished, Didier Trono	Addgene #12259

(*Continued on next page*)

Continued

REAGENT or RESOURCE	SOURCE	IDENTIFIER
pCMVdeltaR8.2	Unpublished, Didier Trono	Addgene#12263
pcDNA-3.2-GW/EmGFP	Invitrogen	K493600
pcDNA-3.2-GW/EmGFP-Scramble	Invitrogen	K493600
pcDNA-3.2-GW/EmGFP-miR-140	This paper	N/A
pCR2.1-Wwp2/miR-140	This paper	N/A
pCX::myr-Venus	Anna-Katerina Hadjantonakis	N/A
pFUGW	Addgene (Lois et al., 2002)	Addgene#14883
pFUGWiCre	Richard Huganir	N/A
pLKO.1-Scramble	Sigma Aldrich	SHC016
pLKO.1-sh-mSox9-2	Addgene (Guo et al., 2012)	Addgene#40645
pLKO.1-sh-mWwp1 #1	Thermo Scientific	#28255
pLKO.1-sh-mWwp1 #2	Thermo Scientific	#28281
pLKO.1-sh-mWwp2 #1	Thermo Scientific	#92098
pLKO.1-sh-mWwp2 #2	Thermo Scientific	#92100
pLKO.1-Venus-Scramble	This paper	N/A
pLKO.1-Venus-sh-mSOX9	This paper	N/A
pLKO.1-Venus-sh-mWwp1 #1	This paper	N/A
pLKO.1-Venus-sh-mWwp2 #2	This paper	N/A
pCAG	Jun-ichi Miyazaki	N/A
pRaichu205X	Michiyuki Matsuda	N/A
pCAG-CTR-Sponge	This paper	N/A
pCAG-miR-140-3p-Sponge	This paper	N/A
pCAG-miR-140-5p-Sponge	This paper	N/A
pWPXL-Sox9	Addgene (Guo et al., 2012)	Addgene#36979
pCR2.1-Fyn	This paper	N/A
pCAG-Fyn-IRES-GFP	This paper	N/A
pCAG-IRES-GFP	This paper	N/A
pXhoI	Frederick Rehfeld (Rybak et al., 2008)	N/A
pXhoI-Fyn 3′UTR	This paper	N/A
pCR2.1-Fyn 3′UTR	This paper	N/A
pMCS-GL	Thermo Scientific	10458
pAPtag	GenHunter Corporation	Q202
pMCS-Wwp1 −1670 to −1663	This paper	N/A
pMCS Wwp2 −1156 to −1150	This paper	N/A
pMCS-Wwp1 −785 to −779	This paper	N/A
pGEM-T-Sox9	This paper	N/A
pCAG-miR-140-IRES-tdTomato	This paper	N/A
pSuper Neo Gfp	Oligoengine	VEC-PBS-0006
pSuper Neo Gfp-sh-Scramble	This paper	N/A
pSuper Neo Gfp-sh-Fyn	This paper	N/A
pCAG-myc-Wwp1	This paper	N/A
pCAG-myc-Wwp2	This paper	N/A
Software and Algorithms		
Fiji	imagej.net	N/A
GraphPad Prism	GraphPad Software	N/A
Photoshop	Adobe	N/A

(*Continued on next page*)

Continued

REAGENT or RESOURCE	SOURCE	IDENTIFIER
Other		
mmu-miR-140-3p, sequence, stabilized by phosphorotioates (3XPTO) at 3′: uaccacaggguagaaccacgg	DNA Core Facility, MPIem, Göttingen	N/A
mmu-miR-140-5p, sequence, stabilized by phosphorotioates (3XPTO) at 3′: cagugguuuuacccuaugguag	DNA Core Facility, MPIem, Göttingen	N/A
Anti-mmu-miR-140-3p miScript miRNA Inhibitor	QIAGEN	MS0000152
Scrambled miRNA, negative control: gguucguacguacacuguuca	Metabion International AG	N/A
LNA-DIG probe for mmu-miR-140-3p detection	Exiqon	Discontinued
LNA-DIG probe for mmu-miR-134 detection	Exiqon	Discontinued
LNA-DIG probe, scrambled control	Exiqon	Discontinued

N/A, not available.

CONTACT FOR REAGENTS AND RESOURCE SHARING

Further information and requests for resources and reagents should be directed to and will be fulfilled by the Lead Contact, Hiroshi Kawabe (kawabe@em.mpg.de).

EXPERIMENTAL MODEL AND SUBJECT DETAILS

Animals

Colonies of wild-type mice (*Mus musculus*) have been maintained in the animal facilities of the Max Planck Institute of Experimental Medicine (MPIem) and the Charité University Hospital. *Wwp1*$^{f/f}$ and *Wwp2*$^{f/f}$ mouse lines were generated in this study by using homologous recombination in ES cells. In both cases, exon 6 of Wwp1 or of Wwp2 was engineered to be flanked by loxP sites. Animals homozygous for the loxP alleles were viable, fertile, and born at the expected Mendelian ratio, and exhibited no overt phenotypic changes in the cage environment. To inactivate *Wwp1* and *Wwp2* in the developing cortex, we crossed *Wwp1/2*$^{f/f}$ mice with the *Emx1*$^{Cre/+}$ line, in which Cre recombinase is expressed from the *Emx1* gene allele (Gorski et al., 2002). In *Wwp1/2*$^{f/f}$; *Emx1*$^{Cre/+}$ animals, the expression of *Wwp1* and *Wwp2* in premitotic progenitors of dorsal telencephalon is ablated from E9.5. To establish conventional KO mouse line, we crossed *Wwp1/2*$^{f/f}$ with *E2A*$^{Cre/+}$ mouse line (Lakso et al., 1996). Other mouse lines used in this study were described previously; *miR-140*$^{-/-}$ line (Nakamura et al., 2011a); *Sox9*$^{f/f}$ line (Akiyama et al., 2002).

All experiments conducted on mice were performed in Max Planck Institute of Experimental Medicine (MPIem) and Charité University Hospital in compliance with the guidelines for the welfare of experimental animals approved by the State Government of Lower Saxony (Niedersächsisches Landesamt für Verbraucherschutz und Lebensmittelsicherheit (LAVES), Permissions 33.9-42502-04-13/1359, /1052, /1954, and /2173 and the Max Planck Society (comparable to National Institute of Health Guidelines) for experiments in MPIem and by the State Office for Health and Social Affairs, Council in Berlin, Landesamt für Gesundheit und Soziales (LAGeSo), permission G0206/16 for experiments in the Charité University Hospital.

Sex and age/developmental stage of animals for *in vivo* experiments

In our experiments, cortical positioning of murine neurons of upper layers was gender-independent (Figure S1K). For this reason, littermates of both sexes were randomly assigned to experimental groups during the procedure of IUE. Our cortical positioning analyses were performed at E14.5 and the brains after IUE were fixed as indicated in the figure legends and in the main text (E15.5, E17.5, E18.5, P0 or P10). Live imaging of migrating neurons in organotypic brain slice was analyzed after IUE at E13.5. Experiments using tissue lysates were performed on animals at developmental stages indicated in the figure legends and in the main text. Detailed information about mouse strains used in this study in IUE experiments is in the Table S3.

Cell lines and primary cultures

HEK293FT, HEK293T and N2A cell line

HEK293FT were used for production of lentiviruses and for transfections (GIBCO; R700–07; RRID:CVCL_6911); HEK293T (RRID:CVCL_0063) were used for luciferase assays. N2A cell line (Thermo Fisher; CCL-131; RRID:CVCL_0470) was used for transfections to validate the efficiency of sh-Fyn vectors and Fyn overexpression. Unless stated otherwise, HEK293FT, or N2A cells were maintained in 6 cm Petri dishes (Corning) in 10 mL HEK cell medium at 37°C in the presence of 5% carbon dioxide in HERA-cell240

(Heraeus) incubator. For passaging, semi-confluent cells were washed with PBS, incubated with 1 mL of 0.05% trypsin solution (GIBCO, Life Technologies) for 1 minute at 37°C and the reaction was stopped by addition of 9 mL of the fresh medium. Sex of HEK293FT/293T cells is female, sex of N2A cell is male.

Murine primary neurons

Brains of P0 mice were dissected in ice-cold Hank's Balanced Salt Solution (HBSS) under stereomicroscope to collect hippocampi in 1 mL of ice-cold Papain solution. For cortical primary neurons, cultured for the analysis of neuronal development *in vitro*, mice at E14.5 developmental stage were used. For cortical primary neurons, cultured for lentiviral infection and cell lysates, mice at E16.5 developmental stage were used. After 1-hour incubation at 37°C with gentle shaking, papain solution was carefully replaced by stop solution and the hippocampi or cortices were further incubated at 37°C for 15 minutes with moderate agitation. Next, the stop solution was discarded, and hippocampi or cortices carefully washed twice with 900 μL of pre-warmed (37°C) Complete Neurobasal medium. Further, the hippocampi or cortices were carefully triturated in 200 μL Complete Neurobasal medium 10 times using P200 pipette tip. The debris were then let sink for 1 minute and 150 μL the supernatant transferred to 900 μL of fresh Complete Neurobasal at 37°C. After second round of trituration, cells were counted with Naubauer counting chamber and neurons were seeded in 24 well-plate formats. For biochemical experiments, 120000 cells and for immunocytochemistry, 40000 cells were plated on one coverslip in 1mL of Complete Neurobasal medium. The day of neuronal prep was counted as day *in vitro* 0 (DIV0). Neurons were cultivated at 37°C in the presence of 5% carbon dioxide in HERA-cell240 (Heraeus) incubator. For counting of axons, neurons were cultivated until DIV4 or DIV6-7 and then fixed with 4% PFA solution. For analysis of protein levels infected cortical neurons were cultivated until DIV15. For analyses of neuronal development *in vitro*, neurons were cultivated until DIV2, 4, or 6, as specified in respective figures.

METHOD DETAILS

Generation of Wwp1/2$^{f/f}$ mouse line

Bacterial artificial chromosome clones covering from the 3rd to the 6th introns of *Wwp1* and form 5th to 6th introns of *Wwp2* were cloned into pL253 plasmid. Two loxP sites flanking 6th exons of *Wwp1* and *Wwp2* together with one neomycin cassette and two FRT sites were integrated in these plasmids (Figure S1A) by recombineering method (Liu et al., 2003). After transfection of one of two targeting vectors to ES cells derived from 129/OlaHsd mouse line, ES cells were cultured in the presence of G418 (Invitrogen) and Ganciclovir (Roche) to select clones with proper homologous recombination. ES cells were validated with Southern blotting (Figures S1C and S1E) and injected into blastocysts (Thomas and Capecchi, 1987). Mice derived from such ES cells were crossed with flip recombinase expressing mouse line (B6;SJL-Tg(ACTFLPe)9205Dym/J; Jackson Laboratory) to delete the Neo cassette. *Wwp1*$^{f/+}$ and *Wwp2*$^{f/+}$ mice were crossed to establish *Wwp1/2*$^{f/f}$ mouse line.

Mutant mouse genotyping

Genotyping for all mutant mouse lines was performed in DNA Core Facility (MPIem, Göttingen) by PCR using oligonucleotide primers listed in Table S4 (wt, wild-type allele; Cre, knock-in allele with Cre; ko, knockout allele; floxed, allele with loxP site).

All genotyping PCRs except for the one for *Sox9*$^{f/f}$ were performed with the following parameters:

Step 1: 96°C for 3 minutes,
Step 2: 94°C for 30 s,
Step 3: 64°C for 1 minute,
Step 4: 72°C for 1 minute (32 cycles from Step2 to 4),
Step 5: 72°C for 7 minutes.

Genotyping of *Sox9*$^{f/f}$ mutation was performed with the PCR protocol with the following parameters:

Step 1: 95°C for 3 minutes,
Step 2: 95°C for 10 s,
Step 3: 58°C for 10 s,
Step 4: 72°C for 30 s (4 cycles from Step2 to 4),
Step 5: 95°C for 10 s,
Step 6: 56°C for 10 s,
Step 7: 72°C for 30 s (4 cycles from Step5 to 7),
Step 8: 95°C for 10 s,
Step 9: 54°C for 10 s,
Step 10: 72°C for 30 s (34 cycles from Step8 to 10),

Expression vectors

pLKO vectors carrying scramble non-silencing shRNA, sh-Wwp1 and sh-Wwp2 were obtained from Thermo Scientific. pLKO-sh-Sox9 was a gift from Bob Weinberg (Addgene plasmid #40645) (Guo et al., 2012). Puromycin resistance cassette of pLKO vectors

was excised using KpnI/BamHI restrictases and replaced by myr-Venus expressing cassette. The expression vector encoding the membrane-anchored variant of Venus was a gift of Dr. Anna-Katerina Hadjantonakis. Control sponge, miR-140-5p and miR-140-3p sponge constructs were synthetized by Life Technologies and cloned into pCAG vector downstream of Venus expression cassette. Hairpin sequences encoded in pLKO.1-sh-mWwp1 and pLKO.1-sh-mWwp2 (Thermo Fisher) to target murine Wwp1 and Wwp2 are listed below.

mWwp1, #28255;
5′-CCGGGCAACAGTGGACTTGAAACAACTCGAGTTGTTTCAAGTCCACTGTTGCTTTTT-3′
mWwp1, #28281;
5′-CCGGGAGTTTGGAGTCACCACACTTCTCGAGAAGTGTGGTGACTCCAAACTCTTTTT-3′
mWwp2 #92098;
5′-CCGGGCCCTCTTGATTCAGTAGCTTCTCGAGAAGCTACTGAATCAAGAGGGCTTTTTG-3′
mWwp2 #92100;
5′-CCGGGCAGCACTTCAGCCAAAGATTCTCGAGAATCTTTGGCTGAAGTGCTGCTTTTTG-3′

Cloning strategies for constructs generated in this study

pCR2.1-Wwp2/miR-140

Intronic sequence of *Wwp2* gene was amplified by PCR using primers 5′-CAGAGCACTGTGTTACCTTCACCC-3′ and 5′-CCTAACC CAGATTTGGATCCATTTAT-3′and subcloned to pCR2.1-TOPO. The constructed plasmid was used for RNA-probe synthesis used in *in situ* hybridization.

pcDNA-3.2-GW/EmGFP-miR-140

To generate pre-miR-140, oligos 5′-TGCTGCAGTGGTTTTACCCTATGGTAGGTTTTGGCCACTGACTGACACCACAGGAGA ACCACGGAC-3′ and 5′-CCTGGTCCGTGGTTCTCCTGTGGTGTCAGTCAGTGGCCAAAACCTACCATAGGGTAAAACCACTGC-3′ were mixed at the ratio 1:1 and incubated at 95°C for 10 minutes. The thermoblock was then switched off and the duplex was let anneal for 10 hours. Next, precursor sequence of miR-140 was cloned into pcDNA-3.2-GW/EmGFP following manufacturer's protocol (Invitrogen).

pCAG-miR-140-IRES-tdTomato

DNA sequence of miR-140 precursor was extracted from P0 mouse brain cDNA library with primers: 5′-gtctcatcattttggcaaag CAGAGCACTGTGTTACCTTC-3′ and 5′-cggccgcgatatcctcgaggAATTGGGGAACAATCGGG-3′ and inserted into pCAG-IRES-tdTomato vector using NEB Builder system.

pCAG-CTR-Sponge

CTR sponge was synthetized as a tandem of 16 DNA repeats: 5′-AAGTTTTCAGTTTGCTAACA-3′ by Life Technologies. The 5′ site was additionally equipped with restriction sites for XhoI, BglII, and BspEI restriction nuclease and 3′ was with EcoRI, SalI, and KpnI. In the downstream of the 5′ restriction sites, three stop codons were added. Synthesized double strand DNA was digested with XhoI and SalI and shuttled to pRaichu-205X, opened with the corresponding restriction enzymes. pRaichu-205X was constructed by Dr. Michiyuki Matsuda's group from pCAGGS vector originally developed by Dr. Jun-ichi Miyazaki, Osaka University Medical School.

pCAG-miR-140-3p-Sponge

miR-140-3p-Sponge was synthetized as a tandem of 16 DNA repeats: 5′ AACTGGTTCCGAACTGTGGTA-3′ and shuttled to pRaichu-205X with the same combination of restriction enzymes as for construction of CTR sponge.

pCAG-miR-140-5p-Sponge

miR-140-5p-Sponge was synthetized as a tandem of 16 DNA repeats: 5′-CTAGCATAGGAGCCAACCACTG-3′ and shuttled to pRaichu-205X with the same combination of restriction enzymes as for construction of CTR sponge.

pLKO.1-Venus-sh-mSOX9

For usage in cell culture experiments and *in utero* electroporation, DNA sequence of myristoylated Venus (myr-Venus) was amplified by PCR using pCX::myr-Venus as a template and 5′ primer with BamHI and 3′ primer with KpnI. PCR product was digested with BamHI/KpnI and the myr-Venus expression cassette was cloned into pLKO-sh-mSox9-2 opened with the same restriction enzymes.

pCAG-Fyn-IRES-GFP

DNA sequence of Fyn was extracted from P0 mouse brain cDNA library with primers:

5′-gtctcatcattttggcaaagATGGGCTGTGTGCAATGTAAG-3′ and 5′-cggccgcgatatcctcgaggTCACAGGTTTTCACCGGG-3′ and inserted into pCAG-IRES-EGFP vector using NEB Builder system.

pCR2.1-Fyn 3′UTR

Fragment of Fyn 3′UTR spanning 4 putative miR-140-3p binding sites (*Mus musculus*, mm10 chr10:39564428-39564977) was amplified from P0 cortex cDNA library using primers 5′-AAAACTCGAGCAGGACAGGTGTTTGGGTTT-3′ and 5′-AAAAGAATTCGGTTGC CATGACTACAATGC-3′ with 4A overhangs for restriction enzymes: XhoI and EcoRI.

pXhoI-Fyn 3′UTR

3′UTR of Fyn was cloned from pCR2.1-Fyn 3′UTR and into pXhoI (Rybak et al., 2008) vector with XhoI and EcoRI enzymes.

pSuper Neo Gfp-sh-Scramble

Oligonucleotides of sequence: 5′- GATCCCCGGTGGATACTATATCACAACGCGAACGTTGTGATATAGTATCCACCTTTTT-3′ and 5′-AGCTAAAAAGGTGGATACTATATCACAACGTTCGCGTTGTGATATAGTATCCACCGGG-3′ were synthetized, hybridized and cloned into pSuper Neo Gfp vector using BglII and HindIII restrictases, accordingly to the manufacturer's protocol (Oligoengine).

pSuper Neo Gfp-sh-Fyn

Oligonucleotides of sequence: 5′-GATCCCCGGTGGATACTATATCACAACGCGAACGTTGTGATATAGTATCCACCTTTTT-3′ and 5′-AGCTAAAAAGGTGGATACTATATCACAACGTTCGCGTTGTGATATAGTATCCACCGGG-3′ were synthetized, hybridized and cloned into pSuper Neo Gfp vector using BglII and HindIII restrictases, accordingly to the manufacturer's protocol (Oligoengine).

pCAG-myc-Wwp1

The cDNA sequence encoding full legth Wwp1 (NM_177327) was amplified from the mouse brain library using primers: 5′-GGCGTCGACTCATTCTTGTCCAAATCCCTCTGTC-3′ and 5′-GGCGAATTCGGTACCATGGCCACTGCTTCACCAAGATC-3′ and cloned into pCAG-myc vector using enzymes EcoRI and SalI.

pCAG-myc-Wwp2

The cDNA sequence encoding full legth Wwp2 (NM_025830) was amplified from the mouse brain library using primers: 5′-GGCGAATTCTCCATGGCATCTGCCAGCTCCAG-3′ and 5′-GGCCCTCGAGTCATTCTTGTCCAAATCCCTCTG-3′ and cloned into pCAG-myc vector using enzymes EcoRI and XhoI.

pMCS-Wwp1 –1670 to –1663

Fragment of Wwp1 promoter (*Mus musculus*, mm10 chr4:19709861-19710845) containing putative Sox9 binding sites 5′-ACAAAGG-3′; (Mertin et al., 1999) (at positions −1670 to −1663; adenine in start codon ATG as position +1) was amplified using primers 5′-GAATTCtctgaaccaatggaggagtg-3′and 5′-GGATCCgttcacgaatcctggcttcttgttg-3′ and cloned into pMCS-Gaussia Luc (Thermo Fisher) vector using EcoRI/BamHII restriction enzymes.

pMCS-Wwp1 –785 to –779

Fragment of Wwp1 promoter (*Mus musculus*, mm10 chr4:19709018-19710005) containing putative Sox9 binding sites (Mertin et al., 1999) at positions −785 to −779 (5′-AACAAT-3′) was amplified using primers 5′-GAATTCcaacggagtgaatcagaaaggt-3′ and 5′-GGATCCctacacctcccttcctcgggagcg-3′ and cloned into pMCS-Gaussia Luc (Thermo Fisher) vector using EcoRI/BamHII restriction enzymes.

pMCS Wwp2 –1156 to –1150

Fragment of Wwp2 promoter (*Mus musculus*, mm10 chr8:107435397-107436288) containing putative Sox9 binding sites (Mertin et al., 1999) at positions −1156 to −1150 (5′-AACAAT-3′) and −529 to −523 (5′-ACAAAGG-3′) (Nakamura et al., 2011b) was amplified using primers 5′-AAAGAATTCaactggtaatcctaacta-3′ and 5′-AAAAGATCTagcgtttgacccgct-3′ and cloned into pMCS-Gaussia Luc (Thermo Fisher) vector using EcoRI/BglII restriction enzymes.

pGEM-T-Fyn

To generate an *in situ* probe for Fyn, a fragment of Fyn mRNA was amplified in a PCR reaction using primers 5′-CAACTGGTACAG CATTACTCAGAGAG-3′ and 5′- TGTCTTGCTGTGTATTCATTGTCTT-3′ and ligated into pGEM-T vector.

pGEM-T-Sox9

To generate a probe for *in situ* hybridization, a fragment of Sox9 mRNA was amplified in a PCR reaction using primers 5′-CTGAAGGGCTACGACTGGACG-3′ and 5′-TGCTGCTGATGCCGTAACTGC-3′ and ligated into pGEM-T vector.

Isolation of RNA

All tools used for RNA work was thoroughly cleaned with 70% ethanol (Sigma) and rinsed with RNA-Zap (Thermo Fisher) before the beginning of the procedure. Brain tissue was isolated from mice and flash-frozen in liquid nitrogen until the purification procedure. The tissue was homogenized in appropriate volume of Trizol (Thermo Fisher) - 1 mL for embryonic cortex, 2 mL per adult cortex - with Ultra Turrax homogenizer (IKA Labtechnik) for 1 minute and incubated in the room temperature for 5 minutes. For every 1 mL of homogenate, 200 μL of chloroform (Merck) was added, mixed well using vortex (Bender and Hobein), incubated at room temperature for 2-3 minutes and centrifuged 15 minutes at 13 krpm. The aqueous phase was transferred to new tubes (Eppendorf), mixed with one volume of 70% ethanol (Sigma-Aldrich) and the solution was applied onto RNeasy columns (RNeasy Mini Kit, QIAGEN). For purification of miRNA fraction, miRNeasy purification Kit (QIAGEN) was used. Further steps were performed according to the manufacturer's protocols. RNA was eluted from the silica membranes using 30 μL of molecular biology-grade (MB)- H_2O.

First-Strand cDNA synthesis

Reverse transcription of purified RNA was carried out with SuperScript III First-Strand Synthesis System (Invitrogen) following the manufacturer's manual. For each reaction, 3 μg of total RNA was used in the final volume of 20 μL. After terminating of the reaction by incubation at 85°C for 5 minutes, the mixture was cooled on ice for 5 minutes and 1 μL of RNaseH (Invitrogen) was added. Reaction was held for 20 minutes at 37°C. Thereafter, 21 μL reaction was supplemented with 63 μL of MB-H_2O and stored at −20°C until further processing.

Real Time PCR (RT-PCR) for mRNA detection and quantification

The RT-PCR was performed in 384 well plates (Roche). For each analyzed gene, master mix including 5 μL of SYBR Green (Invitrogen), 0.1 μL of each RT-primer and 1 μL MB-H_2O per reaction was prepared. Next, 4 μL of cDNA solution was pipetted to each well followed by 6 μL of master mix. Pipetting was performed on ice and the plate covered from light. The reaction was held on Light Cycler 480 (Roche Applied Science) with the parameters listed in the Table S5.

Before each gene analysis by RT-PCR, a standard curve using different concentration of cDNA was plotted and the input amount of cDNA was calculated, enabling the quantification of mRNA levels in the linear range of the input template. Level of transcripts of each analyzed gene: *Wwp1* (detected with quantitative real-time PCR primers 5′-GTTGCTGCCAGACCCAAA-3′ and 5′-TAGGACAGATGATGATTCTCCATTA-3′), *Wwp2* (5′-CTGGGAAGTGTGCCTAATGG-3′ and 5′-GCAGTCCCACTGGATTCTCT-3′), and *Sox9* (5′-GTACCCGCATCTGCACAAC-3′ and 5′-CTCCTCCACGAAGGGTCTCT-3′) was then normalized to the average level of mRNA of housekeeping genes: *Gapdh* (5′-CAATGAATACGGCTACAGCAAC-3′ and 5′-TTACTCCTTGGAGGCCATGT-3′) and *Oaz1* (5′-GCCTGAGGGCAGTAAGGAC-3′ and 5′-GGAGTAGGGCGGCTCTGT-3′). Primers for the reaction were designed with Roche Assay Design Center.

For Figure 5, level of each RNA was expressed relative to component of spliceosome, U6 snRNA - RNU6B. Measurements were performed on cDNA synthetized from RNA isolated from cultured cortical neurons at DIV15 according to the protocols described above with minor modifications.

Detection of miRNA by quantitative real-time PCR

For detection of miRNAs, cDNA was synthetized with miScript II RT system (QIAGEN) using 3 μg of total RNA. Quantitative real-time PCR was carried out with miScript (QIAGEN) primers for miR-140-3p, miR-140-5p, and RNU6B (miRScript Primer Assay) using miScript SYBR Green PCR Kit (QIAGEN). Each step of miRNA detection (including duration and temperatures of RT-PCR) was performed according to the manufacturer's protocol. Level of each miR-140 strand was normalized to the level of RNU6B.

Isolation of the genomic DNA from Embryonic Stem Cells (ES Cells)

The ES cells were grown in 6-well plates (Greiner) until confluency, carefully washed with PBS and incubated with 1 mL of lysis buffer for 16-20 hours at 37°C. Next, cell lysate was collected to 2 mL reaction tubes (Eppendorf) and supplemented with 700 μL isopropanol (Merck). The mixture was inverted several times and centrifuged for 15 minutes at 4°C at 13 krpm. Resulting DNA pellets were subsequently washed with 70% ethanol (Sigma-Aldrich), air-dried, and resuspended in 100 μL of TE Buffer. DNA solutions were kept at 4°C until further processing.

PBS buffer: *8g NaCl, 0.2g KCl, 1.44 g Na_2HPO_4, 0.24 g KH_2PO_4 (all reagents from Merck) in 1L ddH_2O, pH 7.4.*

Lysis Buffer: *100 mM Tris, pH 7.5, 5 mM EDTA, 0.5% (w/v) SDS (Gerbu), 200 mM NaCl, 100 μg/mL Proteinase K (Roche).*

Southern blotting of Wwp1 and Wwp2 mutants

Probes for Southern blotting were prepared using Prime it II kit (Agilent; 300385) with P^{32}-labeled dCTP. After labeling the probe, free P^{32}-dCTP was removed by Bio-Spin size exclusion column (Biorad; 732-6202). DNA templates for labeling was amplified by PCR from ES cell genomic DNA using pairs of primers as following: for *Wwp1* probe, 5′-GAACTAACTGGGGCAGCC-3′ and 5′-CTGTAGCTATGTTATACTTTTTTCAC-3′ and for *Wwp2* probe, 5′-GGATCCGCTGTCTGCAGAC-3′ and 5′-TGGTTAGGAAGCTGGGTGTG-3′.

ES cell DNA obtained from each individual ES cell clone was digested with BsrGI for *Wwp1* floxed ES cells and NcoI for *Wwp2* floxed ES cells. Digested DNA samples were loaded to agarose gel electrophoresis with 0.7% ultrapure agarose (Thermo Fisher; 16500500) buffered with TAE, and DNA was transferred to Hybond-N+ (GE Healthcare; RNP303B) membrane. Membranes were incubated with a Rapid-hyb buffer (GE Healthcare; RPN1635) to avoid non-specific binding of a probe to the membrane. After overnight hybridization with a radioactive probe, membranes were washed with different concentration of SSC supplemented with 0.1% SDS. The membranes were exposed to BioMax film (Sigma-Aldrich; MS-1 143 5726) at −80°C for more than 16 h until signals were detected.

Probe synthesis for *in situ* hybridization

To generate linearized templates for *in vitro* transcription, 7 μg pCR2.1-Wwp2/miR-140 plasmid was linearized by restriction digestion with XhoI for antisense probe synthesis and with HindIII for sense probe transcription. To generate templates for Sox9 – SacI on pGEM-T-Sox9 was used. Digested DNA was subjected to electrophoresis in agarose gel and isolated with gel extraction kit (Invitrogen). The amount of template DNA was estimated by agarose gel electrophoresis using GeneRuler 1 kB ladder (Fermentas) as a standard. Next, DIG-labeled RNA probes were synthetized in an *in vitro* transcription using digoxigenin-11-dUTP (Roche) with SP6/T7 MAXIscript Transcription Kit (Thermo Fisher Scientific) following the manufacturer's protocols. The quality of RNA upon *in vitro* transcription was further analyzed by non-denaturing agarose gel electrophoresis and ethidium bromide staining. Further, RNA was resuspended in Hybmix buffer (50% Formamide, 5x SSC pH 7.0, 1% Boehringer blocking agent, DEPC-H_20, 5mM EDTA, 0.1% Tween-20, 0.1% CHAPS, 0.1mg/ml Heparin, 100μg/ml yeast tRNA and stored at −80°C until use.

In situ hybridization (DIG-labeled probes)

In situ hybridization was performed according to already published protocols with minor modifications (Britanova et al., 2008). In this study, we performed *in situ* hybridization on 16 μm thick cryosections of E15.5, E16 and P20 mouse brains. Briefly, tissue was fixed by intracardial perfusion and overnight incubation with 4%PFA/PB, washed with PBS, and passed through sucrose gradient (10%–30%) prior to freezing. Cryosections were then collected on Superfrost slides and all proceedings were carried out using RNase free reagents. Slides with sections were post-fixed for 10 minutes with 4% PFA/PB, washed with PBS and incubated with 20μg/ml proteinase K in 30mM Tris-HCl pH 8.0, 10mM EDTA pH 8.0, 0.5% SDS buffer for 2 minutes at 37°C, followed by incubation in 0.2% glycine/PBS for 5 minutes in ambient temperature. Slides were then washed with PBS and post-fixed with 4%PFA/0.2% glutaraldehyde/PBS for 20 minutes, followed by PBS washes. Next, slides were incubated with Hybmix solutions in 5XSSC/50% formamide fumes for 2 hours at 65°C. Further, RNA-probes were added to Hybmix solution and incubated with slides at 65°C for 16 hours. Next, slides were washed with 2X SSC pH 4.5 and incubated with 20μg/ml RNase A in 5M NaCl, 1M Tris-HCl pH 7.5 buffer, followed by washing in 2XSSC pH 4.5. Next, slides were incubated at 65°C in 2X SSC pH 4.5 50% formamide solution twice, each time 30 minutes. Prior to application of alkaline-phosphatase coupled anti-DIG antibody, slides with sections were washed in 50mM Tris-HCl pH7.5, 150mM NaCl, 10mM KCl, 1% Triton X-100 buffer and blocked with 20% sheep serum. After 16 hours-long incubation with the primary antibody solution for 16 hours at 4°C, slides were washed and incubated with NBT/BCIP substrate in 100mM Tris-HCl pH 9.5, 100mM NaCl, 50mM $MgCl_2$, 0.05% Tween-20 buffer until color development of requested intensity. Developing reaction was terminated by incubation of sections with PBS.

LNA-based *in situ* detection of miRNA

Wild-type hippocampal neurons grown on poly-L-lysine-coated coverslips at DIV7 were fixed with 4% PFA and washed with PBS. Cells on coverslips were then incubated with acetylation solution, and upon 5-minute-long proteinase K (5 μg/mL PBS) treatment underwent pre-hybridization at room temperature for 4-8 hours, followed by hybridization at 55°C for 16-20 hours. For each coverslip, 1 pM of LNA-DIG labeled probe purchased from Exiqon diluted with hybridization buffer was used. Coverslips were subsequently washed in 5XSSC (pH 4.5) at 60°C for 5 minutes, and with 0.2XSSC at 60°C for 1 hour. Coverslips were incubated for 10 minutes at room temperature with solution B1 followed by application of an anti-DIG antibody coupled with alkaline phosphatase diluted 1:2000 in blocking solution. After 16-20 hours incubation at 4°C, coverslips were washed in B3 solution 3 times for 10 minutes and Developer solution was applied. Color development was stopped with PBS.

Acetylation solution: *0.015% (v/v) Triethanoloamine (Sigma-Aldrich), 0.02% (v/v) HCl (Merck)*

Hybridization solution: *50% deionized (v/v) formamide, 5XSSC, 5 mM EDTA, 0.1% (v/v) Tween-20, 0.1% (w/v) 3-((−3-cholamidopropyl)-dimethyloammonio)-1-propanesulfonate (CHAPS, Biomol), 0.1 mg/mL heparin (Sigma-Aldrich), 1 mg/mL yeats tRNA.*

Solution B1: *0.1 M Tris-HCl, pH 7.5, 0.15 M NaCl*

Blocking solution: *10% (v/v) fetal bovine serum (FBS, GIBCO), 0.5% (v/v) Tween-20 in solution B1*

Soultion B3: *0.1M Tris-HCl, pH 9.5, 0.1 M NaCl, 50 mM $MgCl_2$, 0.1% (v/v) Tween-20, 20 μM levamisole-HCl (Sigma Aldrich) passed through 0.45 μm filter (Nalgene).*

Developer solution: *10 μM levamisole-HCl, 0.02% (w/v) NBT/BCIP in solution B3.*

Biochemical experiments

Preparation of brain and neuron/N2A cell lysates

Cultured primary neurons or N2A cells were washed with PBS and harvested by application of Laemmli buffer. To prepare mouse brain homogenates, tissue was homogenized in 0.32M sucrose supplemented with protease inhibitors (0.1 mM PMSF, 1 mg/L aprotinin and 0.5 mg/L leupeptin) and phosphatase inhibitors (10 mM NaF and phosphatase cocktail inhibitors, Roche).

Protein concentration measurements

Protein concentration was estimated with BCA kit (Thermo, Pierce) following manufacturer's protocol. The absorbance of protein complexes was measured with Plate Reader (Bio-Rad). Protein concentration in sample was calculated based on the absorbance value for BSA standards (Thermo, Pierce).

Sodium dodecyl sulfate polyacrylamide gel electrophoresis (SDS-PAGE)

Proteins were separated under denaturing conditions using SDS-PAGE. Protein samples were dissolved in Laemmli buffer and incubated at 65°C for 15 minutes, loaded on two-layered acrylamide gel and subjected to electrophoresis with Running buffer (Bio-Rad) at 90 V for the stacking gel and 120 V for the separating gel. Protein gel made of stacking and seperating gels was casted according to Bio-Rad Protean II system.

Laemmli buffer: *10% (v/v) glycerol, 50 mM Tris-HCl, pH6.8, 2% (w/v) SDS, 2 mM EDTA, 10 mM DTT, 0.05% (w/v) Bromophenol blue.*

Stacking gel: *3.75% (v/v) acrylamide/N,N'-methylene-bis-acrylamide (35.5:1) solution (National Diagnostics), 125 mM Tris-HCl, pH 6.8, 0.1% (w/v) SDS, 0.05% (w/v) ammonium persulfate (APS, Sigma-Aldrich), 0.005% (v/v) N,N,N',N'-tetramethylethylenediamine (TEMED, Serva).*

Resolving gel: *8 to 15% (v/v) acrylamide/N,N'-methylene-bis-acrylamide (35.5:1) solution, 325 mM Tris-HCl, pH 8.8, 0.1% (w/v) SDS, 0.05% (w/v) APS, 0.005% (v/v) TEMED.*

Running buffer: *25 mM Tris-HCl, 250 mM glycine (Sigma-Aldrich), 0.1% (w/v) SDS, pH 8.8.*

Western blotting

Separated proteins were transferred onto a nitrocellulose membrane (Amersham Protran, 0.2 μm NC, GE Healthcare) in Transfer buffer under a constant current of 80 mA for 10 hours using a tank blotting unit (Hoefer, TE22). After transfer, membrane was rinsed with ddH_2O to remove gel debris and stained with MEM Code (Thermo Scientific) kit to visualize separated proteins. After destaining, the membrane was rinsed with TBS buffer and subjected to blocking with Blocking buffer for 30 minutes at room temperature with moderate shaking, incubated with the primary antibody diluted in blocking buffer for 3 hours at room temperature and washed 3 times with TBS-T for 15 minutes. Next, the membrane was incubated with secondary antibodies conjugated with horseradish peroxidase (HRP) or fluorophores diluted in blocking buffer for 1 hour. After subsequent washing (3 times, 15 minutes), the signal on the membrane was developed with chemiluminescence detection system (ECL) on films (Amersham Hyperfilm ECL, GE Healthcare) or detected with Odyssey CLx Infrared Imaging System (LI-COR).

Transfer buffer: *25 mM Tris-base, 190 mM glycine, 20% (v/v) methanol.*

TBS: *10 mM Tris-HCl, 150 mM NaCl, pH 7.5.*

TBS-T: *TBS, 0.1% (v/v) Tween-20.*

Blocking buffer: *5% (w/v) skimmed milk (Frema), 0.1% (v/v) Tween-20, TBS.*

Quantification of protein levels

Protein levels were normalized to total protein amount in the sample measured as MEM Code staining intensity of respective lane, or relative to β-actin and expressed relative to the level in the reference sample.

Subcellular fractionation of mouse brains

Subcellular fractionation in sucrose gradients of the brain tissue was performed according to published protocols with slight modifications. All described procedures were performed at 0-4°C. Immediately after decapitation, mouse cortex was isolated in Solution A. Cortices from one mouse were homogenized in 3 mL of Solution A supplemented with 0.2 mM PMSF, 1 μg/mL aprotinin, and 0.5 μg/mL leupeptin using Teflon-glass homogenizer with 20 strokes at 1200 rpm (Potter S, Braun). Homogenate was fractionated by centrifugation at 82 500 *g* for 2 hours in discontinuous sucrose density gradient, comprising 0.85 M, 1.0 M, 1.2 M sucrose solutions. The solution on top of the first interface was collected as supernatant, the interface between 0.32 and 0.8 M as the myelin fraction, the one between 0.8 and 1.0 M as the ER/Golgi fraction the one between 1.0 and 1.2 M as synaptosome fraction (P2C), and the pellet as the mitochondria-enriched fraction. Purified P2C fractions were subjected to comparative label-free mass spectrometry.

Solution A: *0.32 M sucrose (Merck), 1 mM $NaHCO_3$ (Merck).*

Label-free protein quantification

Proteolytic digestion. Synaptosomal protein fractions (P2C) corresponding to 20 μg protein were dissolved in lysis buffer and processed according to a filter-aided sample preparation (FASP) protocol modified essentially as described by Distler et al. Unless stated otherwise, all steps were automated on a liquid-handling workstation equipped with a vacuum manifold (Freedom EVO 150, Tecan) by using an adaptor device constructed in-house. Briefly, protein samples were lysed and reduced by shaking for 30 min at 37°C and subsequently loaded on centrifugal filter units (30 kDa MWCO, Millipore). After removal of the detergents by washing twice with wash buffer, proteins were alkylated with 50 mM iodoacetamide in 8 M urea/0.1 M Tris pH 8.5 (20 min at RT), followed by two washes with wash buffer to remove excess reagent. Buffer was exchanged by washing three times with 50 mM ammonium bicarbonate (ABC) containing 10% acetonitrile. After three additional washes with 50 mM ABC/10% acetonitrile, which were performed by centrifugation to ensure quantitative removal of liquids, proteins were digested overnight at 37°C with 500 ng trypsin in 40 μl of the same buffer. Tryptic peptides were recovered by centrifugation followed by two additional extraction steps with 40 μl of 50 mM ABC and 40 μl of 1% trifluoroacetic acid (TFA), respectively. Aliquots of the combined flow-throughs were spiked with 10 fmol/μl of yeast enolase 1 tryptic digest standard (Waters Corporation) for quantification purposes (Silva et al., 2006) and directly subjected to analysis by liquid chromatography coupled to electrospray mass spectrometry (LC-MS).

Lysis Buffer: 7 M urea (Sigma-Aldrich), 2 M thiourea (Sigma-Aldrich), 10 mM DTT, 2% CHAPS, 0.1 M Tris pH 8.5.

Wash Buffer: 8 M urea, 10 mM DTT, 0.1 M Tris pH 8.5.

LC-MS analysis. Nanoscale reversed-phase UPLC separation of tryptic peptides was performed with a nanoAcquity UPLC system equipped with a Symmetry C18 5 μm, 180 μm × 20 mm trap column and a HSS T3 C18 1.8 μm, 75 μm × 250 mm analytical column maintained at 45°C (Waters Corporation). Injected peptides were trapped for 4 min at a flow rate of 8 μl/min 0.1% TFA and then separated over 120 min at a flow rate of 300 nl/min with a gradient comprising two linear steps of 3%–35% mobile phase B in 105 min and 35%–60% mobile phase B in 15 min, respectively. Mobile phase A was water containing 0.1% formic acid while mobile phase B was acetonitrile containing 0.1% formic acid. Mass spectrometric analysis of tryptic peptides was performed using a Synapt G2-S quadrupole time-of-flight mass spectrometer equipped with ion mobility option (Waters Corporation). Positive ions in the mass range m/z 50 to 2000 were acquired with a typical resolution of at least 20,000 full width at half maximum and data were lock mass corrected post-acquisition. Analyses were performed in the ion mobility-enhanced data-independent acquisition mode with drift time-specific collision energies as described in detail by Distler et al. Continuum LC-MS data were processed for signal detection, peak picking, and isotope and charge state deconvolution using Waters ProteinLynx Global Server (PLGS) version 3.0.2. For protein identification, a custom database was compiled by adding the sequence information for yeast enolase 1 and porcine trypsin to the UniProtKB/Swiss-Prot mouse proteome and by appending the reversed sequence of each entry to enable the determination of false discovery rate (FDR). Precursor and fragment ion mass tolerances were automatically determined by PLGS 3.0.2 and were typically below 5 ppm for precursor ions and below 10 ppm (root mean square) for fragment ions. Carbamidomethylation of cysteine was specified

as fixed and oxidation of methionine as variable modification. One missed trypsin cleavage was allowed. Minimal ion matching requirements were two fragments per peptide, five fragments per protein, and one peptide per protein. The FDR for protein identification was set to 1% threshold.

P2C fractions from five *miR-140*$^{+/+}$ and *miR-140*$^{-/-}$ cortices per condition were processed with replicate digestion and injection, resulting in four technical replicates per biological replicate and thus in a total of 40 LC-MS runs to be compared.

Cell culture

Media and solutions

Papain solution: 20 units of papain (Worthington) were added to 1 mL of 0.2 mg/mL cysteine, 1 mM $CaCl_2$ and 0.5 mM EDTA in Dulbecco's Modified Eagle Medium (DMEM, GIBCO, Life Technologies). The solution was then saturated with carbogen – 95% oxygen and 5% carbon dioxide – until clear and filter-sterilized (0.22 μm, Millipore).

Stop solution: 2.5 mg/mL bovine serum albumin (BSA, Sigma-Aldrich), 2.5 mg/mL ovoalbumin (Sigma-Aldrich), 10% (v/v) FBS in DMEM.

Complete Neurobasal medium: 500 mL Neurobasal A (GIBCO, Life Technologies), 10 mL B-27 (GIBCO, Life Technologies), 5 mL GlutaMAX (GIBCO, Life Technologies), 5 mL penicillin/streptomycin (Life Technologies, GIBCO).

HEK cell medium: 500 mL DMEM, 50 mL FBS, 5 mL GlutaMAX, 5 mL penicillin/streptomycin.

RIPA buffer: 20 mM Tris-HCl, pH 7.5 (4°C), 150 mM NaCl, 1 mM EDTA, 1% (v/v) NP-40 (Fluka), 1% (w/v) sodium deoxycholate (Wako Chemicals), PhosphoSTOP (Roche), 10 mM NaF (Sigma-Aldrich), 0.2 mM PMSF, 1 μg/mL aprotinin, 0.5 μg/mL leupeptin.

Murine primary hippocampal neurons

Treatment of coverslips for culturing primary neurons

Prior to cell culture, coverslips (Menzel-Gläser) were incubated with 1 M HCl for 16-20 hours, thoroughly rinsed with dH_2O, incubated with 70% ethanol, again washed with dH_2O, placed in cell culture dishes in sterile conditions (laminar flow hood) and UV-treated for 1 hour. Further, to provide the primary neurons with an adhesion substrate, the coverslips were incubated with poly-L-lysine (Sigma-Aldrich) diluted 1:10 in PBS (GIBCO, Life Technologies) for 1 hour at 37°C. Next, coverslips were rinsed with PBS three times and incubated with Complete Neurobasal medium at 37°C until plating of neurons.

Calcium phosphate transfection

Primary hippocampal or cortical neurons were transfected at DIV1 or DIV4 (as indicated) with calcium phosphate transfection method. Prior to transfection, the DNA-calcium precipitates were prepared accordingly to published works (Jiang and Chen, 2006). For one coverslip of 24 well-plate, 1 μg of plasmid DNA was mixed with 3.1 μL of 2 M $CaCl_2$ and sterile H_2O was added till 25 μL of total volume. The DNA mix was dropwise added to 25 μL of 2XHBS, 1/8 of the solution at a time with gentle agitation for 2 s after each drop. The solution was then incubated at room temperature in darkness for 30 minutes. Complete Neurobasal medium was replaced with the same volume of Neurobasal A, filtered and stored at 37°C. Upon pipetting up and down for 5 times, 50 μL of the DNA-calcium solution was applied on each coverslip and the neurons were placed at 37°C in the incubator until precipitates became visible in the light microscope (approximately 20 minutes). Coverslips were subsequently washed with HBSS equilibrated in 10% carbon dioxide at 37°C until all visible precipitates disappeared. The original complete Neurobasal medium was placed back on the neurons and cells were further cultivated at 37°C/5%CO_2. For the quantification of the number of axons, cells were immunostained with markers for axons and dendrites, and counted were neurites positive for SMI312 (1:2000, Milipore, RRID: AB_509993), or Tau-1 (1:1000, Millipore, MAB3420, clone PC1C6) and negative for MAP2 (1:1000, Novus, RRID: AB_350528).

2XHBS: 274 mM NaCl, 10 mM KCl, 1.4 mM Na_2HPO_4, 15 mM glucose, 42 mM HEPES (Sigma-Aldrich, H3375), pH 7.08 adjusted with 10 M NaOH. Buffer was aliquoted and stored at −20°C.

Ex Utero Electroporation (EUE)

For analysis of development of cortical neurons *in vitro*, particularly to quantify axon growth, branching and extension and dendrite growth, E14.5 mouse heads were collected and subjected to *ex utero* electroporation. Like for *in utero* electroporation, DNA of the final concentration 1 μg/μL was injected with a glass capillary to fill the entire volume of both lateral embryonic ventricles, followed by electroporation using 6 pulses of 35V applied using platinum electrodes. The heads were then placed in ice cold HBSS solution until proceeding with primary neuron culture.

HEK293FT/293T/N2A Transfection

Transfection of HEK293FT/293T/N2A was performed at 80%–90% confluency using Lipofectamine2000 (Invitrogen) following the manufacturer's instructions with 1:2 DNA/Lipofectamine2000 ratio (μg/μL).

Lentivirus production and infection of primary hippocampal cells

Briefly, HEK293FT cells grown in OPTI-MEM supplemented with 10% FBS on 15 cm Petri dish, were co-transfected with 40 μg of pFUGW or 40 μg of pFUGWiCre with 16 μg of packaging plasmid (pMD2.G) and 16 μg of envelope plasmid (pCMVdeltaR8.2). Culture medium was exchanged to DMEM supplied with 1% (v/v) GlutaMax, 1% (v/v) penicillin/streptomycin, 2% FBS, and 10 mM sodium butyrate (Merck) 6 to 16 hours after transfection. Culture medium was harvested 48 hours post-transfection, filtered through 45 μm filters (Millipore), and applied to AMICON filter system (Millipore) to concentrate viral particles by centrifugation at 3500 *g* at 4°C to approximately 100 μL. The filter was subsequently washed with cold Neurobasal A. The virus stock was further dialyzed against TBS at 4°C for 16-20 hours in a sterilized beaker, aliquoted, and flash-frozen in liquid nitrogen. Viruses were stored in −80°C until used.

Upon thawing the aliquot of the virus stock, appropriate volume of the virus stock was added to neuronal medium at DIV1. The virus titer was determined by estimation of GFP expression level in neuronal cultures. At appropriate stage of the culture, infected neurons were washed with PBS four times and lysed with RIPA buffer at 4°C. The homogenate was centrifuged for 10 minutes at 14 *kg* in cold bench-top microfuge and supernatant was used in biochemical experiments.

TBS: 20 mM Tris-HCl, pH 8.0 (4°C), 150 mM NaCl.

Immunocytochemistry

Cells cultured on coverslips were fixed with cold (4°C) 4% PFA, 4% sucrose (Merck) in PB buffer for 20 minutes in room temperature, washed three times with PBS and incubated with Blocking buffer for 30 minutes. Next, cells were incubated with primary antibodies diluted with blocking buffer accordingly for 16-20 hours at 4°C with moderate shaking, followed by washing 3 times for 30 minutes with PBS. Further, secondary antibodies coupled to appropriate fluorophore diluted in blocking buffer were applied for 2 hours at room temperature. After washing 3 times with PBS for 30 minutes, coverslips were briefly rinsed with ddH_2O and mounted on Superfrost Plus glass slides (Thermo Scientific) with Immu-Mount mounting medium (Shandon, Thermo-Scientific).

Blocking buffer: 5% goat serum (GIBCO, Life Technologies), 0.3% Triton X-100 (Roche), 0.1% fish skin gelatin (Sigma-Aldrich) in PBS buffer

Histology

Perfusion

Intracardiac perfusion with 4% PFA in PB buffer was conducted using pump apparatus PA-SF (IKA Labortechnik). Perfusion was performed on animals older than P3. Briefly, mice were intraperitoneally injected with a lethal dose of pentobarbital (Narkoren, Boehringer Ingelheim). Mouse was then placed in darkness to reach unresponsiveness, verified by toe pinch-response. Lateral incision through abdominal wall was followed by separation of the diaphragm from the liver and diaphragm was further incised together with the rib cage until the full exposure of the pleural cavity. Upon fixation of the sternum with hemostat above the animal head, sterile 25-gauge winged cannula was introduced to the heart through the posterior end of the left ventricle. Cannula was fixed to the heart with a hemostat. A small incision with iris scissors was performed in the heart's right atrium preventing damage of the descending aorta to create outlet valve. Initial PBS flush was performed at pump speed 12 for 1 minute and paraformaldehyde solution was then delivered at a constant rate (pump speed 10) for 2 minutes. The brain was further isolated from animal's skull and incubated with 4% PFA in PB buffer at 4°C for 16-20 hours with moderate agitation. Next, brains were transferred to PBS with 0.01% sodium azide (Sigma-Aldrich) and kept at 4°C until further processing.

For animals younger than P3, brains were isolated from the skulls and immediately immersed in 4% PFA in PB for 16-20 hours, followed by incubation with PBS with 0.01% sodium azide (Sigma-Aldrich) at 4°C.

Cryosectioning

For all histological procedures excluding preparation of tissue for *in situ* hybridization, brain sections were prepared on Leica CM3050S cryostat. Prior to cryosectioning, brains were incubated for at least 5 hours with 10% sucrose in PBS, followed by incubation with 30% sucrose in PBS until the organs reached the bottom of the glass beaker. Next, brains were frozen in −38 to −40°C isopentane (Roth). Coronal cryosections of appropriate thickness were either collected immediately on Superfrost Plus glass slides or in PBS/0.01% sodium azide solution. Sections of 50 μm thickness and/or 100 μm-thick sections were used for neuronal distribution and polarity classification studies.

Immunohistochemistry

Brain sections of PFA-perfused mice were washed with PBS three times at room temperature and incubated for 5 minutes with moderate agitation with 1 mg/mL sodium borohydride (Sigma-Aldrich) solution in PBS. Borohydride treatment was skipped for brain sections of non-perfused mice. Subsequently, the sections were thoroughly washed with PBS and incubated with Blocking solution for 1 hour at room temperature. Further, sections were incubated with the primary antibody and DAPI diluted in blocking buffer for 16-20 hours at 4°C, washed in PBS three times for 30 minutes and incubated with secondary antibody coupled to a fluorophore of choice. Next, sections were incubated with PBS for 30 minutes three times and mounted with cover glass (Menzel-Gläser) and Immu-Mount mounting medium (Shandon, Thermo-Scientific).

Blocking solution: 5% goat serum, 0.5% (v/v) Triton X-100, PBS

Antibodies: Details on antibodies used for western blotting (WB), immunocytochemistry (ICC), and immunohistochemitsty (IHC) are listed in Table S6.

Wwp1 (0221) and Wwp2 (7425A) antibodies were generated against GST-fused Wwp1 (149-345 amino acids) and the mixture of two Wwp2 peptides (MASASSSRAGVALPFEKS and RESSGTAIAPETRHQPPSTN) respectively.

Luciferase assay

Luciferase assay was carried out accordingly to manufacturer's protocol (GeneCopoeia). HEK293T cells (Thermo Fisher) were transfected with Turbofect (Thermo Fisher) with pMCS vectors and a pA5-Tag reference vector encoding for secretable alkaline phosphatase with or without pWPXL-Sox9 plasmid. Fragments of *Wwp1* or *Wwp2/miR-140* promoters (precise genomic sequences indicated in Figure 6H) including putative Sox9 consensus binding sequences were cloned upstream of secreted *Gaussia* luciferase coding sequence in pMCS plasmid. Medium was aspirated 72 hours post-transfection, snap-frozen, and stored at −80°C until the measurement. To measure *Gaussia* luciferase activity, the substrate was added to the medium 60 s prior to the measurement and the signals

were integrated for 3 s. For alkaline phosphatase activity measurements, the substrate was automatically added to the medium 0.5 s prior to the measurement, which included integration time of 2 s. Measurements and application of substrates were acquired using Glomax Luminometer (Turner Biosystems). *Gaussia* luciferase activity was then expressed relative to alkaline phosphatase activity for each technical replicate.

Flow cytometry

For the assessment of miR-140-mediated translational Fyn repression, the reporter vector was constructed by fusing Fyn 3′UTR to the down-stream of the stop codon of EGFP coding sequence in pXhoI vector. Scramble miRNA and miR-140 were synthesized by DNA core facility in MPIem. Using Lipofectamine2000 (Life Technologies), HEK293T cells were co-transfected with 80 ng of the reporter vector and 600 ng of scramble RNA, 600 ng of synthetic miR-140, or 50 nM of miR-140 inhibitor (QIAGEN), in each condition with 40 ng of pCAG-tdTomato. 48 hours post-transfection, HEK293T cells were washed with PBS and incubated with 0.25% trypsin-EDTA solution (GIBCO) for 5 minutes at room temperature, triturated and subjected to flow cytometry (BD FACSCanto II). For each assay point, EGFP fluorescence of at least 1000 transfected cells in the living gate was measured. To control for transfection efficiency, GFP fluorescence intensity was measured only in cells gated for tdTomato expression. Measurements were analyzed with FlowJo software.

In utero electroporation (IUE)

Glass capillary preparation

Micropipettes for IUE were prepared from 1.5 – 1.8 X 100 mm borosilicate glass capillaries (Kimble and Chase) using HEKA PIP5 temperature-controlled pipette puller. To ensure the appropriate tip diameter, the filament was heated to 1000°C and pulling of glass capillary was controlled manually, allowing for slow extension of glass.

Plasmid DNA for IUE

Plasmid DNA was prepared with EndoFree Plasmid Maxi Kit (QIAGEN). Prior to IUE, DNA was diluted in endotoxin-free TE buffer and mixed with 0.1% Fast Green FCF (Sigma-Aldrich). Final concentration of DNA used for transfecting cortical progenitors was 200-500 ng/μL. Before injection to embryonic brain, the tip of the microcapillary was broken with fine forceps to enable liquid flow.

Procedure

E13.5 or E14.5 mouse embryos were subjected to IUE as described previously (Hsia et al., 2014), with minor modifications. To electroporate the DNA mixture into the ventricular cells, 4-6 pulses of 32-35V were applied using platinum electrodes. For the analysis of neuronal morphology and laminar distribution, cortical progenitors were *in utero* electroporated at embryonic day 14.5 (E14.5), and brains of treated mice were isolated and fixed at E15.5, E17.5, E18.5, P0, or at P10. Live imaging of cortical slice cultures was performed 24 h after IUE at E13.5. Analysis of laminar distribution of neurons and classification and reconstruction of neuronal morphologies were carried out manually after immunostaining using ImageJ software (NIH). Permeabilization and immunohistochemistry were carried out as described previously (Ripamonti et al., 2017). Slice cultures for live imaging were prepared according to published protocols with slight modifications (Polleux and Ghosh, 2002).

Live imaging

After *in utero* electroporation of E13.5 cortical progenitors, cortical slice culture was prepared from embryos at E14.5. Brains were removed from the skulls and quickly dissected in ice-cold complete HBSS. Next, the brains were embedded in 3% low-melting point agarose (Qbiogene) prepared in Complete HBSS and placed on ice. Further, 350 μm-thick coronal vibratome sections (Microm, HM650V) were placed on laminin/poly-L-lysine (0.1 mg/mL each) coated inserts (35 mm), immersed in Imaging medium. Slice cultures were placed in 37°C, 5% CO_2 for 8 hours to recover. Next, Z stacks of confocal images (Z-step 0.5 μm) throughout developing cortical plates were taken consecutively every 30 minutes using spinning disc confocal microscope (Zeiss ZEN 2012). Imaging was continued for no longer than 40 hours with slices cultures incubated at 37°C in the presence of 5% CO_2 throughout the session. Electroporated neurons were tracked using ImageJ and the plugin TrackMate. The cells were traced in a semi-automatic way with the Laplacian of Gaussian filter to recognize somata. Estimated blob diameter (cell soma) was set at 10 μm, the threshold at 0.3. For the tracker, linking maximum distance was defined as 25 μm, the gap-closing maximum distance 15 μm, and the gap-closing maximum frame gap as 2. Only cells present in the recording for more than two and a half hours (five frames) were analyzed. The total track displacement was measured as the length of the shortest path between the two locations. Total distance traveled was defined as the length of the actual path between the two locations.

Imaging medium: Neurobasal (GIBCO), 5% horse serum (GIBCO), 2 mM glutamine (GIBCO), penicillin/streptomycin, supplemented with B27 (2X final) and N2 (0.5X final).

Complete HBSS: HBSS (GIBCO), 2.5 mM HEPES pH 7.4, 30 mM glucose, 1 mM $CaCl_2$, 1 mM $MgSO_4$, 4 mM $NaHCO_3$.

Image acquisition, analysis and statistics

Confocal imaging of immunostaining signals and analysis

Imaging of brain coronal cross sections after *in utero* electroporation was performed at −1.06 mm to −2.06 mm from Bregma for P10 brains and at the level of anterior commissure for E18.5 and P0 brains.

For imaging of the overview of immunostaining, Leica SPL, Sp2 and Sp8 confocal microscope was used. Imaging of fixed primary cortical neurons was performed using Leica Sp8 microscope.

For quantitative imaging of Sox9 signal from *Sox9*$^{f/f}$ neurons expressing GFP or GFP and iCre, Leica Sp5 microscope with 40X objective with confocal scanning zoom 2.5 was used. Quantification of Sox9 signals was performed using ImageJ measure tool on manually selected somata. Intensities were normalized to the average signal intensity of control neurons.

Stitching of images after acquisition was performed using ImageJ Pairwise Stitching Plugin or using Photoshop. Analyses of length and cell tracings were performed using confocal Z stack and ImageJ Simple Neurite Tracer. Total extension of the axon was measured as total length of all axons emerging from a single neuron, identified by immunostaining for SMI312 or Tau and lack thereof for MAP2. Sholl analyses were performed on maximum Z-projections of confocal images of neurons, whose axon(s) was first identified using immunostaining and manually removed, using ImageJ Sholl Analysis command. Starting radius was defined as 10 μm and ending radius 100 or 150 μm, as indicated. Radius step size was set as 1 μm. Sum of Crossing Dendrites was quantified per a single neuron.

Colocalizations with fate markers and % neurons with a single TP was performed manually counted using Cell Counter Plugin in ImageJ software. Multiple TPs were defined as emerging from different positions on the soma and projecting toward the ventricle.

Light and epifluorescence microscopy

Apochromatic fluorescence stereomicroscope Leica MZ16F was used to acquire images of *in situ* hybridization results.

QUANTIFICATION AND STATISTICAL ANALYSIS

Quantitative western blotting

Quantification of protein levels was performed with ImageStudioLite (Li-Cor) software using scans of films after exposure to ECL chemiluminescence or data acquired by Odyssey cLX. The bands representing respective proteins were manually outlined and the signal intensity was measured. Signal intensity (x) is defined as the sum of the individual pixel intensity values for a selected shape (a) subtracted by the toatal background signal [i.e., average intensity value of the pixels in the background (b) multiplied by the total number of pixels within the region of interest (c)]; x = a-b*c. Protein level was expressed relative to the signal for β-actin detected in respective lane, or to the total protein amount as measured by the integral of MEM Code Staining intensity estimated with Tracing tool of ImageJ software (Schneider et al., 2012). For statistical analysis of the difference between two groups, t test was used and p value of less than 0.05 was considered as significant.

Label-free protein quantification

The freely available software ISOQuant (http://www.immunologie.uni-mainz.de/isoquant/) was used for post-identification analysis including retention time alignment, exact mass and retention time (EMRT) and ion mobility clustering, data normalization, isoform/homology filtering, and calculation of absolute in-sample amounts for each detected protein according to the TOP3 quantification approach. Only peptides with a minimum length of seven amino acids, which were identified with PLGS scores above or equal to 5.5 in at least two runs, were considered. FDR for both peptides and proteins was set to 1% threshold and only proteins reported by at least two peptides were quantified using the TOP3 method. The parts per million (ppm) abundance values (i.e., the relative amount (w/w) of each protein in respect to the sum over all detected proteins) were log2-transformed and normalized by subtraction of the median derived from all data points for the given protein. Significant changes in protein abundance were detected by moderated t-statistics with an empirical Bayes approach and false discovery (FDR)-based correction for multiple comparisons (Kammers et al., 2015). For this purpose, the Bioconductor packages "limma" (Ritchie et al., 2015) and "q-value" (Storey and Tibshirani, 2003) were used in RStudio, an integrated development environment for the open source programming language R.

Axon counting assays *in vitro*

For quantification of the number of axons projected by single primary neurons, numbers of cells projecting 0, 1, or multiple axons were counted. Axons were defined as processes with prominent SMI312 or Tau-1 staining and no detectable MAP2 signals. Cells were imaged and scored by a blind observer. Images of transfected hippocampal neurons were acquired with AxioImager Z.1 (Carl Zeiss), 40X objective and water immersion and analyzed with AxioVision software. For analyses of cortical primary neurons, confocal Z stacks were acquired using 40X objective of Sp8 Leica microscope. Each quantification represents data from at least two independent primary culture experiments. For statistical analyses of axon acquisition in groups, χ^2 test was employed and for comparison of frequencies in contingency table format, Fisher's exact test was employed.

Quantification of distribution of cortical neurons and polarity classification

Z stacks of 100 μm-thick mouse cortices after IUE were acquired with Leica SPL, Sp2, or Sp8 confocal microscope with 10X or 20X objective lens with digital zoom 1.5 for E18 and P0 cortices and without any digital zoom for P10 cortices. Maximum projections of confocal stacks were divided into 5 bins of identical dimensions. Numbers of transfected neurons in each bin were manually counted with Cell Counter plug-in of ImageJ software and the number of neurons in each bin expressed relative to the total number of transfected nerve cells. Based on previously published works (Barnes et al., 2007; Namba et al., 2014; Sasaki et al., 2002), neurons were manually scored based on their morphologies into respective classes. Neurons in E18 or P0 mouse cortices were classified into two groups; BP neurons with two processes emerging from opposite poles of the soma parallel to the axis perpendicular to pia, and non-BP neurons with more or less than two neurites or with misoriented neurites. Neurons in P10 mouse brains were sorted

into a pyramidal morphology group (one prominent apical dendrite oriented perpendicular to the pial surface) or non-pyramidal (no apparent dendrite with prominent apical shaft, multiple prominent dendrites, or apical dendrite forms an angle larger than 15° with an axis perpendicular to the pial surface). Frequencies of neurons in BP or pyramidal class within a bin or entire cortical plate were quantified using Cell Counter plug-in of ImageJ software. Numbers of neurons with BP or pyramidal morphology were expressed as a fraction of electroporated nerve cells in each bin or in the entire cortex. Tracing of representative neurons were performed manually after binarizing of thresholded images. For statistical analyses, two-way ANOVA with appropriate post hoc test indicated in the figure legend was used.

Statistical analyses

All statistics were performed using SPSS v.17 (San Diego, USA) or Prism Graph Pad software. All statistical details of experiments can be found in Supplementary Tables and description of statistical tests used, definition of center, dispersion, precision and definition of significance are additionally in the figure legends. On numerical data, first normal distribution of datapoints was tested for using D'Agostino and Pearson omnibus normality test. For normally distributed data, we then used unpaired two-tailed t-test or one/two-way ANOVA with Bonferroni post-hoc test; for data with not normal distribution, we employed Mann Whitney test to compare two groups or Kruskal-Wallis test with Dunn's Multiple comparison test for comparison between multiple groups.

Neuron, Volume *100*

Supplemental Information

Polarity Acquisition in Cortical Neurons Is Driven by Synergistic Action of Sox9-Regulated Wwp1 and Wwp2 E3 Ubiquitin Ligases and Intronic miR-140

Mateusz C. Ambrozkiewicz, Manuela Schwark, Mika Kishimoto-Suga, Ekaterina Borisova, Kei Hori, Andrea Salazar-Lázaro, Alexandra Rusanova, Bekir Altas, Lars Piepkorn, Paraskevi Bessa, Theres Schaub, Xin Zhang, Tamara Rabe, Silvia Ripamonti, Marta Rosário, Haruhiko Akiyama, Olaf Jahn, Tatsuya Kobayashi, Mikio Hoshino, Victor Tarabykin, and Hiroshi Kawabe

SUPPLEMENTARY FIGURES AND FIGURE LEGENDS

Supplementary Figure S1.

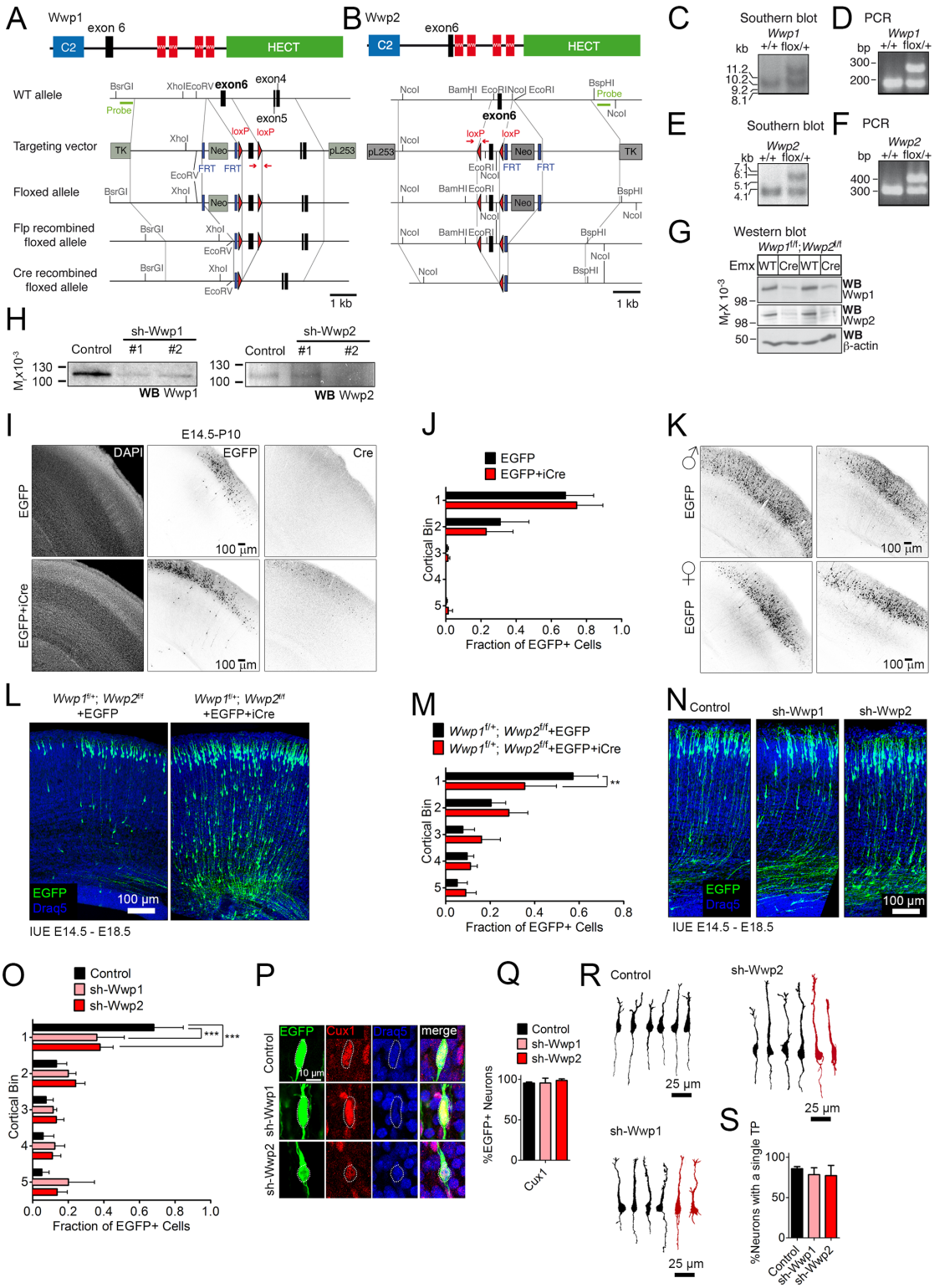

Supplementary Fig. S1. Generation and basic characterization of *Wwp1*$^{f/f}$, *Wwp2*$^{f/f}$, and *Wwp1/2*$^{f/f}$ mouse lines and sh-RNA vectors to knock down Wwp1 and Wwp2. Related to Fig. 1.

(A, B) Targeting strategies for *Wwp1* (A) and *Wwp2* (B) genes. Domain structures of Wwp1 and Wwp2 proteins (top schemes), structures of the wild type (WT) *Wwp1* and *Wwp2* alleles, Wwp1 and Wwp2 targeting vectors (Targeting vector), floxed mutant alleles (Floxed allele, Flp recombined floxed allele, and Cre recombined floxed allele) of *Wwp1* and *Wwp2*. Exons are represented as black boxes. Flp recombinase targets (FRT) and loxP sites are represented as blue rectangles and red triangles, respectively. After homologous recombination and germ line transmission of mutant alleles, *Wwp1*$^{fl/+}$ and *Wwp2*$^{fl/+}$ mice were crossed with the FLP-deleter to excise the neomycin resistance cassettes. Subsequently, exons flanked by loxP sites in mutant alleles were floxed-out by Cre. Genomic DNA fragments for Southern blotting probes are represented as green bars in WT alleles, and genotyping PCR primers are represented as red arrows in Targeting vectors. pL253, pL253 gene targeting vector; Neo, Neomycin resistance cassette; TK, herpes simplex virus thymidine kinase expression cassette. (C-G) Verification for gene targeting. (C, E) Southern blot analyses of genomic DNA samples of the WT (+/+) and targeted (flox/+) embryonic stem cells. BsrGI and NcoI were used for digestion of the genomic DNA purified from cloned embryonic stem cells of *Wwp1*$^{fl/+}$ line (C), and *Wwp2*$^{fl/+}$ line (E), respectively. 10.7 kb and 12.7 kb bands represent WT and Wwp1 floxed alleles in (C), 4.0 kb and 6.0 kb bands represent WT and Wwp2 floxed alleles in (E). (D, F) Genotyping PCR analyses of genomic DNA samples from WT (+/+) and heterozygous (flox/+) mice. (G) Western blotting in cortical lysates of P5 mice of indicated genotypes using anti-Wwp1, anti-Wwp2, and anti-β-actin antibodies. (H) Western blotting using anti-Wwp1 and anti-Wwp2 antibodies using lysates of primary cortical neuronal cultures, infected with lentiviruses expressing scramble sh-RNA (Control), sh-RNA for Wwp1 knock-down (sh-Wwp1 #1, sh-Wwp1 #2) and sh-RNA for Wwp2 knock-down (sh-Wwp2 #1, sh-Wwp2 #2). For all experiments we used sh-Wwp1 #1 and sh-Wwp2 #2. (I-K) Laminar distribution and morphology in cortical neurons are independent of Cre expression and gender in wild type mice. Related to the entire manuscript. (I) Representative images of DAPI staining, anti-EGFP immunolabeling, and anti-Cre immunolabeling in P10 cortices after IUE at E14.5 with plasmids for EGFP or for simultaneous expression of EGFP and Cre. (J) Distribution of EGFP-, and EGFP- and Cre-expressing neurons *in vivo* (Table S1G). (K) Representative images of anti-EGFP immunolabeling in P10 cortices after IUE at E14.5 with plasmids for

EGFP and myristoilated Venus expression in male and female wild type mice. Note no qualitative difference in neuronal distribution and normal pyramidal morphology. (L-S) Phenotype of the single KD of Wwp1 and Wwp2 and single *Wwp2* KO. Related to Fig. 1. (L) Representative images of EGFP immunostaining signals and Draq5 labeling in E18.5 cortices of $Wwp1^{f/+}$; $Wwp2^{f/f}$ mice electroporated *in utero* to express EGFP, or EGFP and Cre at E14.5. (M) Quantification of laminar distribution of cortical neurons in $Wwp1^{f/+}$; $Wwp2^{f/f}$ mouse brains after electroporation with EGFP, or EGFP and iCre (Table S1H). (N) Representative images of EGFP/Venus immunostaining signals and Draq5 fluorescence in E18.5 cortices of wild type mice electroporated *in utero* to express EGFP/Venus and control sh-RNA, or EGFP/Venus and sh-Wwp1, or EGFP/Venus and sh-Wwp2 at E14.5. (O) Quantification of laminar distribution of cortical neurons in mouse brains after electroporation with indicated constructs (Table S1I). (P) Representative images of immunostaining against EGFP and Cux1 antibody and Draq5 fluorescence after electroporation with indicated vectors. Cell soma is marked with a dotted line. (Q) Quantification of fraction of neurons expressing indicated vectors, positive for Cux1 (Table S1J). (R) Representative EGFP-fluorescence based tracings of neurons expressing indicated vectors. Neurons with aberrant morphology (i.e. multiple trailing processes) are colored red. (S) Quantification of the number of neurons with a single and multiple trailing process (TP) (Table S1K). Results on graphs are represented as averages ± S.D. For statistical analyses, (J), (M), (O), two-way ANOVA with Bonferroni post-hoc test; (Q) and (S), one-way ANOVA with Bonferroni post-hoc test. *** $p < 0.001$; ** $0.001 < p < 0.01$.

Supplementary Figure S2.

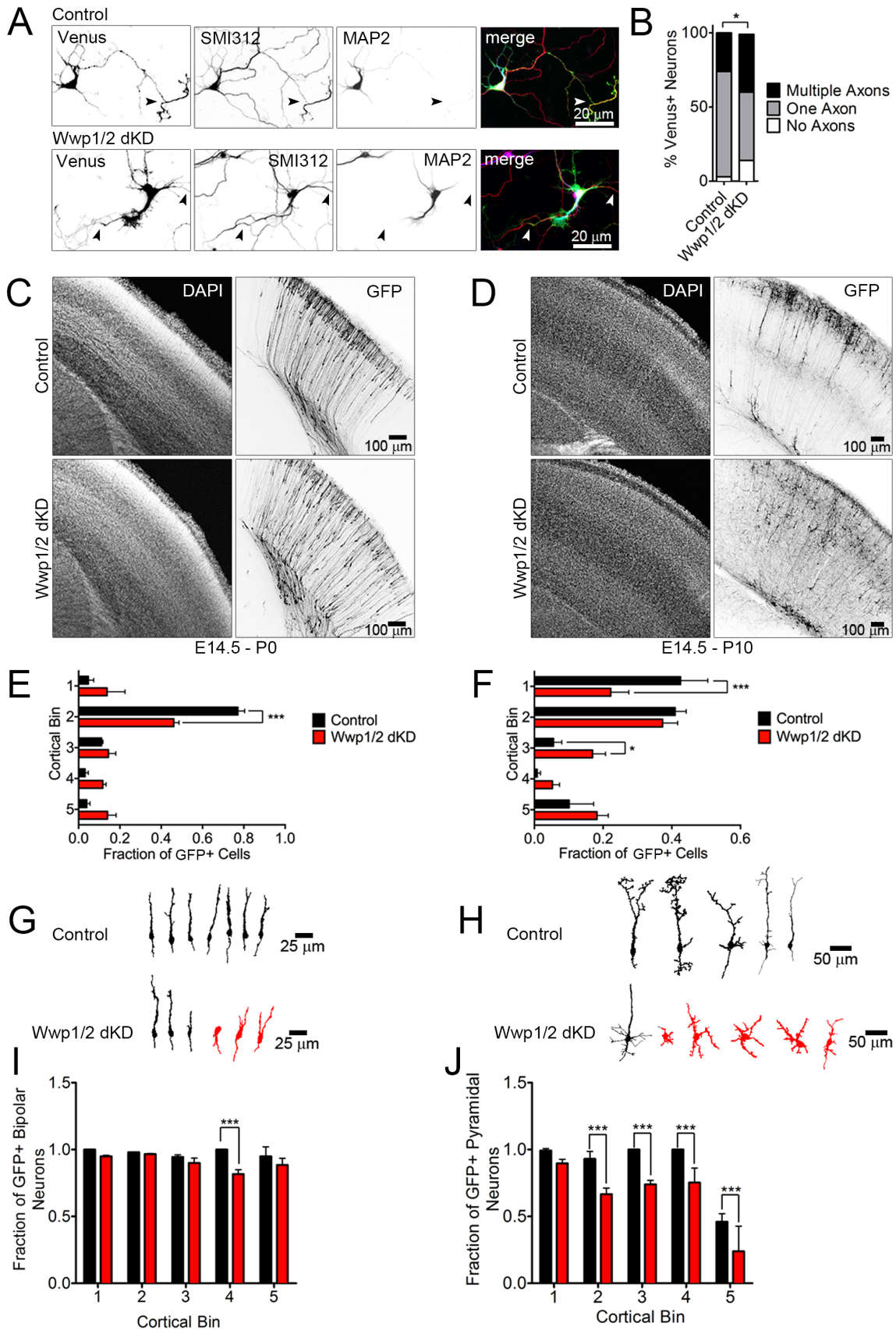

Supplementary Fig. S2. Induction of multiple axons, aberrant distribution and morphology of cortical neurons upon Wwp1 and Wwp2 double knock-down. Related to Fig. 1.

(A) Representative images of cultured primary hippocampal neurons transfected with plasmid encoding control scramble sh-RNA, or with two plasmids encoding sh-RNAs for double knock-down of Wwp1 and Wwp2 (Wwp1/2 dKD). Neurons were transfected at DIV1 and fixed at DIV7. Arrowheads indicate axons positive for SMI312 and negative for MAP2 staining. (B) Quantification of the number of axons projected from a single neuron. Quantification of the number of axons projected by a single neuron (Table S1L). (C-J) Cortical progenitors of wild type mice were transfected *in utero* at E14.5 with a plasmid encoding myristoilated Venus (myr-Venus) and control non-silencing sh-RNA, or co-transfected with two plasmids, one encoding myr-Venus together with sh-RNA to downregulate Wwp1, and another one encoding myr-Venus and sh-RNA for Wwp2. Brains were then fixed at P0 (C, E, G, I), and at P10 (D, F, H, J). (C, D) Representative maximum intensity projections of 100 μm thick Z-stacks of DAPI signals and immunostaining with anti-GFP antibody in coronal cryosections. (E, F) Distribution of control and Wwp1/2 dKD neurons in P0 (E) or P10 (F) cortex. Images of cortices were divided into 5 bins of identical dimensions and the relative number of neurons was counted in each bin (Table S1M and S1N). (G, H) Representative morphologies of neurons in bin 3 and 4 of P0 (G) or P10 (H) control or Wwp1/2 dKD brains. (I) Quantification of neuronal polarities. Numbers of BP neurons were counted in each cortical bin (Table S1O). (J) Fractions of pyramidal neurons in control and Wwp1/2 dKD in P10 cortices. Relative numbers of neurons with a single prominent dendritic shaft projecting towards the pia in each bin were expressed as averages ± S.D. (Table S1P). Results on graphs are represented as averages ± S.D. For statistical analyses, (B), Chi-square test; (E), (F), (I), (J), two-way ANOVA. *** $p < 0.001$; ** $0.001 < p < 0.01$; * $p < 0.05$.

Supplementary Figure S3.

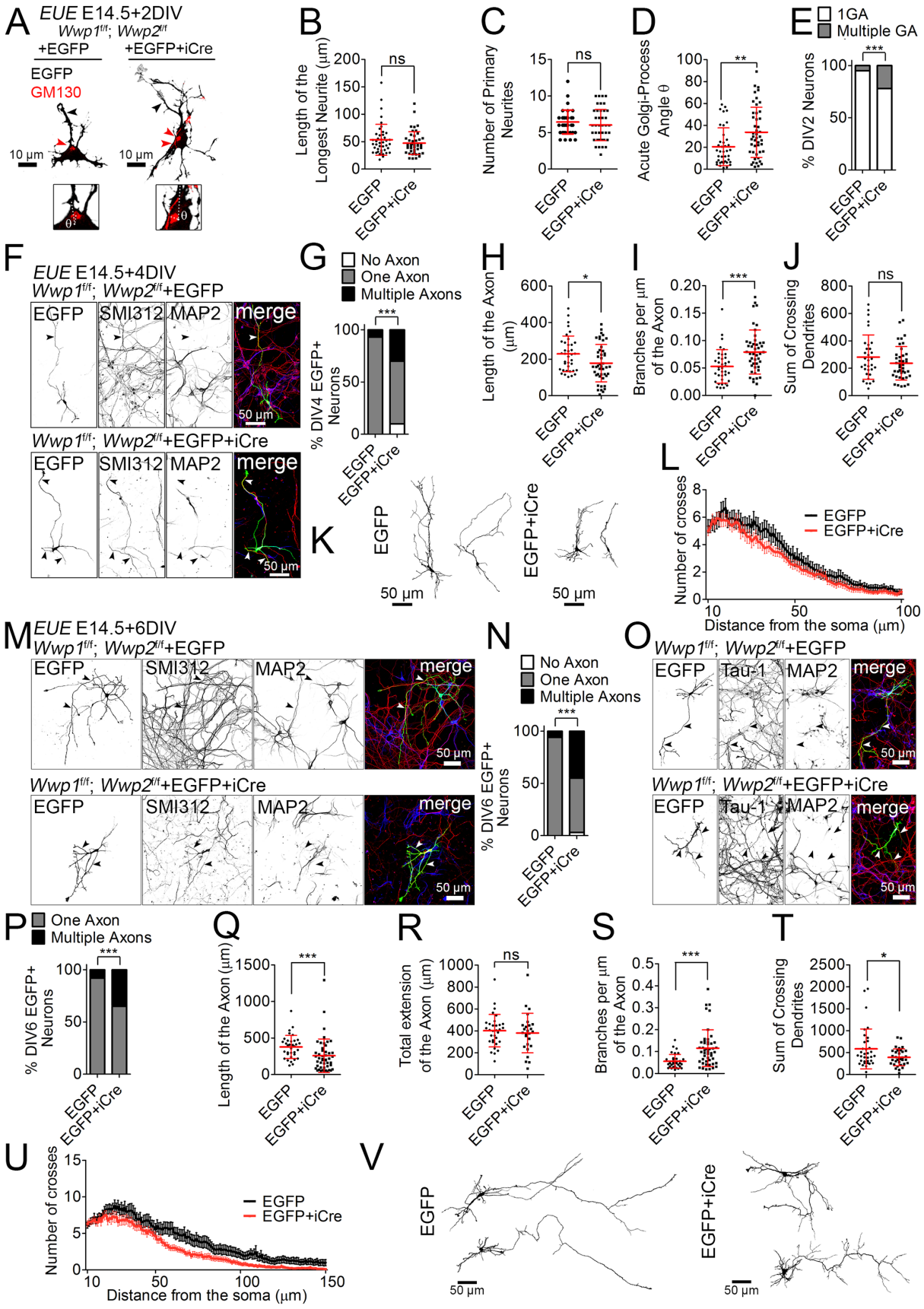

Supplementary Fig. S3. Double knock-out of *Wwp1* and *Wwp2* induces multiple axons and aberrances in neurite growth in cortical primary neurons. Related to Fig. 1.

(A) Images of representative primary cortical *Wwp1/2*$^{f/f}$ neurons after *ex utero* electroporation (EUE) at E14.5. Control neurons expressing EGFP and *Wwp1/2* dKO expressing GFP and Cre recombinase were fixed at DIV2, and immunostained for EGFP and cis-Golgi marker protein GM130. Black arrowheads indicate the longest neurite, red arrowheads point to Golgi apparatus (GA). Quantification of the length of the longest neurite (Table S1Q) (B), the number of primary branches (Table S1R) (C), and the acute angle of Golgi apparatus and the emergence of the longest neurite θ (Table S1S) (D). (E) Quantification of the number of Golgi apparatus (GA) stacks in a single neuron (Table S1T). (F) Images of representative primary cortical *Wwp1/2*$^{f/f}$ neurons after EUE at E14.5. Control neurons expressing EGFP and *Wwp1/2* dKO expressing GFP and Cre recombinase were fixed at DIV4, and immunostained for axonal (SMI312) and dendritic (MAP2) marker proteins. Arrowheads indicate axons. (G) Quantification of the number of axons projected from a single neuron (Table S1U). Quantification of the length (Table S1V) (H) and branching (Table S1W) (I) of the axon, identified as SMI312-positive and Map2-negative neurite. (J) Quantification of the sum of crossings of neurites with Sholl circles in control and *Wwp1/2* dKO neurons (Table S1X). (K) Representative reconstructions of DIV4 control and *Wwp1/2* dKO neurons, based on EGFP fluorescence. (L) Sholl analysis diagram of DIV4 control and *Wwp1/2* dKO neurons. Axons were manually removed from the analysis. (M to P) Polarity of neurons estimated by two axonal markers, SMI312 and Tau-1. (M, O) Images of representative primary cortical *Wwp1/2*$^{f/f}$ neurons after EUE at E14.5. Control neurons expressing EGFP and *Wwp1/2* dKO neurons expressing GFP and Cre recombinase were fixed at DIV6, and immunostained for axonal (SMI312 in M; Tau-1 in O) and dendritic (MAP2) marker proteins. Arrowheads indicate axons. (N, P) Quantification of the number of axons, defined as Map2-negative and SMI-312-positive (Table S1Y) (N), or Tau-1-positive (Table S1Z) (P) neurite, projected from a single neuron. Quantification of the length (Table S1A') (Q), total extension (Table S1B') (R) and branching (Table S1C') (S) of the axon, identified as SMI312-, or Tau-1-positive and Map2-negative neurite. (T) Quantification of the sum of crossings of neurites with Sholl circles in control and *Wwp1/2* dKO neurons (Table S1D'). (U) Sholl analysis diagram of DIV6 control and *Wwp1/2* dKO neurons. Axons were manually removed from the analysis. (V) Representative reconstructions of DIV6 control and *Wwp1/2* dKO neurons after EUE at E14.5. Results on (L) and (U) are represented as averages ± S.E.M. Results on other graphs are represented as averages ± S.D. For statistical analyses, (B to D), (I), (Q to S), D'Agostino-

Pearson normality test and Mann-Whitney test; (H), (J), (T), D'Agostino-Pearson normality test and unpaired t-test; (E), (P), Fisher's exact test; (G), (N), Chi-square test. *** $p < 0.001$; 0.001 **$0.001 < p < 0.01$; * $0.01 < p < 0.05$.

Supplementary Fig. S4.

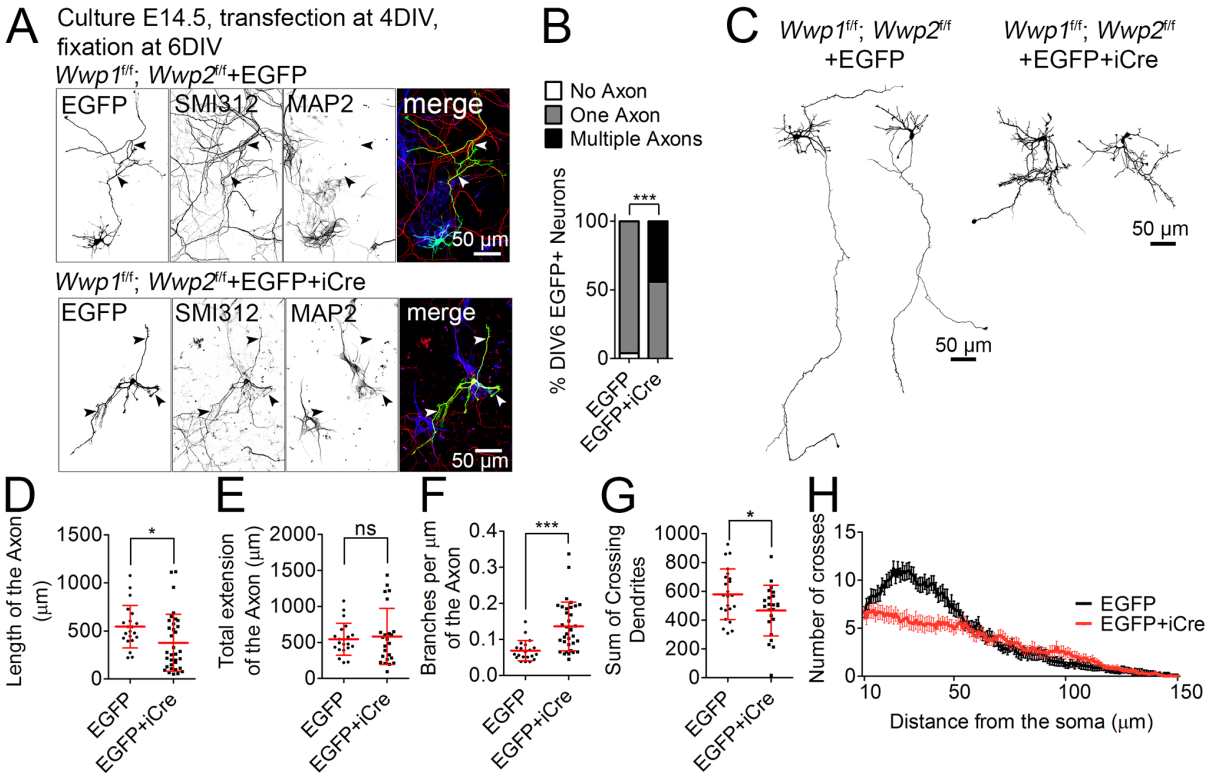

Supplementary Fig. S4. Double knock-out of *Wwp1* and *Wwp2* after initial axon specification induces multiple axons in cortical primary neurons. Related to Fig. 1.

(A) Images of representative primary cortical *Wwp1/2*$^{f/f}$ neurons. Neurons were transfected at DIV4. Control neurons expressing EGFP and *Wwp1*/2 dKO expressing GFP and Cre recombinase were fixed at DIV6, and immunostained for axonal (SMI312) and dendritic (MAP2) marker proteins. Arrowheads indicate axons. (B) Quantification of the number of axons, defined as Map2-negative and SMI-312-positive neurite, projected from a single neuron (Table S1E'). (C) Representative reconstructions of DIV6 control and *Wwp1/2* dKO neurons after transfection with EGFP or EGFP and Cre expression vectors at DIV4. Quantification of the length (Table S1F') (D), extension (Table S1G') (E), and branching (Table S1H') (F) of the axon, identified as SMI312-, or Tau-1-positive and Map2-negative neurite. (G) Quantification of the sum of crossings of neurites with Sholl circles in control and *Wwp1/2* dKO neurons (Table S1I'). (H) Sholl analysis diagram of DIV6 control and *Wwp1/2* dKO neurons. Axons were manually removed from the analysis. Results on (H) are represented as averages ± S.E.M. Results on other graphs are represented as averages ± S.D. For statistical analyses, (B), Chi-square test; (D-F), D'Agostino-Pearson normality test and Mann-Whitney test; (G), D'Agostino-Pearson normality test and unpaired t-test. *** $p < 0.001$; * $0.01 < p < 0.05$.

Supplementary Fig. S5.

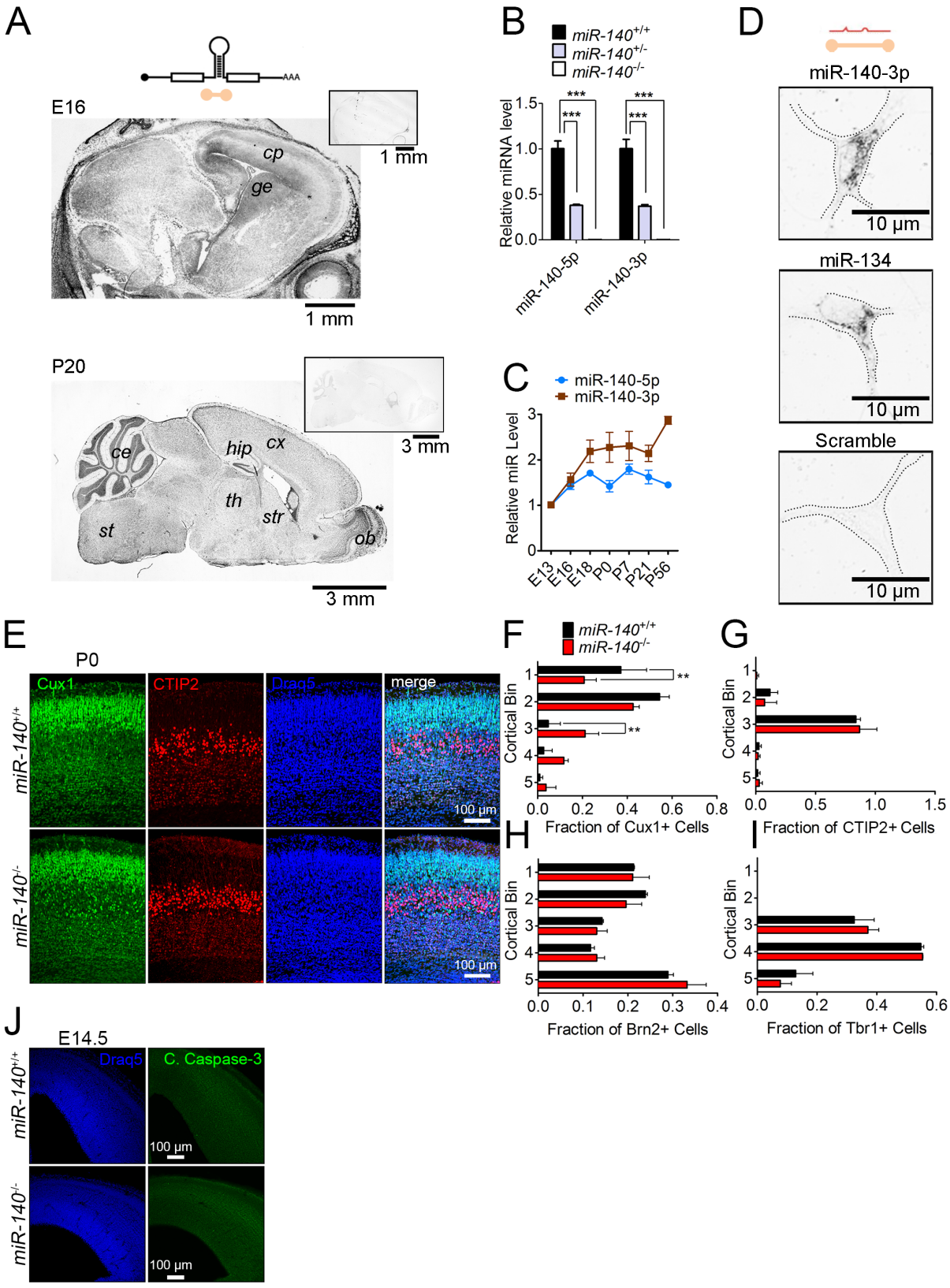

Supplementary Fig. S5. miR-140 is expressed in murine central nervous system and its knock-out engenders aberrant lamination of Cux1-positive neurons. Related to Fig. 2.

(A) Results of *in situ* hybridization of the antisense probe for intronic *miR-140* spanning *Wwp2* locus (upper scheme) on sagittal sections of E16 and P20 wild type mouse brain. Images in the top right inserts represent signals from the control sense probe; cortical plate (cp), ganglionic eminence (ge); cortex (cx), hippocampus (hip), cerebellum (ce), brain stem (st), thalamus (th), striatum (str) and olfactory bulb (ob). (B) Validation of qRT-PCR primer specificity for miR-140-5p and -3p. cDNA samples were prepared from total RNA extracted from cerebral cortices of *miR-140*$^{+/+}$, *miR-140*$^{+/-}$, and *miR-140*$^{-/-}$ mice at P21. The level of each miR-140 strand was expressed relative to component of spliceosome, U6 snRNA - RNU6B (Table S1J'). (C) Developmental profile of miR-140-3p and -5p expression in developing mouse cortex. Total RNA was isolated from cortices of mice of depicted ages. The level of each miRNA strand was expressed relative to RNU6B and to the miR level at E13 (Table S1K'). (D) *In situ* hybridization with locked-nucleic acid probes (upper scheme) for mature miR-140-3p (top panel), dendritic miR-134 (middle panel), and scramble control (bottom panel) in DIV7 primary hippocampal neurons. Edges of cell bodies are outlined with black dotted lines. (E) Representative images of immunostaining against Cux1, CTIP2 and Draq5 labeling in P0 *miR-140*$^{+/+}$ or *miR-140*$^{-/-}$ cortices. (F-I) Quantification of laminar distribution of cortical neurons positive for indicated fate markers in *miR-140*$^{+/+}$ or *miR-140*$^{-/-}$ mouse brains (Tables S1O' – S1R'). (F), Cux1; (G), CTIP2; (H), Brn2, expressed in neuronal progenitors and upper layer neurons; and (I), Tbr1, a deeper layer neuron marker. (J) Representative images of immunostaining against cleaved caspase-3 and Draq5 labeling in P0 *miR-140*$^{+/+}$ or *miR-140*$^{-/-}$ cortices. Results on (C) are represented as averages ± S.E.M. Results on (B) and (F-I) are represented as averages ± S.D. For statistical analyses, (B) one-way ANOVA with Bonferroni post-hoc test; (F-I) two-way ANOVA with Bonferroni post-hoc test. *** $p < 0.001$; ** $0.001 < p < 0.01$.

Supplementary Fig. S6.

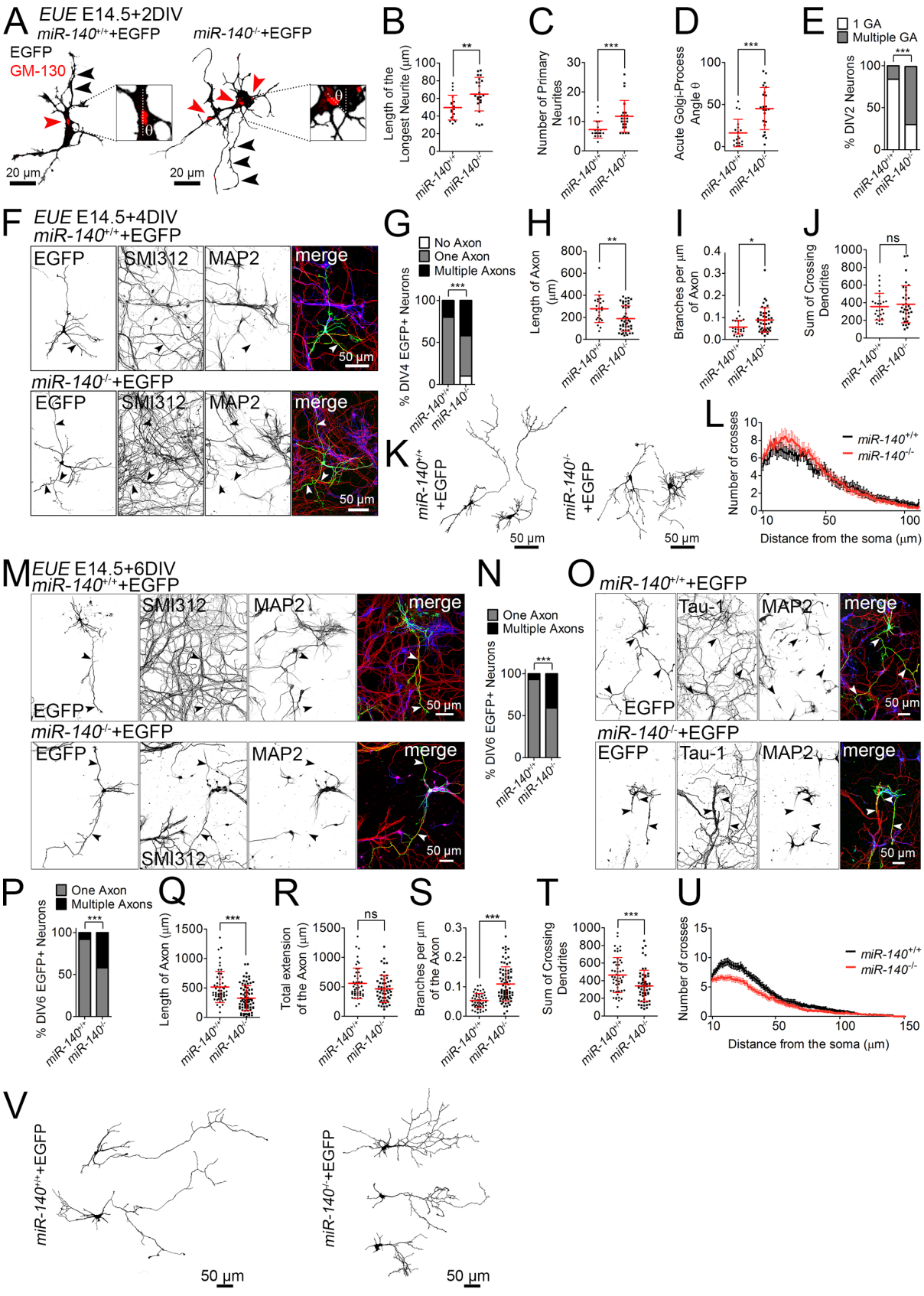

Supplementary Fig. S6. Knock-out of *miR-140* induces multiple axons and aberrances in neurite growth in cortical primary neurons. Related to Fig. 2.

(A) Images of representative primary cortical *miR-140*$^{+/+}$ and *miR-140*$^{-/-}$ neurons after EUE at E14.5. Neurons of both genotypes expressing EGFP were fixed at DIV2, and immunostained for EGFP and cis-Golgi marker protein GM130. Black arrowheads indicate the longest neurite, red arrowheads point to Golgi apparatus (GA). Quantification of the length of the longest neurite (Table S1V') (B), the number of primary neurites (Table S1W') (C), and the acute angle of Golgi apparatus and the emergence of the longest neurite θ (Table S1X') (D). (E) Quantification of the number of Golgi apparatus (GA) stacks in a single neuron (Table S1Y'). (F) Images of representative primary cortical *miR-140*$^{+/+}$ and *miR-140*$^{-/-}$ neurons after EUE at E14.5. Neurons of both genotypes expressing EGFP were fixed at DIV4, and immunostained for axonal (SMI312) and dendritic (MAP2) marker proteins. Arrowheads indicate axons. (G) Quantification of the number of axons projected from a single neuron (Table S1Z'). Quantification of the length (Table S1A") (H) and branching (Table S1B") (I) of the axon, identified as SMI312-positive and Map2-negative neurite. (J) Quantification of the sum of crossings of neurites with Sholl circles in control and *miR-140* KO neurons (Table S1C"). (K) Representative reconstructions of DIV4 control and *miR-140* KO neurons, based on EGFP fluorescence. (L) Sholl analysis diagram of DIV4 control and *miR-140* KO neurons. Axons were manually removed from the analysis. (M and O) Images of representative primary cortical *miR-140*$^{+/+}$ and *miR-140*$^{-/-}$ neurons after EUE at E14.5. Neurons of both genotypes expressing EGFP were fixed at DIV6, and immunostained for axonal (SMI312 in M; Tau-1 in O) and dendritic (MAP2) marker proteins. Arrowheads indicate axons. (N, P) Quantification of the number of axons, defined as Map2-negative and SMI-312-positive (N), or Tau-1-positive (P) neurite, projected from a single neuron (Table S1D" and S1E"). Quantification of the length (Table S1F") (Q), extension (Table S1G") (R), and branching (Table S1H") (S) of the axon, identified as SMI312-, or Tau-1-positive and Map2-negative neurite. (T) Quantification of the sum of crossings of neurites with Sholl circles in control and *miR-140* KO neurons (Table S1I"). (U) Sholl analysis diagram of DIV6 control and *miR-140* KO neurons. Axons were manually removed from the analysis. (V) Representative reconstructions of DIV6 *miR-140*$^{+/+}$ and *miR-140*$^{-/-}$ neurons after EUE at E14.5. Results on (L) and (U) are represented as averages ± S.E.M. Results on other graphs are represented as averages ± S.D. For statistical analyses, (B), (D), D'Agostino-Pearson normality test and unpaired t-test; (C), (H to J), (Q to T), D'Agostino-Pearson normality test and Mann-Whitney

test; (E), (N), (P), Fisher's exact test; (G), Chi-square test. *** $p < 0.001$; ** $0.001 < p < 0.01$; * $0.01 < p < 0.05$.

Supplementary Fig. S7.

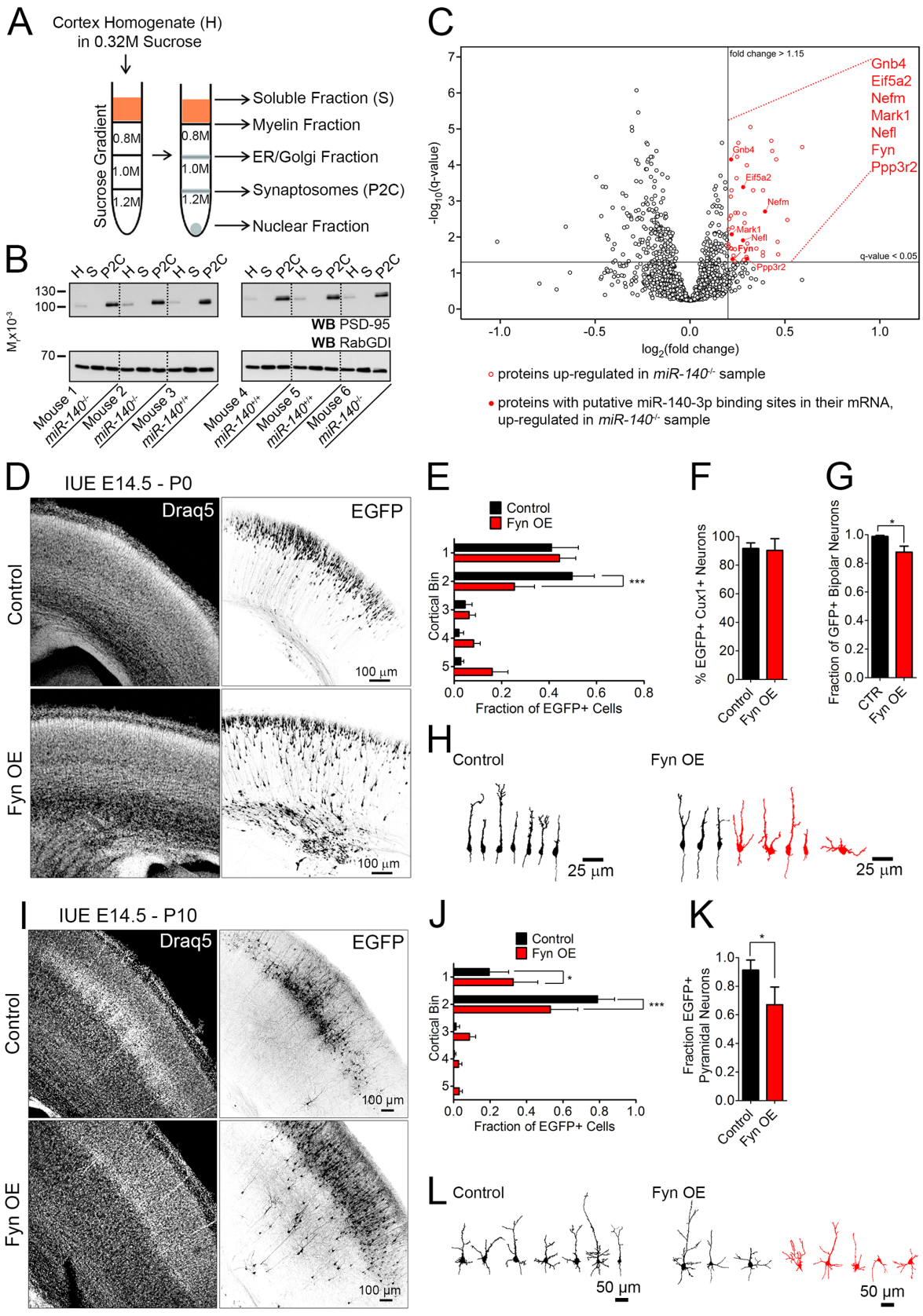

Supplementary Fig. S7. Identification of miR-140 downstream targets and overexpression of Fyn in wild type neurons resembles the loss of miR-140 in migrating cortical neurons. Related to Fig. 3.

(A) Schema of synaptosome purification from *miR-140*$^{+/+}$ and *miR-140*$^{-/-}$ mouse brains. Homogenate (H), Soluble fraction (S), and Synaptosome fraction (P2C) were used in validation in (B). (B) Validation of synaptosomal preparation by Western blotting using anti-PSD-95 and anti-RabGDI antibodies. Same protein amounts of H, S, and P2C were loaded for SDS-PAGE. Note enrichment of PSD-95 in synaptosomes (P2C), and persistent levels of RabGDI in all fractions. (C) Volcano plot with proteins identified by quantitative proteomics. Putative targets of miR-140 are listed in red, the $\log_2$ fold-change of protein level in *miR-140*$^{-/-}$ samples relative to *miR-140*$^{+/+}$ samples, and the corresponding q-values of moderated t-statistics with false discovery-based correction for multiple comparisons. q-values < 0.05 were considered significant. Proteins with fold change > 1.15 and with putative miR-140-3p binding sites along their 3'UTR were selected as putative miR-140 targets. (D) Representative images of Draq5 fluorescence and EGFP immunofluorescence in P0 cortices. Cortical progenitors of wild type mice were transfected *in utero* at E14.5 to express GFP (Control), or simultaneously over-express EGFP and Fyn (Fyn OE). (E) Distribution of Control and Fyn overexpressing (OE) neurons (Table S1R"). (F) Quantification of Cux1-positive neurons relative to total number of control or Fyn OE cells (Table S1S"). (G) Quantification of Control and Fyn OE neurons with BP morphology (Table S1T"). (H) Representative morphologies of Control and Fyn OE neurons in bin 3 and 4 at P0. Neurons with aberrant, non-BP morphology are colored red. (I) Representative images of EGFP immunostaining signals and Draq5 labeling in P10 cortices of mice electroporated *in utero* to express EGFP, or EGFP and Fyn overexpression vector (Fyn OE) at E14.5. (J) Quantification of laminar distribution of cortical neurons in mouse brains after electroporation with EGFP or EGFP and Fyn overexpression vector (Table S1U"). (K) Quantification of the number of neurons with a pyramidal morphology (Table S1V"). (L) Representative EGFP-fluorescence based tracings of neurons expressing indicated vectors. Neurons with aberrant, non-pyramidal morphology are colored red. Results on graphs are represented as averages ± S.D. For statistical analyses, (F), (G), (K), unpaired t-test; (E), (J), two-way ANOVA with Bonferroni post-hoc test. *** $p < 0.001$; * $0.01 < p < 0.05$.

Supplementary Fig. S8.

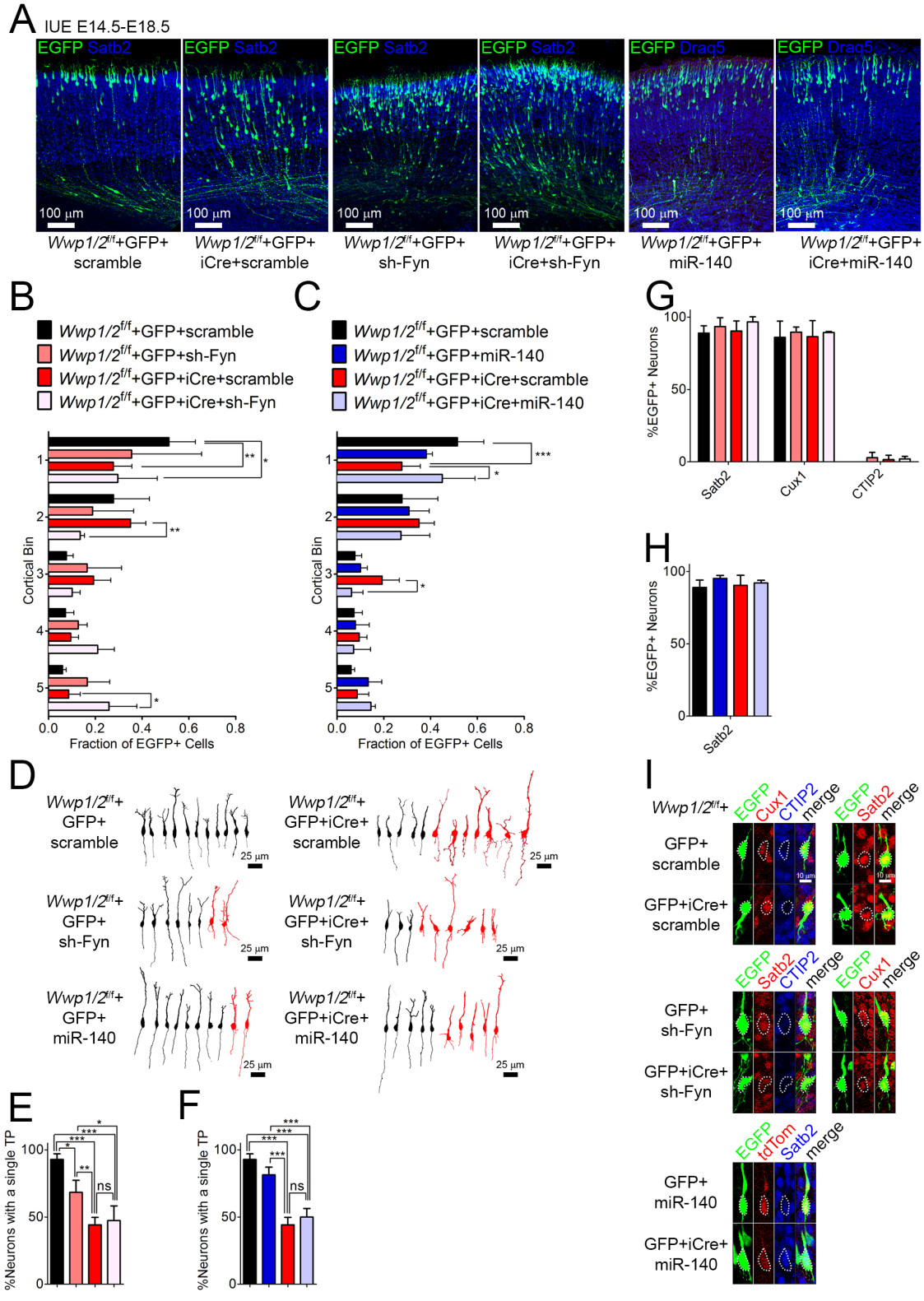

Supplementary Fig. S8. Wwp1/2 operate in Fyn-independent manner. Related to Fig. 1, 2, 3, and 4.

(A) Representative images of immunostaining against EGFP and Satb2 or Darq5 labeling in E18.5 *Wwp1/2*$^{f/f}$ cortices electroporated *in utero* at E14.5 to express indicated vector combinations. (B, C) Quantification of laminar distribution of cortical neurons in *Wwp1/2*$^{f/f}$ mouse brains after electroporation with indicated vectors (Table S1A''' and S1B'''). (D) Representative EGFP-fluorescence based tracings of *Wwp1/2*$^{f/f}$ neurons expressing indicated vectors. Neurons with aberrant morphology (i.e. multiple trailing processes) are colored red. (E, F) Quantification of the number of neurons with a single trailing process (TP) (Table S1C''' and S1D'''). Legends for the graphs are on panel (B, C). (G) Quantification of the fraction of EGFP-positive *Wwp1/2*$^{f/f}$ neurons expressing indicated fate markers after IUE with vectors indicated on (B) (Table S1E'''). (H) Quantification of the fraction of EGFP-positive *Wwp1/2*$^{f/f}$ neurons expressing Satb2 after IUE with vectors indicated on (C) (Table S1F'''). (I) Representative images of immunostaining against EGFP, Cux1, CTIP2, Satb2, and tdTomato after IUE with indicated vectors. tdTomato is a reporter used to visualize expression of miR-140. Cell soma is marked with a dotted line. Results on graphs are represented as averages ± S.D. For statistical analyses, (B) and (C), two-way ANOVA with Bonferroni post-hoc test; (E-H), one-way ANOVA with Bonferroni post-hoc test. *** $p < 0.001$; ** $0.001 < p < 0.01$.

Supplementary Fig. S9.

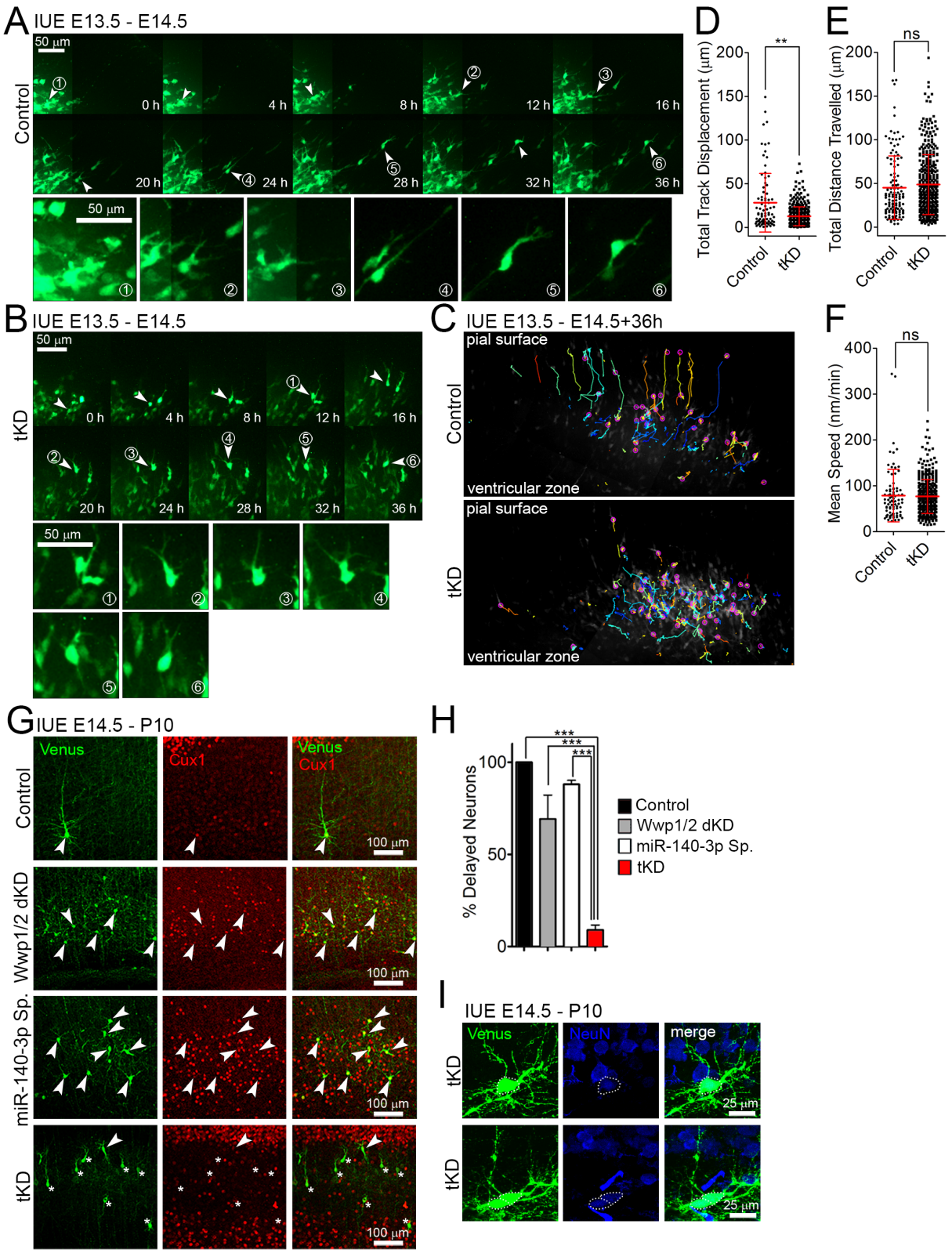

Supplementary Fig. S9. Wwp1/2 and miR-140-3p triple knock-down neurons translocate in a non-radial fashion and lose their terminal differentiation marker expression. Related to Fig. 4.

(A) Montage of a representative control neuron. Arrowhead points to one neuron over the course of 36 hours-long imaging experiment. Magnifications of respective cell states are depicted under pictures 1-6 on the bottom panel. (B) Montage of a representative tKD neuron. Arrowheads point to a single neuron. Magnifications of respective cell states are depicted under pictures 1-6 on the bottom panel. Neuronal progenitors at E13.5 were *in utero* electroporated with vectors encoding for non-silencing sh-RNA and control sponge (A), or with plasmids for the expression of sh-RNAs to downregulate Wwp1 and Wwp2 and miR-140-3p-Sponge (tKD) (B). Slice culture was prepared at E14.5 and images of developing cortical plate were taken every 30 minutes using spinning disc confocal microscope. (C) Representative reconstruction of tracks of control and tKD neurons. (D to F) Quantifications of (D) total track displacement (Table S1N'''), (E) total distance travelled (Table S1O'''), (F) and the mean speed of movement (Table S1P''') of control or tKD neurons. (G) Immunolabeling with anti-GFP antibody and anti-Cux1 antibodies in Wwp1/2 dKD, miR-140-3p-Sponge-expressing, and Wwp1/2; miR-140-3p tKD P10 cortices after IUE at E14.5. Presented is a fragment of bin 3 of cortical coronal cryosection. Arrowheads point to Venus- and Cux1-positive neurons. Asterisks mark neurons positive for Venus and negative for Cux1. (H) Quantification of Cux1-positive neurons delayed in deeper cortical layers in control and upon Wwp1/2 dKD, miR-140-3p-Sponge expression, or Wwp1/2; miR-140-3p tKD. (Table S1Q'''). (I) EGFP/myrVenus-expressing tKD neurons (green) are positive for a neuronal marker NeuN (blue). Cell soma is highlighted by the dashed line. Results on graphs are represented as averages ± S.D. For statistical analyses, (D-F), D'Agostino and Pearson omnibus normality test and Mann Whitney test; (H), one-way ANOVA with Bonferroni post-hoc test. *** $p < 0.001$; ** $0.001 < p < 0.01$.

Supplementary Fig. S10.

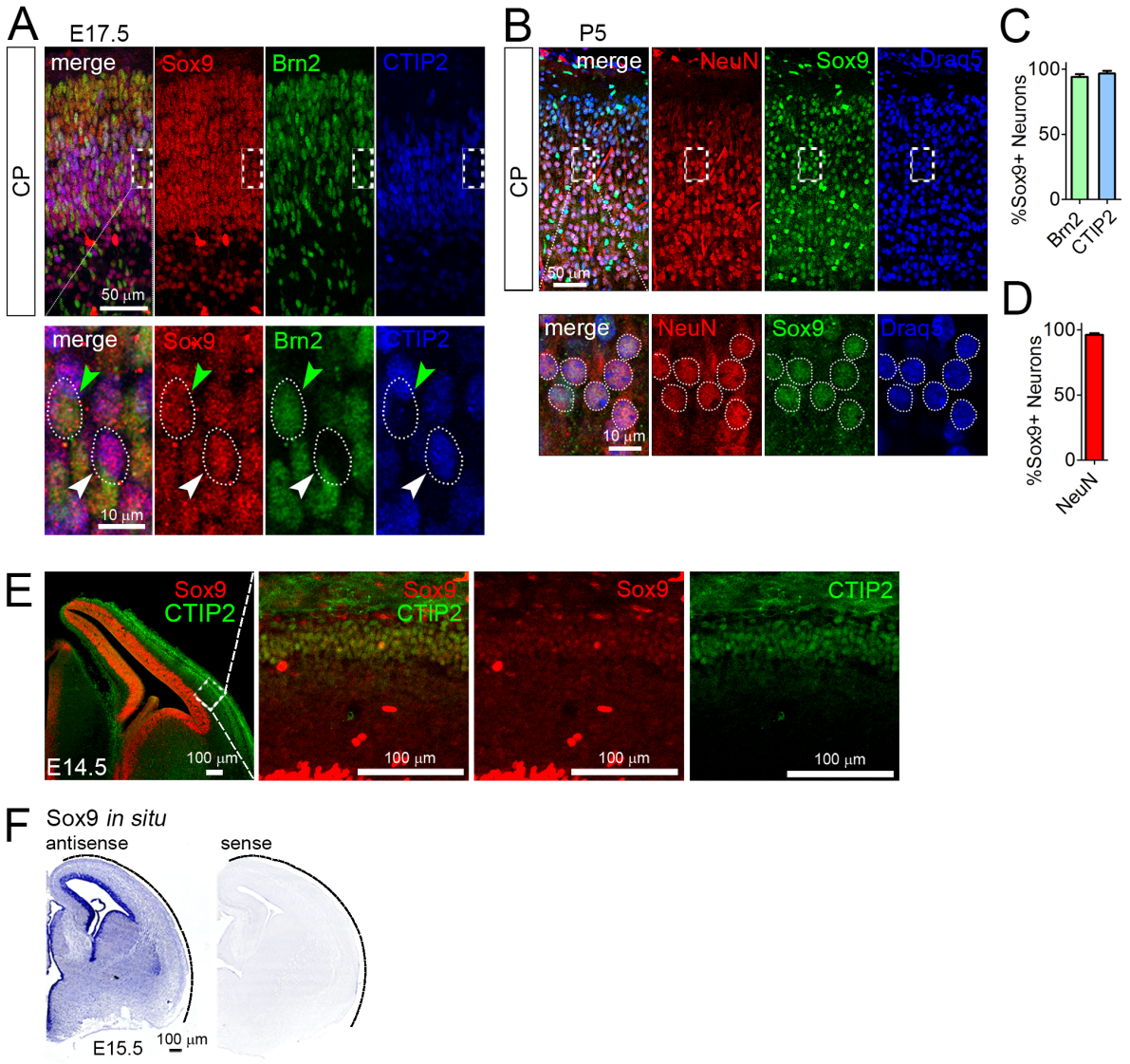

Supplementary Fig. S10. Sox9 is expressed in the ventricular zone and postmitotic neurons of the cortical plate. Related to Fig. 5.

(A) Representative images of immunostaining signals in E17.5 cortical plate (CP) of wild type mice to visualize expression of Sox9, Brn2 and CTIP2. White arrowhead points to CTIP2+ Sox9+ neuron, green arrowhead points to Brn2+ Sox9+ neuron. Cell nucleus is marked with a dotted line. (B) Representative images of immunostaining signals in P5 cortical plate (CP) of wild type mice to visualize expression of NeuN, Sox9, and and Draq5 labeling. Cell nucleus is outlined with a dotted line. (C) Quantification of fraction of Brn2+ or CTIP2+ neurons that express Sox9 (Table S1S'''). (D) Quantification of NeuN+ neurons that express Sox9 (Table S1T'''). (E) Immunohistochemistry in E14.5 brain coronal cryosection with antibodies for Sox9 and CTIP2, a marker for deeper layer postmitotic neurons. Note that CTIP2 positive neurons are also positive for Sox9 (F) Results of *in situ* hybridization on E15.5 coronal cryosection of embryonic brain using an antisense and sense probe for *Sox9*. Bars on (C-D) represent averages ± S.D.

Supplementary Fig. S11.

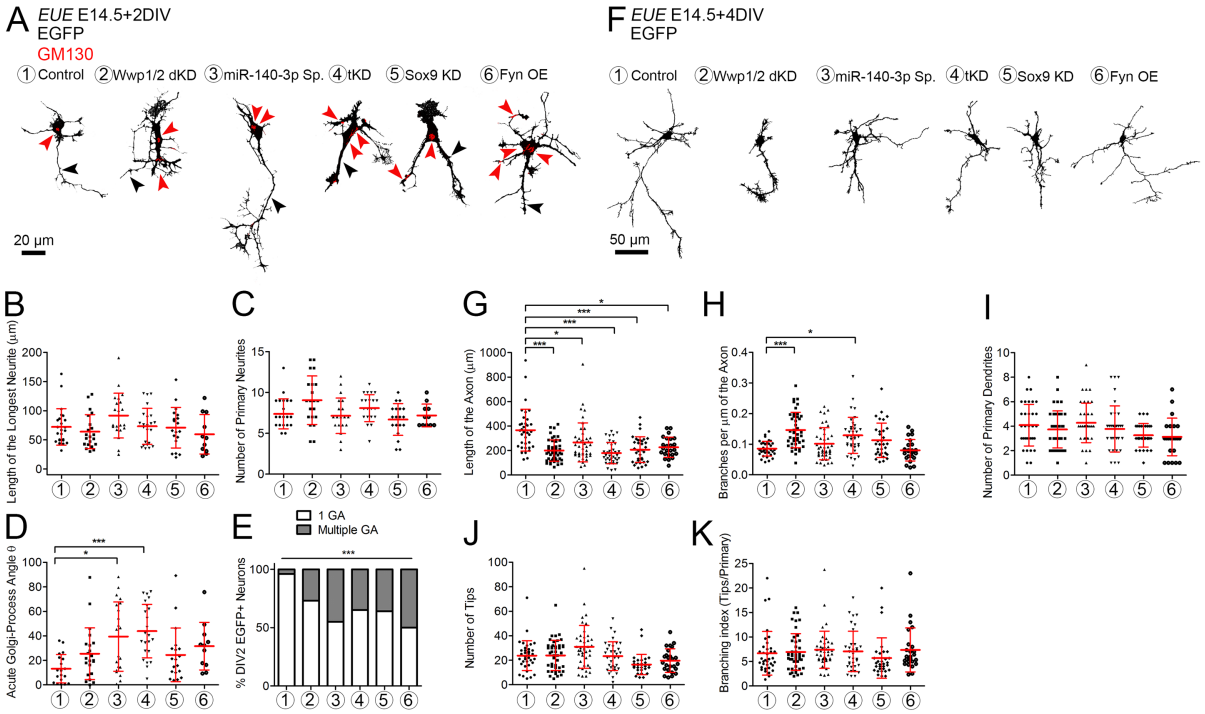

Supplementary Fig. S11. Development of cortical neurons upon disruption to Sox9-Wwp1/2-miR-140-Fyn pathway. Related to Fig. 6, 7, and 8.

(A) Images of representative primary cortical neurons after *ex utero* electroporation (EUE) at E14.5 with indicated plasmids. (1) Control: plasmids encoding EGFP+scramble-sh-RNA-Venus+Control Sponge+mock DNA; (2) Wwp1/2dKD: EGFP+sh-RNA-Wwp1+sh-RNA-Wwp2-Venus+Control Sponge+mock DNA; (3) miR-140-3p Sponge: EGFP+scramble-sh-RNA-Venus+miR-140-3p Sponge+mock DNA; (4) tKD: EGFP+ sh-RNA-Wwp1+sh-RNA-Wwp2-Venus +miR-140-3p Sponge+mock DNA; (5) Sox9 KD: EGFP+sh-RNA-Sox9-Venus+Control Sponge+mock DNA; (6) Fyn OE: EGFP+scramble-sh-RNA-Venus+Control Sponge+Fyn overexpression plasmid. (A to E) Neurons expressing indicated vectors were fixed at DIV2, and immunostained for EGFP and cis-Golgi marker protein GM130. (A) Representative images of neurons at DIV2. Black arrowheads indicate the longest neurite, red arrowheads point to Golgi apparatus (GA). Quantification of the length of the longest neurite (Table S1L"") (B), the number of primary branches (Table S1M"") (C), and the acute angle of Golgi apparatus and the emergence of the longest neurite θ (Table S1N"") (D). (E) Quantification of the number of Golgi apparatus (GA) stacks in a single neuron (Table S1O""). (F to K) Neurons expressing indicated vectors were fixed at DIV4, and immunostained for EGFP. (F) Representative images of neurons at DIV4. (G) Quantification of the length of axon identified as a neurite expressing SMI312 or Tau-1 and negative for MAP2 (Table S1P""). (H) Quantification of axon branching (Table S1Q""), (I) number of primary dendrites (Table S1R""), (J) number of dendritic tips (Table S1S""), (K) branching index as a ration between the number of dendritic tips and number of primary dendrites in a single neuron (Table S1T""). Results on (B to D) and (G to K) are represented as averages ± S.D. For statistical analyses, (B to D) and (G to K), D'Agostino and Pearson omnibus normality test and Kruskal-Wallis test with Dunn's Multiple comparison test; (E), Chi-square test. *** $p < 0.001$; ** $0.001 < p < 0.01$; * $0.01 < p < 0.05$.

Supplementary Fig. S12.

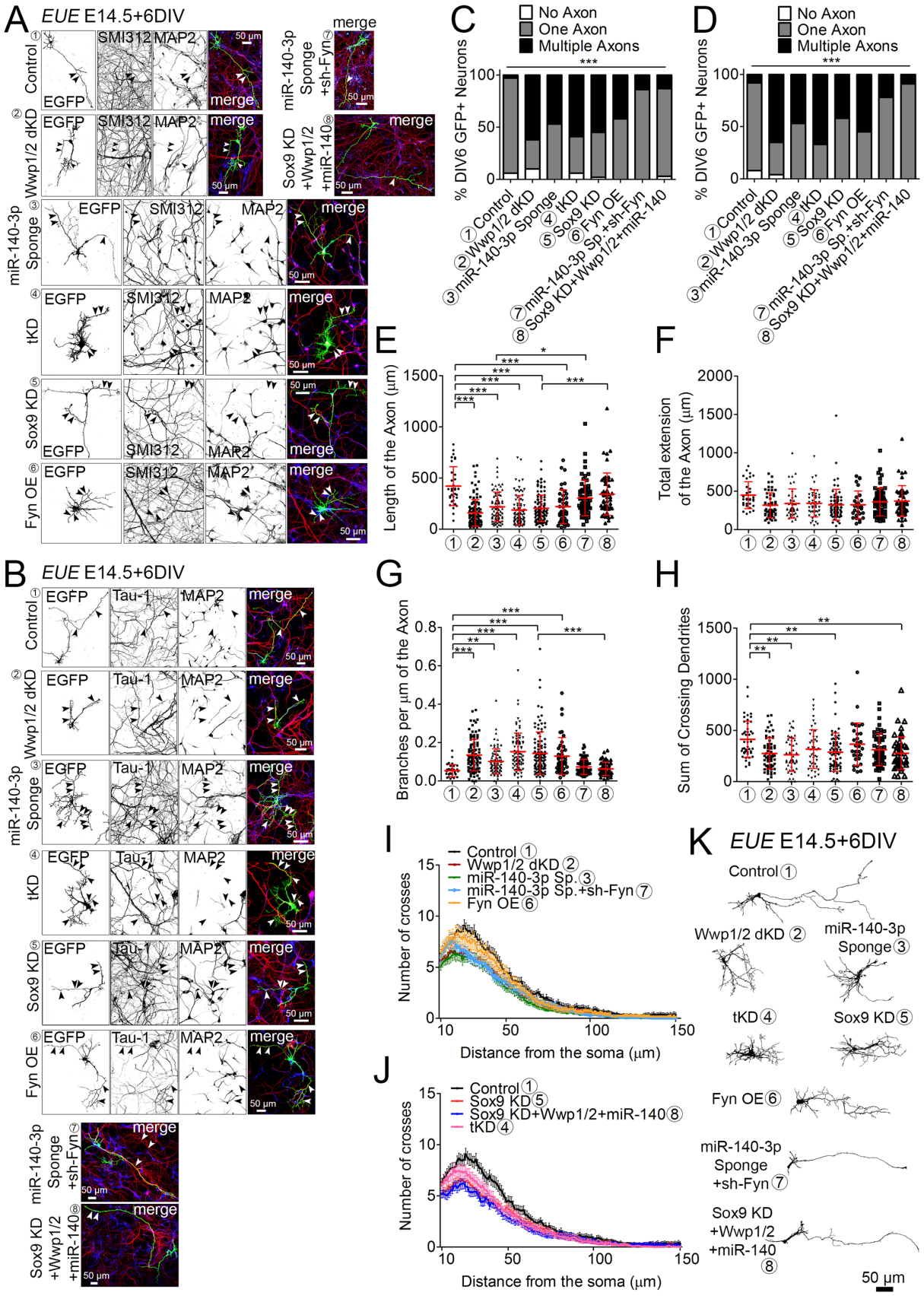

Supplementary Fig. S12. Induction of multiple axons and aberrances to axon-dendrite growth upon disruption to Sox9-Wwp1/2-miR-140-Fyn pathway. Related to Fig. 7 and 8.

(A, B) Images of representative primary cortical neurons after *ex utero* electroporation (EUE) at E14.5 with indicated vectors. (1) Control: plasmids encoding EGFP+scramble-sh-RNA-Venus+Control Sponge+mock DNA; (2) Wwp1/2dKD: EGFP+sh-RNA-Wwp1+sh-RNA-Wwp2-Venus+Control Sponge+mock DNA; (3) miR-140-3p Sponge: EGFP+scramble-sh-RNA-Venus+miR-140-3p Sponge+mock DNA; (4) tKD: EGFP+ sh-RNA-Wwp1+sh-RNA-Wwp2-Venus +miR-140-3p Sponge+mock DNA; (5) Sox9 KD: EGFP+sh-RNA-Sox9-Venus+Control Sponge+mock DNA; (6) Fyn overexpression (OE): EGFP+scramble-sh-RNA-Venus+Control Sponge+Fyn overexpression plasmid; (7) miR-140-3p Sp.+sh-Fyn: EGFP+sh-RNA-Fyn +miR-140-3p Sponge+mock DNA; (8) Sox9KD+Wwp1/2+mIR-140: EGFP+sh-RNA-Sox9-Venus+Control Sponge+Wwp1 OE+Wwp2 OE+miR-140 OE plasmids. Neurons were fixed at DIV6, and immunostained for axonal marker SMI312 (A) or Tau-1 (B) and dendritic MAP2 proteins. Arrowheads indicate axons. (C, D) Quantification of the number of axons, defined as MAP2-negative and (C) SMI-312-, or (D) Tau-1-positive neurite, projected from a single neuron, Chi square tests (Tables S1U"" and S1V""). Quantification of the length of the axon defined as a SMI312- or Tau-1-positive an MAP2-negative neurite (Table S1W"") (E), total extension of the axon defined as total length of all axons projected from a single neuron (Table S1X"") (F), branching of the axon (Table S1Y"") (G), and total number of crossing dendrites with Sholl circles (Table S1Z"") (H). (I, J) Sholl analysis diagrams of DIV6 primary cortical neurons expressing indicated vectors. Axons were manually removed from the analysis. (K) Representative EGFP-based tracings of primary cortical neurons after EUE at E14.5 with indicated vectors. Results on (E-H) are represented as averages ± S.D. Results on (I, J) are represented as averages ± S.E.M. For statistical analyses, (E), (G), (H), D'Agostino and Pearson omnibus normality test and Kruskal-Wallis test with Dunn's Multiple comparison test; (F), D'Agostino and Pearson omnibus normality test and one-way ANOVA with Bonferroni post-hoc test; (C and D), Chi-square test. *** $p < 0.001$; ** $0.001 < p < 0.01$; * $0.01 < p < 0.05$.